NMR measurements of wettability alternation in Berea Sandstone

Joar Vevle

Master`s Thesis in

Petroleum Technology – Reservoir Physics

Centre for Integrated Petroleum Research

Department of Physics and Technology

University of Bergen

2011

uniCIPR

This page is intentionally left blank

Abstract

When a new oil reservoir is discovered and a production strategy is chosen the knowledge about wettability characteristics for the field is of outermost importance. Wettability is a key factor for fluid distribution and fluid displacement. Many laboratory methods have therefore been developed and used over the years in order to measure wettability. Common to many of these methods are that they only give indirect information about wettability based on other parameters like imbibition rate, capillary pressures curves and relative permeability data. Displacement based methods are also often quite time consuming.

In this thesis we will investigate the use of Nuclear Magnetic Resonance (NMR) as a tool to find wettability data for 3 different systems of oil and water. Because of the NMR techniques natural sensitivity to position and surface effects between pore fluid and pore surface in a porous media it is ideal for investigating the wettability of a rock. Because the wetting state of the rock will have a big impact on the fluid distribution both on the micro scale inside a single pore, and on a larger scale in the porous media, NMR is capable of giving an indication for the wetting state.

In order to find sufficient information about the system, we applied specialized NMR sequences order to separate the signal from the two phases based on diffusion coefficient and by the effects from internal gradients. Specialized NMR sequences were also used find the correlation between transverse and longitudinal relaxation rate. When combining these sequences with standard CPMG experiments it increases the amount of information obtained from the porous media.

We have chosen Berea sandstone as a basis for the experiments and will be looking at a system of crude oil in aged cores, mineral oil in non-aged cores and crude oil in non-aged cores. A reference system at 100% water saturation n was also investigated. Because the aging of the cores changes the wettability of the core, we believe that it is possible to detect this by the use of NMR and find how it differs from the non-aged cores. We will also include a traditional USBM/Amott test in order to correlate this to the NMR-response in each system.

The cores that have been chosen to undergo ageing were flooded with crude oil at 110˚C for a period of 4 weeks. All of the cores have then been subjected to the combined USBM/Amott test to establish the wettability of each core. We found that the aged cores had changed significantly towards neutrally wet, and the non-aged cores were strongly water wet.

In the NMR part of the experiment we found that when doing only a standard CPMG test of the cores the broadening of the peaks originating from each phase made it hard to separate the response from each phase. This made it difficult to use the CPMG data as a wettability indicator. Despite this we were able to find some indicators of a change in the aged cores. When comparing the T_2 distribution

from the aged and the non-aged core we found that there had been a reduction in the main peak and increase in intensity at shorter T_2 values of the aged core`s T_2 distribution. This is described as an effect of changed wettability state, where the altered wetting conditions cause the oil to come into contact with the pore surface.

When including a sequence for diffusion encoding we observed that we were not able to distinguish between the signals from each phase. In the case of S_{wi} this is caused the nature of the sequence itself. We are however able to detect an increase in the measured diffusivity of oil that may be caused by a more continuous oil phase. In the case of S_{or} the peaks from water and oil has merged forming a larger combined peak. But because the diffusion encoding is preserved in the large peak we are able to separate the aged core from the non-aged core. In this case we see a decrease in diffusion that may be caused by oil trapped in films at the pore surface, where the diffusion is limited.

When applying the internal gradient encoding sequence no information was collected at S_{wi}, but at S_{or} good indicators of wettability alternation was detected. Because the oil is behaving more like the wetting phase no shift in DG_0/T_2 ratio was observed in the aged cores. In the non-aged cores on the other hand a hinge point was found that corresponded to the oil phase.

After applying the T_1-T_2 correlation sequence we found that the altered wettability of the aged cores caused the oil phase to behave more like the wetting phase. This caused a reduction in the signal from the bulk oil and an increase in the signal that had a T_1/T_2 ratio close to 1. This situation was found in both the S_{wi} case and in the S_{or} case.

We have found that the use of specialized NMR sequences is able to detect the alternation of wettability due to aging in Berea sandstone. When only relying on the standard CPMG experiment we only found small indicators on the changed wettability, but when combining this with the other three mechanisms described above results were made. In particular we show the strength of the internal gradient encoding sequence as a tool to detect change in wettability.

Acknowledgments

Firstly, I would like to express my gratitude to my main supervisor, Professor Arne Skauge, for his guidance and feedback throughout this work, and for finding the practical solutions in the problems we encountered.

Secondly I want to thank Ketil Djurhus for his help in understanding the physics behind NMR and for always keeping his door open when I needed to discuss the progress and analysis of the experimental work.

Thanks to Behruz Shakur for valuable discussions and for lending me his aged cores. All the ageing procedures in this thesis have been performed by Behruz Shakur.

Special thanks go to Jonas Solbakken, Sverre Hetland, Per Arne Ormhaug and Bartek Vik for helping out on the experimental work and to all my friends and colleagues on CIPR that has made these two years a memorable experience.

Finally I want to thank my wife, Liv Elin, and my son, Sigurd, for putting up with me, and supporting me while I was working long shifts at the laboratories, and for giving me a valuable lesson on what's important in life when I was home.

Nomenclature

A	Cross-sectional area, Work
$\mathbf{B_0}$	Static magnetic field (flux density)
BVI	Capillary bound water
BVW	Mobile water
CBW	Clay bound water
CPMG	Carr, Purcell, Meiboom, Gill
χ	Magnetic susceptibility
D	Diffusion coefficient
δ	Absolute error
F	Force
FWL	Free Water Level
FW	Fractionally wet
FFL	Free fluid index
f_j	Volume fraction
f_{RF}	Radio or Larmor frequency
ϕ	Porosity
$\mathbf{g}$	Acceleration of gravity
γ	Gyromagnetic ratio
$\hbar$	Planck's constant divided by 2π
I	Angular momentum quantum number
I_{USBM}	USBM wettability index
I_{AH}	Amott-Harvey fluid displacement index
K	Absolute permeability
$\mathbf{L}$	Nuclear angular momentum
L	Length
m	Mass
$\mathbf{M}$	Macroscopic magnetization
MWL	Mixed wet large
m_z	spin magnetic quantum number
μ	Fluid viscosity
$\boldsymbol{\mu}$	Magnetic moment
N	Number of data points
NMR	Nuclear magnetic resonance
OWC	Oil-water contact
ω	Centrifuge speed
ω_L	Larmor angular frequency
PSD	Pore size distribution
PV	Dimensionless unit normalized with respect to pore volume
P_c	Capillary pressure
P_w	Pressure in wetting phase
P_{nw}	Pressure in non-wetting phase
Q	Rate of flow
R	Pore radius
ρ	Fluid density
S	Surface area
S_o	Oil saturation
S_{or}	Residual oil saturation
S_{iw}	Irreducible water saturation
S_w	Water saturation
$\overline{S_w}$	Average water saturation
s	Standard deviation
SW	Acquisition bandwidth
σ	Interfacial tension

T_1	Longitudinal relaxation time
T_2	Transverse relaxation time
t	Time
T_E	Echo spacing
q	Wetting angle
U	Potential energy
USBM	United States Bureau of Mines
V	Volume
W	Work

Table of contents

1. Introduction

In a world that has become increasingly oil dependent the need for efficient oil production is more important than ever. Having the full knowledge of the reservoir characteristics is essential in order to ensure maximum production and to further squeeze the last drop of oil out of every field. This is where the understanding of wettability comes into place. In a multicomponent system there will be a contrast in the magnitude of the forces acting between the pore wall and the fluids in the system[3]. These forces will in turn strongly affect the fluid distribution, the mobility of the pore fluids and the residual oil saturation, both in micro and macro scale. The concept of wettability is related to these forces so the knowledge of the wetting state of the reservoir rock is of great importance for a petroleum engineer. The term wettability is however not unambiguous. From the two extreme wetting states, water-wet and oil-wet there exist a range of intermediate wetting states which are difficult to separate. In addition when measuring the wettability in the traditionally manner your result could be influenced by other rock and fluid parameter like viscosity and permeability to name a few. Finally the preferred experimental techniques are related to time consuming procedures. All of these factors make wettability to one of the most challenging features of the petroleum industry[2].

There are two preferred methods for conventional wettability measurements. The Amott method[4] introduced by Earl Amott in 1958, and the USBM method[5] introduced by Donaldson et al in 1969. Both of these methods involve displacement experiments where the mobility of the fluids and the permeability of the rock will play a part.

The concept of NMR has been known since the 1950`s, and experiments to utilise the technology in the petroleum industry has been performed since the 1960`s. The main focus for NMR research in the petroleum industry have been on porosity and mobility measurements, because of excellent distinguishing between matrix and pore fluids, and between mobile and immobile fluids respectively[6].

In this thesis we will look into the use of NMR technology to find wettability characteristics. A fluid close to the pore surface will relaxate at a higher rate than a fluid in the interior of the pore because of the effect from surface relaxation. Because wettability play a key role in the fluid distribution in a rock on both micro and macro scale the use of NMR as a tool to probe the wetting state of a rock has proven usefull[7-10].

2. Basic rock properties

2.1. Porosity, φ

P*orosity* is one of the fundamental properties of an hydrocarbon bearing formation and it`s defined as "the void part of the rock`s total volume, unoccupied by the rock grains and mineral cement" [1]. In this way the magnitude of the porosity tells us the fluid storage capacity of the rock and we can write it as

$$\varphi_{tot} \overset{\text{def}}{=} \frac{V_b - V_s}{V_b} = \frac{V_{p,tot}}{V_b} \tag{2-1}$$

where V_s is the solid volume, V_b is the bulk volume of the rock and $V_{p,tot}$ is the total pore space. Because not all pores are connected and will contribute to the fluid transportation in the rock, we introduce the effective porosity. It is defined as the ratio of volume of interconnected pore space, $V_{p,eff}$, and the bulk volume of the rock.[1]

$$\varphi_{eff} \overset{\text{def}}{=} \frac{V_{p,eff}}{V_b} \tag{2-2}$$

For simplicity we will use φ for effective porosity and V_p for effective pore volume in this thesis. It is also common practice to distinguish between two main categories of porosity, namely the primary and the secondary porosity. The former one is caused by the sedimentation process and the latter are those pores developed in a rock some time after the deposition. These two categories are again divided in to subgroups, after their origin and type [11].

In figure 2-1 we can see an idealized schematic of various pores. The fluid in the closed pore is trapped, thus its volume is not a part of the effective porosity.

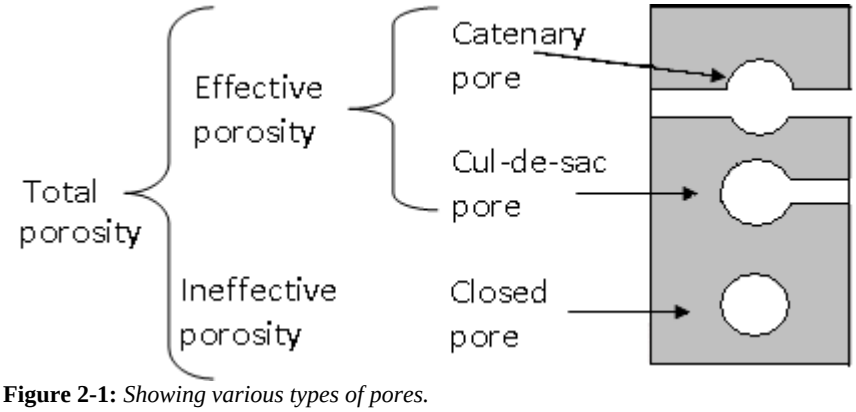

Figure 2-1: *Showing various types of pores.*

2.2 Permeability, K

Permeability is another important property of a reservoir rock. If the pores in chapter 2.1 are connected, a fluid inside the pore will be able to pass through the porous material. *Permeability* will then be the potential of the medium to allow transportation of fluid through its interconnected pores. A

good analogy to this phenomenon is the conductivity of an electrical wire which allows transportation of electrical current.

The relationship between fluid, medium and fluid transportation was first discovered by a 19th-century engineer named Henry Darcy who experimented with water and different types of sand filters [1]. Rewritten to a more modern form Darcy law states that:

$$\boldsymbol{q} = \frac{\boldsymbol{kA}}{\mu}\,(\nabla p - \rho g) \qquad \textbf{2-3}$$

where q is the rate, A is the cross-sectional area, μ is the viscosity of the fluid, ∇p is the pressure gradient, ρ is the fluid density and **g** is the gravity and **k** the permeability tensor.

The Darcy law will in this form is only valid for a system with one fluid present. This is because the different fluids will obstruct each other`s flow pattern, hence reducing the *apparent permeability* of the system. For such a system with multiple immiscible fluids there will be an *effective permeability, k_{eff},* for each fluid, that is different (and lower) than the *absolute permeability K*. The effective permeability depends highly on fluid saturation, but is also controlled by the pore- and pore throat geometry, the wettability and the hysteresis of the rock [11-12].

2.3 Saturation

Because most reservoirs are occupied by more than one reservoir fluid we introduce the unit s*aturation*. The saturation of a fluid is the volumetric ratio of the respective fluid to the total fluid volume in the reservoir. As a rule of thumb, the reservoir fluids fill all of the pores in the reservoir, hence the total fluid volume equals the pore volume V_p. This gives the three saturation equations for water, oil and gas respectively.

$$S_w = \frac{V_w}{V_p}, \qquad (2\text{-}4) \qquad\qquad S_o = \frac{V_o}{V_p}, \qquad (2\text{-}5) \qquad\qquad S_g = \frac{V_g}{V_p}, \qquad (2\text{-}6)$$

where V_w, V_o, V_g is the volume of water, oil and gas respectively. Because we assumed that all of the pore volume is filled by reservoir fluid, the following is always true:

$$S_w + S_o + S_g = 1 \qquad (2\text{-}7)$$

As a consequence of wettability and capillary pressure that we will discuss later in this chapter there exists a lower limit for the saturation of any fluid in a reservoir. The oil that will remain in the rock after production is called the *residual oil, S_{or}*[1]. At this value, the remaining oil is immobile, and will not move by any conventional method. The *irreducible water saturation, S_{wi},* is the lowest level of water. The remaining water is retained in the smallest pores by *capillary trapping.*

2.4 Wettability

Wettability can be defined as "the tendency of one fluid to spread on or adhere to a solid surface in the presence of other immiscible fluids"[13] and arise because of the difference in molecular interaction between the solid and the fuids in the system. For an ideal system of oil and water on a flat surface the energies are explained by the Young-Dupre equation:

$$\sigma_{os} - \sigma_{ws} = \sigma_{ow} cos\theta \qquad 2\text{-}8$$

Where the subscripts o_s, w_s and o_w denotes the oil solid, water-solid and oil-water interface respectively and θ is the *contact angle* at the oil-water-solid interface measured through the water (as shown in Figure 2-1).

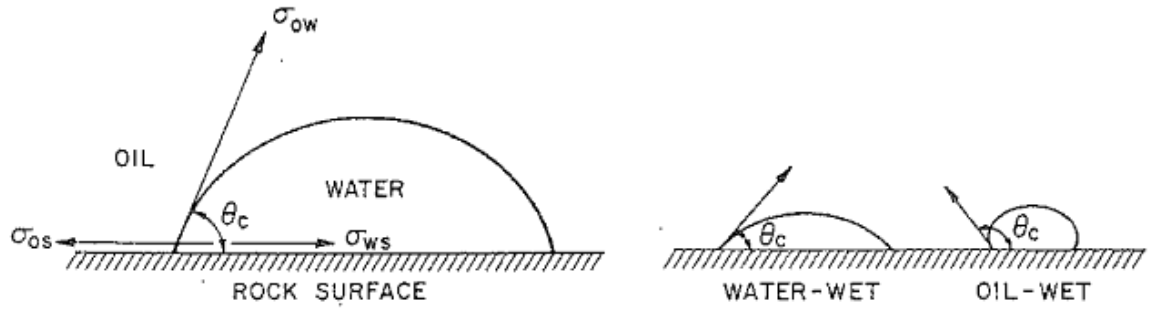

Figure 2-2: *Schematics of fluid configuration and the interfacial tensions in an water-oil-solid system. Modified reprint from Graig[13]*

The *contact angle* has become a significant measure of wettability and is commonly referred to as the *wetting angle*. For a solid with a tendency for water, the contact angle is less than 90° and the surface is referred to as water-wet. If, on the other hand the surface has a tendency for oil, the contact angle is greater than 90° and we label the surface as oil-wet. A contact angle of exactly 90° would indicate that the surface has equal tendency for water and oil. In addition the term *strongly oil wet* and *strongly water wet* have been used to for wetting angle near the extreme points according to table 2-1.

Table 2-1: *Wettability classes for water-oil system. Reprint from Zolotukhin[1]*

Wetting angle (degree)	Wettability preference
0-30	Strongly water-wet
30-90	Preferentially water-wet
90	Neutral wettability
90-150	Preferentially oil-wet
150-180	Strongly oil-wet

The wettability is of great importance since it is a major factor in controlling the location and flow of the reservoir fluids. Given that sufficient amounts of the fluids are present and that the system is in

equilibrium, the wetting fluid will occupy the smallest pores and the majority of the rock surface in the larger pores. The nonwetting fluid will on the other hand only appear in the center of the large pores forming globules. This distribution of the fluids will have great impact on the mobility of the phases and consequently the residual oil saturation after water flooding. Skauge and Ottesen [14], reviewed special core analysis data from 30 north sea fields and found a relationship between the wetting state and remaining oil saturation after water flooding. The investigation showed the smallest oil saturation for intermediate wet oil cores (ref. figure 2-3).

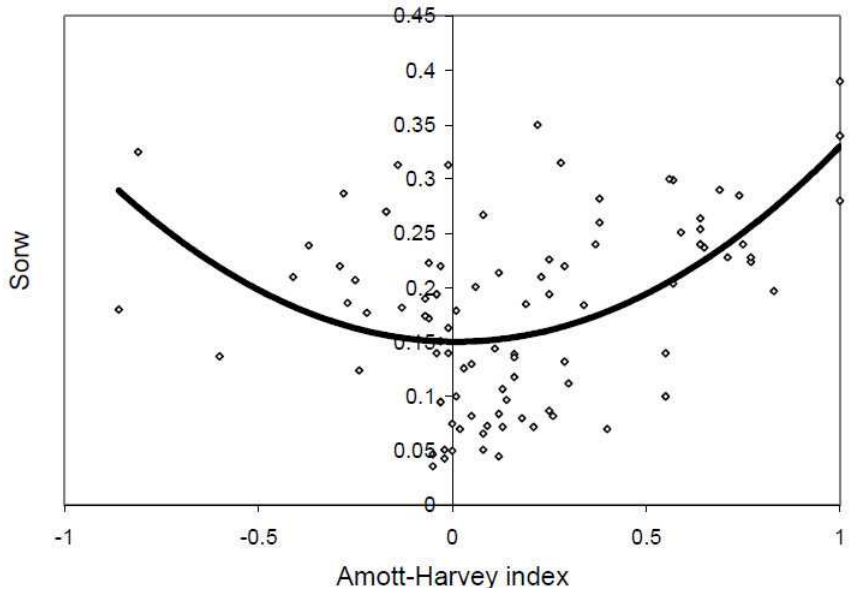

Figure 2-3: *The relationship between residual oil saturation after water flooding and Amott-Harvey index.* Reprint from Skauge and Ottesen[14].

Fractional wettability

Until now we have given that the wettability is uniform in the rock. This would in most cases not be true. Because the wettability could be altered through absorption of polar components in the crude oil and the rock consist of a range of minerals with various surface chemistry it would develop a heterogeneous form of wettability[15]. In fractional wettability (FW), the absorption of crude oil components are only affecting one part of the rock, leading to certain areas is strongly oil-wet, while leaving the rest strongly water-wet.

Mixed Wettability

The term mixed wettability (MW) refers to a special type of fractional wettability. According to Salathiel[16] this situation develops when oil migrates in to the originally water-wet reservoir, and fills the larger pores. Over time the absorption of crude oil components will only happen in the oil filled pores causing them to develop an oil-wet surface, leaving the smaller pores water-wet. Salathiel has also shown that this condition gives a very favourable situation for waterflood because the oil phase will remain mobile down to very low saturations, giving a microscopic recovery factor of up to

90 percent. The situation with large oil-wet pores is commonly referred to as *mixed wet large* (MWL). The opposite condition where the oil-wet surfaces are located in the smaller pores are called *mixed wet small* (MWS). The main difference between MW and FW are that there are no correlation between pore size and wettability in rocks with FW nature. Both small pores and large pores could have oil-wet surfaces.

Sandstone and carbonate wettability

The mineral surface of the rock is of great importance in determining the wettability. It is generally believed that carbonate reservoirs are more prone to be oil-wet than sandstone reservoir. Chilingar and Yen [17] found after extensive research that most reservoirs range from neutral-wet to strongly oil-wet. The experiment includes 161 core plugs with various carbonate minerals from all over the world and result are shown in table 2-2.

	Contact angle	Percent of reservoirs
Water-wet	0-80	8
Neutral-wet	80-100	12
Oil-wet	100-160	65
Strongly oil wet	160-180	15

Table 2-2: *Distribution of carbonate reservoir wettabilities. Note that the range of contact angles considererd is different than in Table 2-1. Modified reprint from Chilingar and Yen[15]*

Sandstone reservoir got a completely different mineral surface than carbonate reservoirs, and this gives another wettability regime. Treiber et al.[18] conducted in 1972 a wettability evaluation of fifty fields and found a broad spectrum of wettability. Most of the fields were located in North America, but some South America and Middle East field were also considered. Treiber found that almost half of the fields were weakly oil-wet and the rest in the range neutral to strongly water-wet, but he states that it should not be considered representative for all fields. Today there is a general understanding that most sandstone reservoirs are in the range weakly water-wet to neutral-wet[14].

Natural alteration of wettability in reservoir rock

Most sedimentary rocks are naturally water wet, and in fact all reservoirs was considered strongly water wet in the early years of reservoir engineering. This was believed to be true because most minerals constituting the rock are water-wet, and the fact that most sediment is deposited in an aqueous environment. The oil which migrated in to the rock at a later time would then be prevented from touching the pore surface by the presence of connate water and water films. However, during the

1930 researchers found that some producing reservoirs actually was strongly oil-wet. The original strong water-wet mineral surface in the reservoir could be altered by deposition of organic matter from the crude oil, or by absorption of polar components containing oxygen, nitrogen or sulphur. These polar components, sometimes called the *surface active compounds* consist of both a polar end and a hydrocarbon end which makes them ideal for altering the wetting nature of the rock. The polar end absorbs on the mineral surface exposing the hydrocarbon end making the rock more prone to oil. The absorption of these components have been shown experimentally by i.e. Lyutin and Burdy take place even in the presence of thin water film because of the soluble nature of hydrocarbon compound[19].

Alteration of sandstone and carbonate surfaces

The minerals constituting the rock surface will to some extent affect the wettability alteration. Sandstone constituting mainly of silica got a negatively charged, weakly acidic surface, while carbonates on the other hand have a positively charged, weakly alkaline surface. This governs the kind of chemicals which are attracted to the surface and could alter the wettability. Because of the attraction in differences, the components will prefer the opposite polarity. Wettability of carbonates will be most affected by organic acids, while sandstone will be most affected by organic bases[15]. This is of great importance because the same reservoir fluids will alter the reservoir in different ways depending on the mineral surface of the rock. However, this is only valid in reservoirs where the pH is near neutral. Where the pH of the brine is different from neutral, the surface charge of the mineral could be altered, hence changing the preference for organic compounds.

Oil-wet minerals

Though almost every mineral in sedimentary rocks are strongly water wet, there have been evidence of a few minerals are weakly water wet, and even oil wet. This minerals include graphite, coal talc and sulphides[15]. Most of this minerals are however not a present in such quantities that they got a significant impact on the wettability. Nevertheless, some researchers have in a limited numbers of reservoirs found core samples with such a high percentage of coal that it could only be cleaned to neutral wet.

Artificial alteration of wettability

Several methods exist for artificial alteration of wettability in cores, but all of them are based on the principle of reproducing the conditions that are taking place within the reservoir. The simplest method consist only of submerging the cores in crude oil at elevated temperature, but other procedures like high temperature crude oil flooding[20-21] and submerging the core in specific chemicals have also been performed[15]. The main objective of all these procedures is to have the surface active compounds react with the pore surface, and alter the wettability to a more oil-wet condition. Carefully considerations of both the mineral chemistry and the composition of all of the pore fluids must be taken to secure an efficient alteration of the wettability.

2.6 Capillary pressure, P_c

In a porous media containing more than one phase the *capillary pressure* is an important parameter. "Capillary pressure P_c can be defined as the molecule pressure difference across the interface of two fluids" [1]. This pressure difference could be illustrated in a thin capillary tube with radius *R* in a container filled with oil and water.

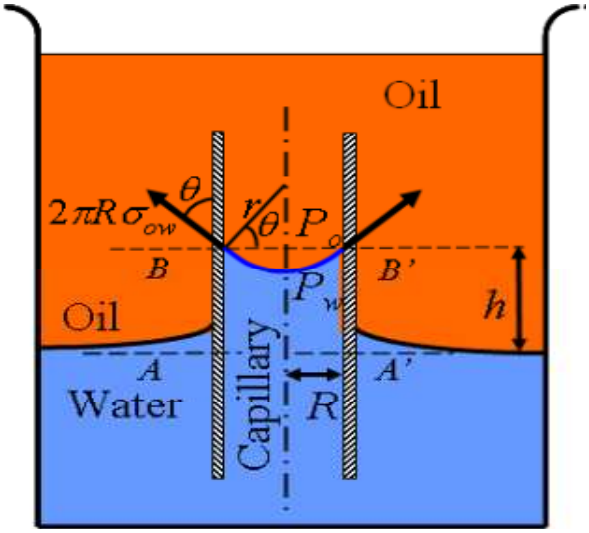

Figure 2-3 – *Schematics of capillary pressure in a thin tube filled with oil and water. Reprint from Lien [22]*

If we assume that the surface of the tube is water-wet the surface-fluid forces, i.e σ_{ow}, will cause the water level to rise inside the tube as shown in figure 2-3. For the fluids and their interfaces to be in equilibrium this calls for a stronger pressure in the non-wetting phase. The vertical component of the forces acting on the total area of the circular meniscus inside the capillary tube could in this example be written as:

$$F_{ow}^{v} = 2\pi R\sigma_{ow}\cos\theta \qquad 2\text{-}9$$

Where σ_{ow} is the interfacial tension acting between the two fluids and θ is the angle defined on the figure. This upward force is balanced by the pressure difference in the two fluids. In figure 2-4 we examine a small area *d*A of the interface between oil and water. The vertical component of dF_c can be written as

$$dF_c^{v} = (P_o - P_w)dA\cos\alpha \qquad 2\text{-}10$$

and P_o and P_w is the pressure in oil and water respectively.

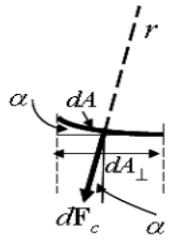

Figure 2-4: *A small surface element dA on the interface between water and oil. Reprint from Lien*[22]

The size of the projection of *dA* into the horizontal plane is given by $dA_{\perp} = dA\ Cos\ \alpha$. It follows that the total vertical component of the forces acting on the interface can be found by integrating equation 2.10 over the meniscus surface A so that

$$dF_c^v = (P_o - P_w) \int_A \cos\alpha\, dA = (P_o - P_w) \int_A dA_{\perp} = (P_o - P_w)\, \pi R^2 \qquad 2\text{-}11$$

For a fluid in static equilibrium, the meniscus separating the fluids has stabilized. This condition implies that $F_c = F_{ow}$ and equation 2-9 and 2-10 can be written:

$$(P_o - P_w)\pi R^2 = 2\pi R \sigma_{ow} \cos\theta \qquad 2\text{-}12$$

Since capillary pressure is defined as pressure difference between the non-wetting and the wetting fluid this could in our example be rewritten to the following equation:

$$P_c = (P_o - P_w) = \frac{2\sigma_{ow}\cos\theta}{R} \qquad 2\text{-}13$$

It is quite clear that the radius of the capillary tube is a controlling factor in capillary pressure. This could be further visualized if multiple capillary tubes with various sizes are placed together in a container filled with oil and water.

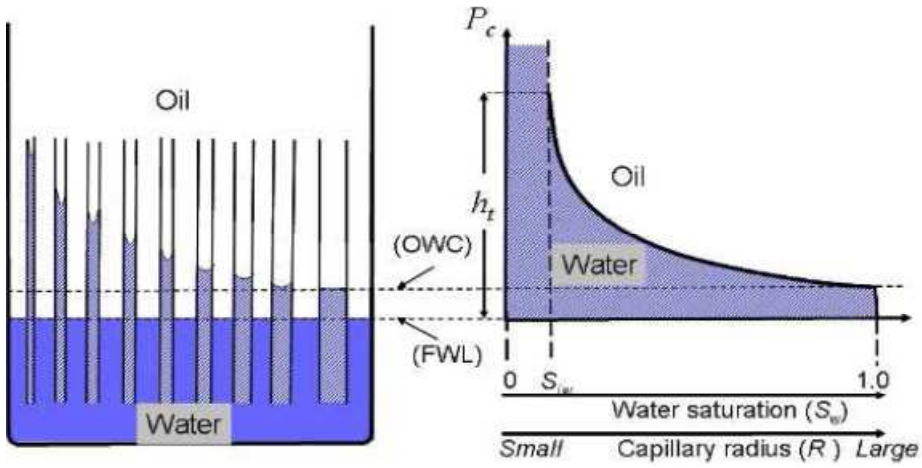

Figure 2-5: *Schematics of how the radius of the capillary tubes governs the capillary pressure.* Reprint from Lien[22]

The capillary tubes are water-wet causing the water to cling to the tube surface and to rise inside the tubes. On the right side of the figure this has been converted into a continuous curve called capillary pressure curve. Three important properties can be drawn from this figure.

- The height in the tube can be converted to capillary pressure with the following equation.

$$P_c = \Delta\rho g h \qquad 2\text{-}14$$

  Where $\Delta\rho = \rho_w - \rho_o$ is the density difference between oil and water respectively.

- The *Free Water Level* (FWL) is the boundary line between oil and water if no capillary pressure was present (e.g. inside the wellbore where the size of the "pore" is too large for any capillary pressure). The Oil Water Contact (OWC) is the level where the water saturation is less than 100%.
- With increasing height the water is only able to occupy the smaller tubes. Hence the water saturation is decreasing as a function of height.

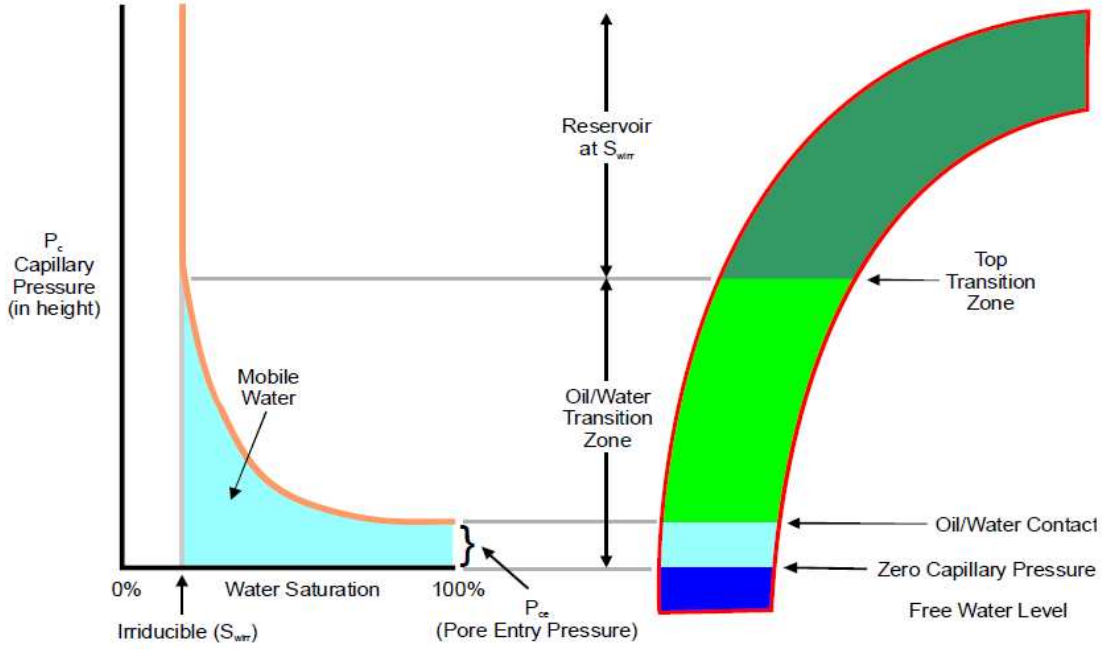

Figure 2-6: *Schematics of the capillary pressure and how it effects the distribution of oil and water in a uniform reservoir. Reprint from Holmes[23].*

If we transfer this knowledge to the reservoir we discover an oil-water transition zone just above the aquifer where water has displaced oil in the smaller pores because of the higher capillary pressure. In this zone both oil and water are mobile. Above the transition zone only oil is mobile and below the transition zone only water is mobile.

Imbibition and drainage flooding

Because the capillary pressure is affecting the flow dynamics of the fluids, there are two categories of fluid displacement process based on the function of the capillary pressure. In *drainage* the non-wetting fluid, i.e. oil, displaces the wetting, i.e. water. As shown in figure 2-5 a force is needed to reduce the saturation of the water, allowing the oil to occupy the largest pores. For oil to displace water from a pore the oil pressure must exceed the combined pressure of capillary pressure and water pressure ($P_o > P_w + P_c$). As the pressure increases the oil displaces water from smaller and smaller pores until a threshold value is obtained. If we plot the capillary pressure as a function of the fluid production we get the capillary pressure curve. In special core analysis it is common practice to do three flooding cycles (as in figure 2-7).

1. Oil flood in 100% water saturated core.
2. Water flood in core driven to S_{wi}
3. Oil flood in core at start saturation S_{or}.

Intuitively the pressure curves between point two and three should be similar in shape and size, but because of a *hysteresis* this is not the case. As shown on figure 2-7 the "spontaneous water imbibition" follows a much steeper decline than the "secondary drainage curve". The major factors controlling hysteresis is snap off of oil film and contact angle hysteresis.

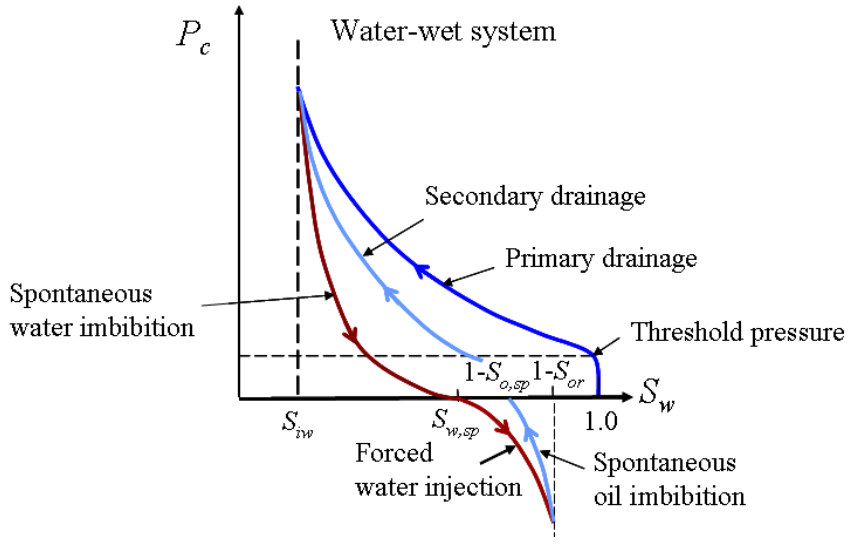

Figure 2-7: *Capillary pressure curves for drainage and imbibition in a porous media. Reprint from Lien [22]*

2.5 Review of wettability measurement procedures

Since reservoir engineers found that the wettability of reservoir rock was different from strongly water-wet, they have been in search for a convenient and accurate method for the determination of wettability. Several methods exist today, and in this chapter we will look into three methods frequently used, each with their advantages and limitations.

2.5.1 Wetting angle

The wetting angle, or contact angle measures the wettability of a specific surface. There have been developed a number of different methods to measure the wetting angle, but the most frequently used is the sessile drop method. First a clean, flat slab of reservoir minerals is covered with brine. Then a droplet of reservoir oil is formed and brought into contact with the mineral surface. The contact angle is measured after a period of ageing according to figure 2-8.

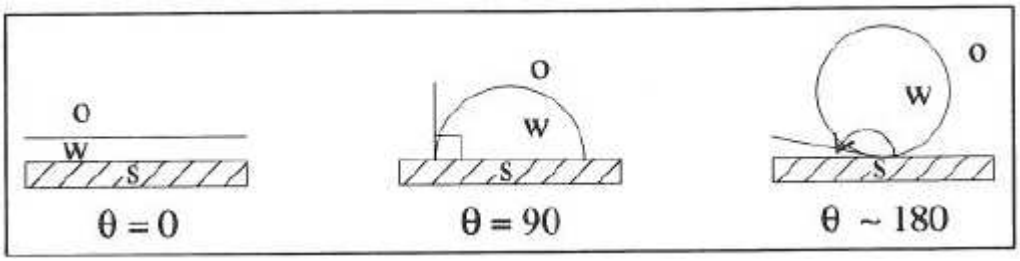

Figure 2-8: *Schematics of contact angle in different solid for strongly water-wet, neutral-wet and strongly oil-wet respectively from left to right. Reprint from Zolotukhin[1]*

The strength of the wetting angle procedure is that the result is not affected by surfactant or other contaminations in the rock. The resulting contact angle is clearly only a function of fluid-surface interactions. Despite of this the question of how representative these results are in terms of predicting the wettability of the core arises. It is hard to assume that a value from the strictly controlled environment of a clean, flat slab of mineral could yield a valid result for the heterogeneity of a rock.

2.5.2 Amott Wettability Test

While the contact angle method measures the wettability of a specific surface, the Amott wettability test combines imbibition and forced displacement in a flooding experiment to find the mean wettability of the rock[24]. The foundation of the test is that the wetting fluid will spontaneously imbibe into the core, displacing the non-wetting fluid. The original test consists of a four step process.

1. In the first step a core at irreducible water saturation is submerged in water allowing the water to seep in while the volume of oil diplaced is recorded.
2. In step two, the water is forced into the core by the use of a pump or a centrifuge. This process is called *forced imbibition* and continues until *residual oil saturation* is reached. We define the "displacement-by-water ratio".

$$\delta_w = \frac{V_{o,sp}}{V_{ot}} = \frac{S_w - S_{wi}}{1 - S_{or} - S_{wi}} \quad \text{2-15}$$

Where $V_{o,sp}$ is the oil displaced by water in spontaneous imbibition alone, and V_{ot} is the total volume of oil displace in step one and two.

3. Step three reverses the process in step 1, and oil is allowed to imbibe in to the core at water saturated core. Amott proposed that the imbibition should continue for 20 hours in both step one and three, but this could pose a problem. If the imbibition is allowed too short period of time the measured imbibition volume will be too low, causing an under *or* overestimation of the wettability. For example in core samples of low permeability the 20 hour time limit of Amott could cause a significant impact on the measured volume. Anderson[2] suggested that the imbibition should continue until no more water will enter the core sample or a time limit of 1-2 weeks is reached.
4. Finally the core is exposed to forced imbibition of oil. We define the "displacement-by-oil ratio".

$$\delta_o = \frac{V_{w,sp}}{V_{wt}} = \frac{(1 - S_{or}) - (1 - S_{o,sp})}{1 - S_{or} - S_{wi}} - \frac{S_{o,sp} - S_{or}}{1 - S_{or} - S_{wi}} \quad \text{2-16}$$

Where $V_{w,sp}$ is the water displaced by oil in spontaneous imbibition alone, and V_{wt} is the total volume of water displaced in step three and four. A modification of the Amott test frequently used by researchers over the world is the "Amott-Harvey relative displacement index"

$$I_{AH} = \delta_w - \delta_o = \frac{V_{o,sp}}{V_{ot}} - \frac{V_{w,sp}}{V_{wt}} = \frac{(S_{w,sp} - \boldsymbol{S_{wi}}) - (S_{o,sp} - \boldsymbol{S_{or}})}{1 - S_{or} - S_{wi}} \quad \text{2-17}$$

The different wettability classifications proposed for this method are:

- $0{,}3 < I_{AH} < 1$: Water-wet
- $-0{,}3 < I_{AH} < 0{,}3$: Neutral-wet
- $-0{,}3 < I_{AH} < -1$: Oil-wet

The main limitation in the Amott test is its insensitivity near neutral wettability, where neither fluid will spontaneously imbibe into the core.

2.5.3 USBM

The USBM test developed by Donaldson et al [5] compares the work necessary for one fluid to displace the other. Because of the reduction in surface tension on the fluid-surface interface when the wetting fluid replaces the nonwetting fluid, the amount of work required is less than the work required for the opposite displacement.

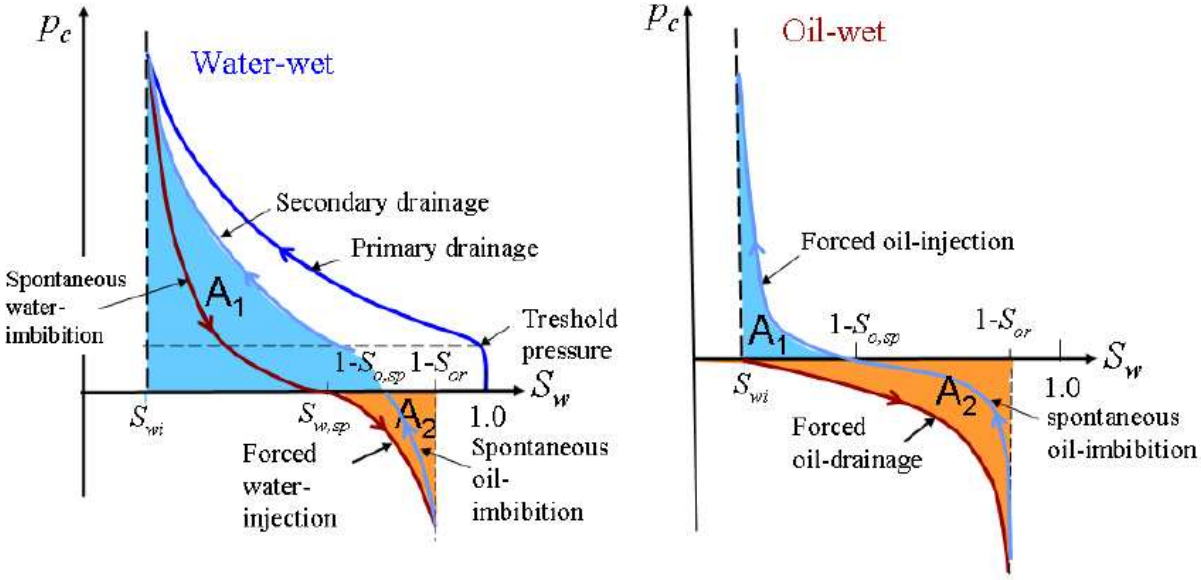

Figure 2-9: *Capillary pressure curves for a water-wet and an oil-wet system. Reprint from Lien [22]*

As shown in figure 2-9 the capillary pressure curves are greatly affected by the wettability of the porous media. For a secondary drainage process the work executed is proportional to the area A_1 below the drainage curve. Because the work is calculated with respect to the change in water saturation (which is negative for a secondary drainage process) there is need for a minus sign in the equation. S_{wi} is the irreducible water saturation, and $S_{o,sp}$ is the saturation of oil after spontaneous oil-imbibition.

$$A_1 = -\int_{1-S_{o,sp}}^{S_{iw}} P_c(S_w)\, d\, S_w \qquad 2\text{-}18$$

The work needed to displace the oil is proportional to the area A_2 defined by the *forced water injection curve*. The saturation subscripted $S_{w,sp}$ denotes the water saturation after the spontaneous water-imbibition.

$$A_2 = \int_{S_{w,sp}}^{1-S_{or}} P_c(S_w)\, d\, S_w \qquad 2\text{-}19$$

In a water-wet medium, the work needed for oil to displace water is far greater than for the opposite displacement, hence the area A_1 is larger than area A_2. In an oil-wet medium on the other hand, the work needed for water to displace oil outweighs the opposite displacement, hence the area A_2 is larger than area A_1. Donaldson found this relationship and introduced the USBM-index classifying the average wettability in the rock.

$$I_{USBM} = log\left(\frac{A_1}{A_2}\right) \qquad 2\text{-}20$$

The different wettability classifications for this method are similar to the ones proposed for the Amott method:

- $0,3 < I_{AH} < \infty$: Water-wet
- $-0,3 < I_{AH} < 0,3$: Neutral-wet
- $-0,3 < I_{AH} < -\infty$: Oil-wet

We observe that the USBM index ranges from ∞ to $-\infty$ while the Amott index ranges from 1 to -1. Despite this fact, comparing the two indexes proves to be valuable. The USBM test got a major advantage over the Amott test because of its sensitivity near neutral wettability. On the other hand, the USBM test is insensitive to fractional or mixed wettability, and can only be measured on plug sized samples because the samples must be spun in a centrifuge.

2.5.4 Combined Amott/USBM method

Developed by Sharma and Wunderlich[25] a new procedure to measure the wettability has been introduced that allows both the Amott and the USBM wettability indices. A 5 step sequence of capillary pressure and spontaneous imbibition tests is performed on the sample in the order suggested by figure 2-10 which allows both indices to be found. The test start with a sample 100% water saturated and the following steps are performed:

1. Oil displaces water.
2. Spontaneous imbibitions
3. Forced water drive
4. Spontaneous imbibition of oil
5. Forced oil drive

According to Sharma et al, this process has 2 advantages over the standard wettability test. First it allows both the USBM and the Amott index to be measured, second, the resolution of the USBM index is improved because the technique takes into account the saturation change at zero capillary pressure.

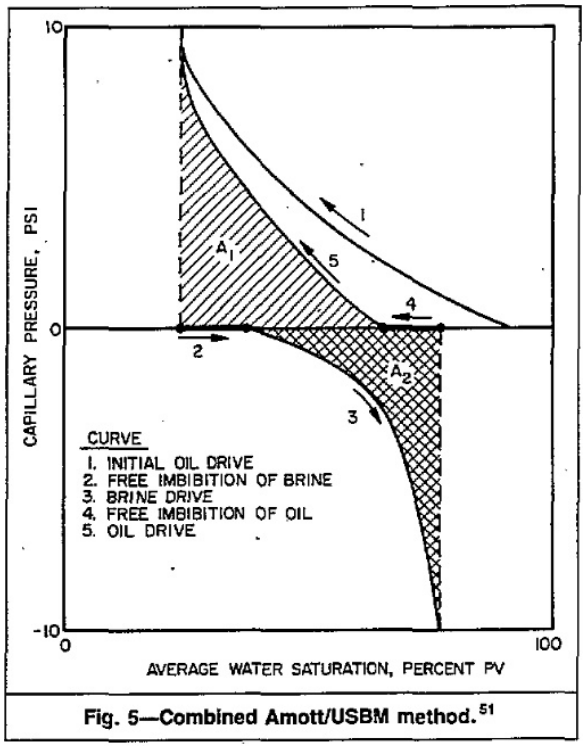

Figure 2-10: *Illustration of the capillary pressure curve and the imbibition test found by the combined Amott/USBM wettability test.* Reprint from Anderson[2]

A second strength of the combined Amott/USBM method is the ability to distinguish between the different intermediate wetting states. Dixit et al[26] found an analytical relationship between the

USBM and Amott tests and found that for a intermediate wetting state where $-0,5 < I_{AH} < 0,5$ the following holds:

MWS : $I_{AH} > I_{USBM}$
FW: $I_{AH} \approx I_{USBM}$
MWL: $I_{AH} < I_{USBM}$

If the larger pores are more oil wet (MWL) snap of effect in the water wet pores will cause the USBM index to indicate a more water wet state than the Amott-Harvey. For a situation where the smallest pores are more oil wet (MWS) the snap-off effect will be suppress and consequently $I_{USBM} < I_{AH}$. This relationship have later been experimentally found by Skauge and Ottesen[14] who analysed USBM and Amott-Harvey data from 13 north sea fields.

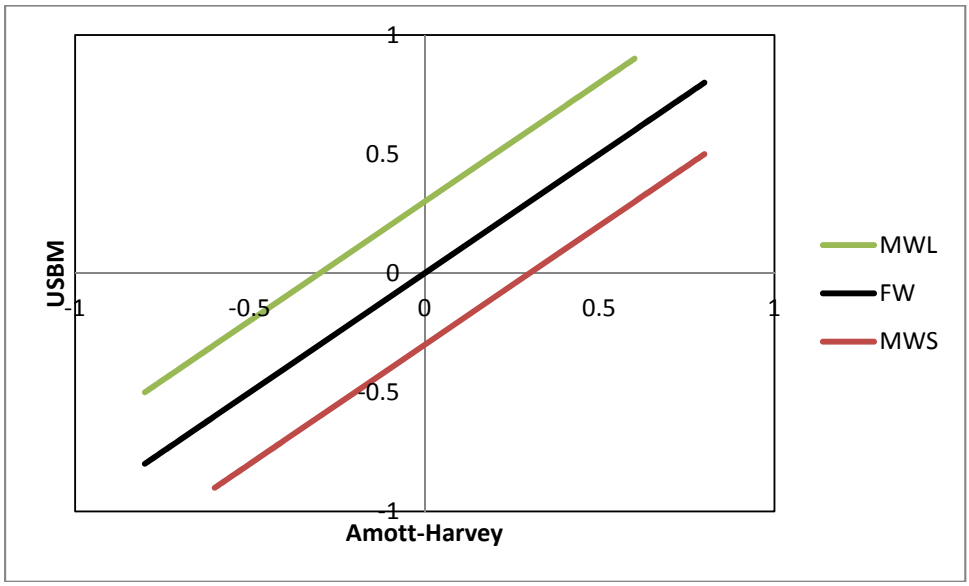

Figure 2-11: *Graph showing the analytical relationship between Amott Harvey and USBM. Skauge and Ottesen[14] found a similar relationship for experimental data, however not as distinct.* Modified reprint from Dixit et al[26].

3. NMR – technology

3.1. Introduction to basic concepts

The concept of nuclear magnetic resonance was first discovered in 1946 by the American physicist Purcell and Bloch at Harvard and Stanford University respectively[27-28]. They observed the absorption of radiofrequency energy in a sample of paraffin when a magnetic field brought the hydrogen nucleis into resonance with the applied radiofrequency field. Now the technology is applied with ground breaking results in fields like chemistry, medicine and petroleum industry.

Nuclear magnetic resonance is related to the properties of nuclei with odd number of protons or neutrons placed in a magnetic field. These nuclei possess a property referred to as *spin angular momentum*. Despite the name, spin in quantum physics is not the same as the angular movement of a classical object, i.e. the spinning of a billiard ball. Elementary particles simply *have* spin and it should be regarded as one of the fundamental characteristics of an elementary particle along with charge, mass and magnetism [29]. The angular moment L is in accordance with quantum physics quantified into

$$\mathrm{L}=\sqrt{I(I+1)}\hbar \qquad 3\text{-}1$$

where ħ is the reduced Planck constant and I is the angular momentum quantum number. The quantum number is related to the elementary particles and takes integer values for *boson* particles like photons, and half integer values for *lepton* like electron. For the component in z-direction

$$L_z = \hbar m_z \qquad 3\text{-}2$$

where $m_z = \pm I$ which is referred to as the *azimuthal quantum number*, which will quantify the z-component of the angular momentum. For a proton $m_z = \pm ½$ which gives only two possible orientations of the angular momentum in z direction. For the rest of this these we will only referee to the proton 1H NMR. Associated with the nuclear spin angular momentum there is a magnetic momentum parallel to the angular moment

$$\boldsymbol{\mu} = \gamma \mathbf{L} \qquad 3\text{-}3$$

where γ is called the gyromagnetic ratio. γ is uniqe for every type of nuclei and reflects the inner structure of the nuclei. Since we stated in equation 3-2 that the angular moment is quantified along the z-axis it consequently follows that the magnetic moment also must be quantified. Hence, along the z-axis we got

$$\mu_z = \gamma \hbar m_z \qquad 3\text{-}4$$

In a petroleum reservoir, there will be an abundance of hydrogen in the pore fluids compared to the matrix. Because of this contrast in hydrogen content NMR gives us a good way of distinguish pore fluids from the matrix. For a hydrogen nuclei (a single proton), $\gamma = 267{,}522 \cdot 10^6$ rad/s·T[29].

The orientation of the magnetic moment in the hydrogen nuclei is randomly orientated, but when placed in a magnetic field $\mathbf{B}_0$, it will experience a torque from the field forcing the magnetic moment to align with the external field.

$$\boldsymbol{\tau} = \boldsymbol{\mu} \times \mathbf{B_0} \tag{3-5}$$

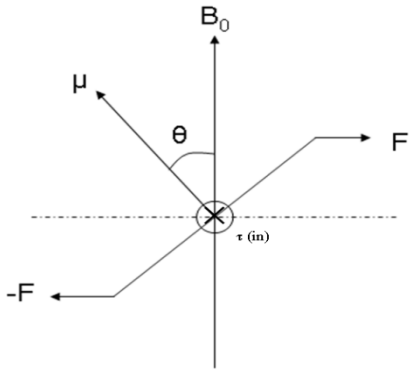

Figure 3-1: *Schematics of the forces acting on the magnetic moment from the external magnetic field* $\boldsymbol{B_0}$**.** Reprint from Lien[30].

The potential energy in the system is a function of the magnetic momentum and the external magnetic field. It can be shown that the potential energy in the system is given by

$$U = -\boldsymbol{\mu} \cdot \boldsymbol{B_0} \tag{3-6}$$

which combined with equation 3-4 gives us the potential energy along the z-axis.

$$U_z = -\gamma \hbar m_z B_0 \tag{3-7}$$

The magnetic quantum number, m_z can have two values, one parallel to the field $\mathbf{B_0}$ (positive), and one anti-parallel to $\mathbf{B_0}$ (negative). This refers to the two possible energy states that the nuclei could obtain, the α- and the β-state. To understand this we could think of the magnetic momentum as a tiny magnet as in figure 3-2-a. When placed in a magnetic field the magnet tries to align whit the field in order to obtain a lower potential energy, but because the azimuthal quantum number, m_z = ½ for a proton it got two possible ways of orientate in the z direction. There is a low energy state where the poles are aligned north-south (fig 3-2-b), and a higher energy level when the poles are aligned north-north (fig 3-2-c).

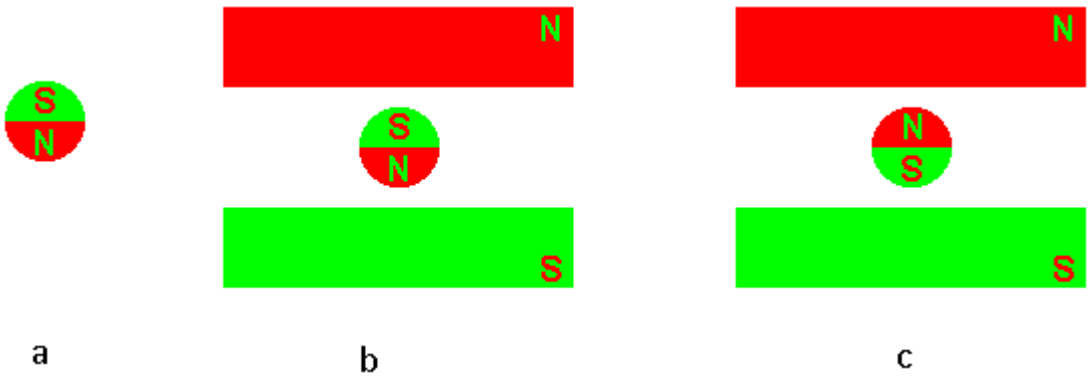

Figure 3-2: A proton behaves like a magnet and would orientate to an external magnetic field as shown in b) and c). Modified reprint from Hornak [31]

Now we have two energy states where the contrast in potential energy **ΔU** increases proportional to the external magnetic field:

$$\Delta U = \gamma \hbar B_0 \qquad 3\text{-}8$$

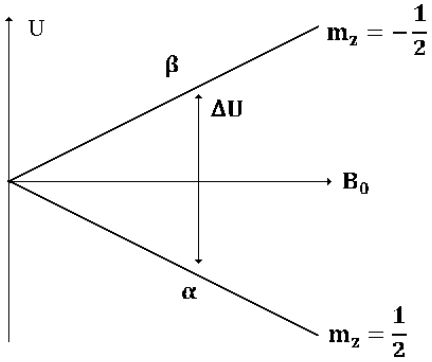

Figure 3-3: *Energy states for a proton in a magnetic field B_0. ΔU increases for increasing field strength.*

The proton will not align perfectly with the external $\mathbf{B_0}$ field. Because of the angular momentum it will be precessing about the external magnetic field, in much the same way as a child`s spinning top would precess in the gravitational field (figure 3-4). If the axis of the spindle top is slightly skew relative to the gravitational field it will produce a torque that will pull the tip towards the ground. However when the spinning top is spinning fast, it will not fall. Instead it will rotate around the gravitational field in a precessional motion.

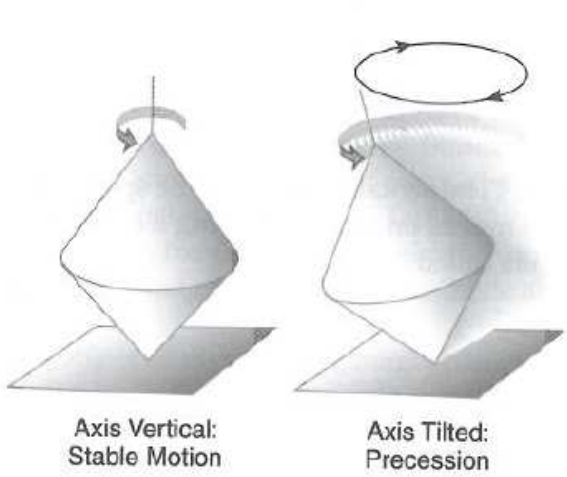

Figure 3-4:*The precessing motion of a spinning top, for a tilted and a vertical axis.* Reprint from Levitt[29]

A nucleus in a static magnetic field experiences the same effect from the magnetic field. A full quantum mechanical description of the system is beyond the scope of this thesis, but semi-classically we could say that the magnetic momentum will precess about the axis of the external magnetic field, and that the precessing would follow the Larmor frequency, ω_L. The frequency of the precession is proportional to the strength of the magnetic field $\mathbf{B_0}$ giving

$$\omega_L = -\gamma B_0 \tag{3-9}$$

In thermal equilibrium the distribution between the two possible energy states follows Boltzmann statistics and the ratio is given by

$$\frac{n_\alpha}{n_\beta} = exp[-\Delta E/kT] \cong 1 - \frac{\gamma \hbar B_0}{kT} \tag{3-10}$$

where k is Boltzmann`s constant, T the temperature and n_α and n_β the number of nuclei in α- and β-state respectively. In typical temperature and magnetic field strengths the population of nuclei in α-state is slightly higher than the β-state. Because the magnetization on macro scale is simply the vector sum of the individual magnetization this causes a net nuclear magnetization, $\mathbf{M_0}$ of the sample.

Transition from the α-state to the β-state in figure 3-3 can be induced by absorption of a photon. In modern NMR-instruments this is done by introducing a second magnetic field, $\mathbf{B_1}$, referred to as a radio frequency field (RF) that is perpendicular to both $\mathbf{B_0}$ and **L**. As seen in figure 3-5 the angular moment **J** is precessing about $\mathbf{B_0}$ with the Larmor frequency ω_L. This means that the secondary magnetic field $\mathbf{B_1}$ must rotate about $\mathbf{B_0}$ with the Larmor frequency in order to be perpendicular to both $\mathbf{B_0}$ and **J** simultaneously.

$$f_{RF} = \frac{\omega_L}{2\pi} = \frac{\gamma}{2\pi} B_0 \tag{3-11}$$

The energy of the photon capable of excite the proton from the α- to the β-state is exactly the same as the difference in potential energy between the two states. This is given by the Planck`s equation:

$$hf = \gamma \hbar B_0 \qquad 3\text{-}12$$

$$f = \frac{\gamma}{2\pi} B_0 \qquad 3\text{-}13$$

We can now observe that $f_{RF} = f$, so that the frequency of the photon equals the frequency of the magnetic momentum`s precession about the external magnetic field $\mathbf{B_0}$. For a low frequency NMR apparatus which we will use in this thesis the Larmor frequency is 12 MHz. Each proton spin completes 12 million full cycles of precession every second and in order to be in resonance the $\mathbf{B_1}$ field must do the same. Introduction of the $\mathbf{B_1}$ field causes an alternation of the magnetization vector $\mathbf{M_1}$. This is easily described in a new reference frame (x´,y´,z´) rotating about the z-axis with an angular velocity ω_0 equal to the Larmor frequency (figure 3-5).

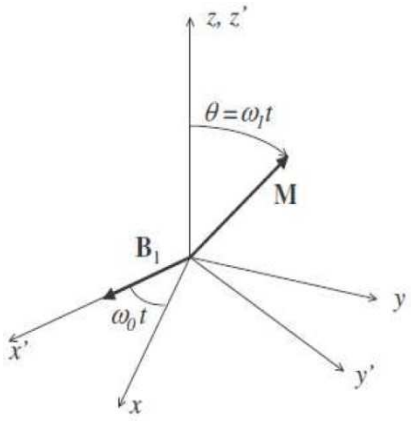

Figure 3-5: The frame of reference (x´,y´,z´) rotates with angular velocity ω_0 causing $\mathbf{B_1}$ to appearing fixed. The effect of $\mathbf{B_1}$ is to rotate the magnetization vector **M** about $\mathbf{B_1}$ with angular velocity ω_1. Reprint from Lien[30]

In this new frame of reference, (x´,y´,z´), $\mathbf{B_1}$ appears to be fixed. As $\mathbf{B_1}$ normally is defined along the x´-axis, the introduction of the new magnetic field causes **M** to rotate about the x´-axis with velocity ω_1, and down to the x´y´-plane (figure 3-5). The distance **M** is rotated is dependent on how long $\mathbf{B_1}$ is applied to the sample and is controlled by the equation:

$$\theta = \omega_1 \tau_p = \gamma B_1 \tau_p \qquad 3\text{-}14$$

The pulse is named by what angle and which axis **M** is rotated about. A $90^\circ_{x'}$ rotates **M** 90˚ about the x´-axis while a $180^\circ_{x'}$ inverts **M** about the x-axis. The pulse might even be in a negative direction, making us able to control **M** in all positions. In a modern NMR-experiment it is common to send

several pulses. This is called pulse sequences and the design of new pulse sequences is a major research field, with new pulse sequences being published frequently.

The application of the RF-field on microscale are quite complex and the exact behaviour will not be examined in this thesis. We are however able to explain the effect on the net-magnetization sufficiently with the introduction of two simultaneously working processes. When the RF-pulse is applied it causes the magnetization **M** to tip down into the x-y-plane. This involves that the population in the two energy states are equal, ie $n_\alpha = n_\beta$. Because of basic quantum mechanical laws the magnetic momentum is only allowed two different directions relative to the z-axis, parallel or anti-parallel. We are however able to detect a magnetization in the x-y-plane because the RF-puls forces the spin-system into phase coherence as shown in figure 3-6. This lumping of the individual magnetic momentum causes a transverse magnetization even though the individual **μ**`s cannot have x´- or y´-components.

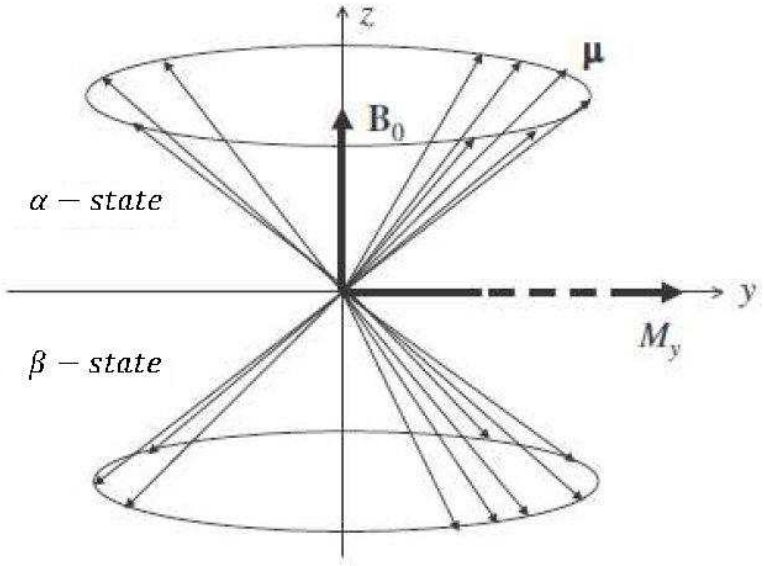

Figure 3-6: *The RF-puls causes the energy states to be equally distributed, and forces the precessing of the magnetic momentum into phase. The combination of these two effects causes a net magnetization in the y-direction.*

When the RF-field is applied the spin experience two magnetic fields. The strong static magnetic field $\mathbf{B_0}$ provided by the magnet and an oscillating field from the transverse coil. The static field is many orders of magnitude larger than the oscillating field, so how is the transverse field able to introduce such a large effect on the nuclear spin? This is solely a result of the *resonance* with the nuclear spin. As the spin precesses, the RF-field follows it allowing the effect of the weak RF-field to accumulate as time goes by. In a NMR experiment the duration of the RF-pulse is commonly several microseconds, equivalent to a multitude of Larmor precession cycles, so even if each push from the $\mathbf{B_1}$ field is weak it sums up to a significant effect. The process is analogous to a child`s swing. Each push on the swing is

weak, but when the force is applied in resonance with the natural oscillating frequency of the swing the accumulated effect could be significant.[29]

3.2 Relaxation

Immediately after the RF-pulse is turned off the spin system will tend to fall back to the equilibrium state. As a result, the magnetization vector that was tipped into the x-y-plane will deflect from its excited state and return to the thermal equilibrium condition, $\mathbf{M_0}$, with the $\mathbf{B_0}$ field. The process is called relaxation and is of great importance in NMR experiments. The process associated with increasing magnetization in the z direction is called *transverse relaxation* or *spin-lattice relaxation*. This process involves interaction between the spin system and the surroundings, sometimes referred to as the *lattice*. A magnetization vector which is tipped out off its equilibrium state got three components, $M_{x,}$, M_y and M_z in the frame of reference. The rate of growth in z- direction would then be proportional to the deviation of M_z to the originally equilibrium state according to equation 3-15[27, 30]

$$\frac{dM_z}{dt} = \frac{M_z - M_0}{T_1} \qquad 3\text{-}15$$

T_1 is a time constant and was first introduced by Bloch. It is called longitudinal or spin-lattice relaxation time and indicates how effectively the energy of the spin system is transferred to the surroundings. T_1 for a hydrogen nuclei is typically in the range $0.1 > T_1 > 10$ seconds. Sometimes T_1 relaxation is referred to as polarization time because the time allowed for the T_1-relaxation indicates the degree of proton alignment (polarization). At $t = T_1$, 63% of the equilibrium magnetization is achieved, and at $t = 3xT_1$ 95% of the magnetization is achieved. In order to get a strong NMR signal a full magnetization is favourable, but the knowledge of the polarization could also be exploited in some NMR application in order to get an artificially suppressed signal.

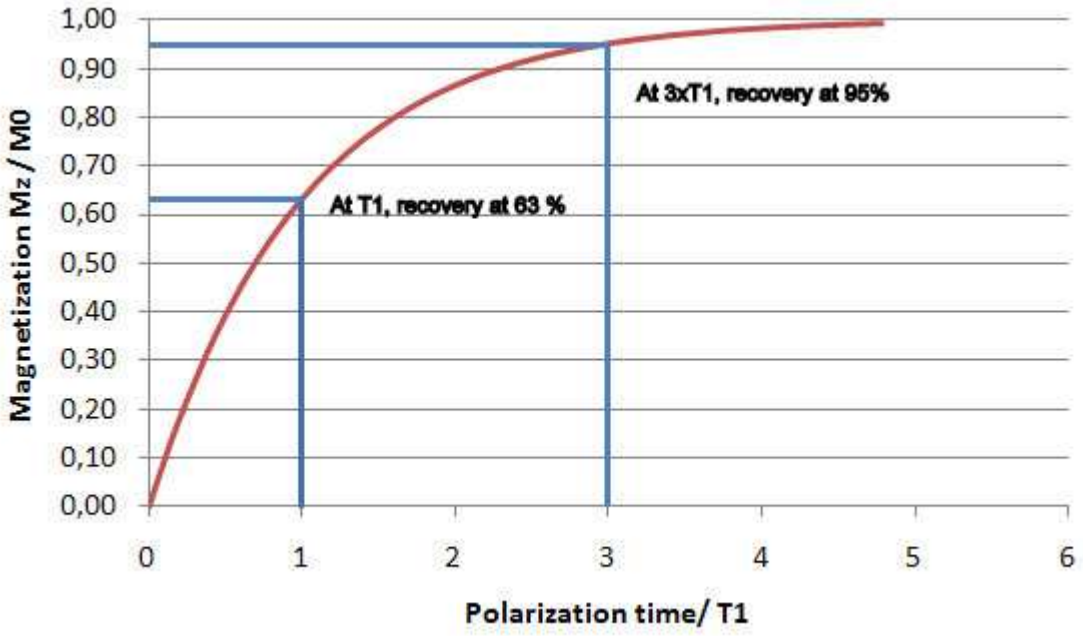

Figure 3-7: *T_1 relaxation curve for M_z when applying B_0-field on a completely non-polarized sample.*

The dissipation of the phase coherence which is generated by the transverse coil is called spin-spin or transverse relaxation, labelled T_2^*. This dissipation comes as a consequence of two separate mechanisms.

The first and dominating effect comes from the NMR system. At the end of the RF-pulse the spin-system is in phase coherence, but because the applied field is non-perfect the spins will feel slightly different magnetic fields, which causes them to precess with slightly different Larmor frequency's according to equation 3-9. The variation in the magnetic field could come as a consequence of inhomogeneity in the static field, interference from neighbouring nuclei or nearby ferromagnetic metals. The nuclei that experience a stronger static field must precess with a higher frequency and the nuclei experiencing a weaker static field must precess with a lower frequency. Over time this variation in Larmor frequency leads to a dissipation of the phase coherence acquired during the RF-pulse and eventually it will fan out zeroing the transverse magnetization M_y. Because of the tremendous speed of the precession there is very little room for error in the variation of the magnetic field. For a 1 Tesla magnet a one part per million variations between two regions of the static field causes the precession to be 180˚ out of phase in about 10 ms. Hence it is obvious to see that nuclei`s variation in experienced magnetic field strength cause a large impact on the measured magnetization.

The second effect comes from dissipating of phase coherence trough the direct interaction with other nuclei. In this mechanism the dissipating of phase coherence is not a function of variation in Larmor frequency, but rather as a consequence of energy transfer between individual nuclei. Classically this can be seen as the population of spin in the two energy states is kept unchanged, and that the rate of spins going from α-state to β-state equals the rate of spins going from β-state to α-state. Hence the

energy of the spin system is kept constant and $n_\alpha = n_\beta$. The decay of the M_y and M_x caused by loss of phase coherence can be described by the following equation.

$$\frac{dM_x}{dt} = -\frac{M_x}{T_2^*}, \qquad \frac{dM_y}{dt} = -\frac{M_y}{T_2} \tag{3-16}$$

By direct integration of equation 3-15 and 3-16 it yields the following solution for the characteristic time constant T_1 and T_2.

$$M_z = M_0\left(1 - e^{-\frac{t}{T_1}}\right) \tag{3-17}$$

$$M_x = M_y = M_0 e^{-\frac{t}{T_2^*}} \tag{3-18}$$

As we can see the characteristic time constant T_2^* consist of two separate contributors. One that is a system effect caused by imperfect magnetization and lack of purity of the sample, and the other a mechanism that is more dependent on the fluids in the system. In the next section we will discuss how we can manipulate our experiment so that only the latter is found.

Longitudinal and transverse relaxation occurs simultaneously. However, T_2^* is always smaller or equal to T_1. This is because T_1 cannot reach its equilibrium state as long as a transverse magnetization in the x- or y-direction exists.

3.3 Measuring the relaxation

A sample of protons that have been subjected to a transverse magnetic RF-field at resonance with the nuclei produces a transverse magnetization. Immediately after the pulse is turned off, the protons start to relaxate, due to the transfer of energy from the spin system to the surroundings, causing a reduction in the transverse magnetization and increasing the longitudinal magnetization. In a NMR experiment the decay of the transverse magnetization is recorded as a function of time and referred to as *free induction decay (FID)* curve. Because the protons are only loosely coupled to the surroundings this process requires what for atomic particles is a very long time. Several seconds is common, and even minutes have been recorded [32]. The technique for measuring the longitudinal magnetization is called *inversion recovery*. The sequence consists of an 180˚ pulse that inverts the spin population, followed by a 90˚ pulse after a variable waiting time which flips the magnetization into the x-y-plane for acquisition. This trick gives solely the effect from longitudinal relaxation. The 180˚ pulse shifts the magnetization from the positive z axis to the negative z axis. Hence immediately after the 180˚ pulse there will exist a slightly higher population of spins in β-state. Since this is not an equilibrium state for the sample, immediately after the stimuli, the spin starts to flip back to the positive z direction in order to re-establish a population between the two energy states in accordance with Boltzmann statistics

(equation 3-10). The rate of re-establishing the magnetization in positive z direction follows the equation

$$M(t) = M_0(1 - 2e^{-\frac{t}{T_1}}) \qquad 3\text{-}19$$

where the only difference from equation 3-17 is that the exponential function is multiplied by two. The purpose of the subsequent 90˚ pulse is to tilt the magnetization into the plane of the receiver coil in order to read the free induction decay that follows the 180 pulse. The start intensity of the FID is related to the growth of magnetization in accordance with equation 3.19. Hence an increase in the "wait time" from the 180˚ pulse to the 90˚ read pulse gives an increase in the measured magnetization. By conducting a sequence of experiments with increasing "wait times" a plot of signal strength vs the variable recovery time can be produced as shown in figure 3-8. T_1 is then computed by curve fitting using equation 3-19.

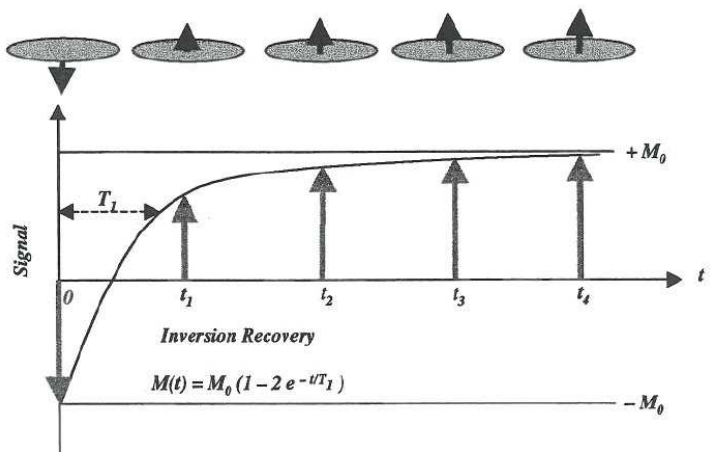

Figure 3-8: *A typical example of inversion recovery for obtaining T_1.*

Measurement of transverse relaxation follows a somewhat different outline. When physicist first started to record the decay of transverse magnetization they found that the recorded decay was much faster than anticipated[33]. As noted in section 3.2 this is because another process which is not related to the transfer of energy to the surroundings happens at a much faster rate. This is caused by variation in the Larmor precession which causes the phase coherence to fan out, cancelling the transverse magnetization. The two main contributors to a distribution in the Larmor frequency are [29, 34-35]:

- A time independent part that arises due to inhomogeneities in the applied static magnetic field, *and* variation in magnetic field caused by susceptibility differences between the solid and the pore fluid known as internal magnetic field gradients.
- A time dependent part caused by local fluctuation in the magnetic field due to random vibration and rotation of the neighbouring nuclei.

The transverse relaxation included the combined effect from both a) and b) are characterized by the time constant T_2^*. However, this relaxation is often governed by the effect from the applied field which is not of interest for our experiment. To avoid this, a trick has been developed in order to measure only the contribution from the local fluctuation. The most popular technique has taken its name from the authors Carr-Purcell-Meiboom-Gill[36-37], CPMG.

CPMG measurement

The technique utilizes a property of the spin system first recognized by American physicist E. L. Hahn [33] and is commonly referred to as Hahn-echoes. He found that decay in transverse magnetization came from loss of phase coherence due to variance in Larmor frequencies. In any sample, and in particularly in a fluid filled porous media there will exist a variance in the magnetic field caused by the factors explained in the previous paragraph. Nuclei that experience similar magnetic fields are referred to as isochromates and will precess with identical Larmor frequency. At the end of the RF-pulse all of the nuclei will precess in phase coherence, but since some of the isochromates experience a weaker magnetic field than the others they must have a slower Larmor frequency and consequently fall behind compared to the average nuclei. The isochromates experiencing a stronger magnetic field will precess with a faster Larmor frequency pulling ahead. Together it causes the phase coherence to fan out. Hahn found that by applying an 180˚ pulse to the sample a time τ after the initial 90˚ pulse, it inverts the precessing motion, putting the slower precessing nuclei to the front and mowing the faster precessing nuclei to the back. In a system where the different isochromates do not change their Larmor frequency during the experiment the now fanned out phase coherence will start to build up again as schematically shown in figure 3-9.

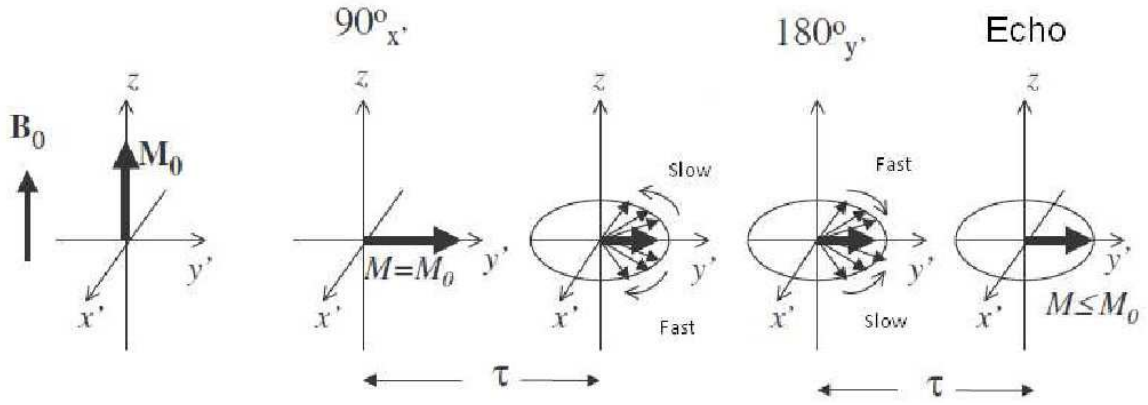

Figure 3-9: *A 90˚ pulse flips the magnetization down in the transverse plane and immediately the phase coherence starts to fan out. After a time interval τ an 180˚ pulse inverts the signal, "resurrecting" the phase coherence. The transverse magnetization reaper as a Hahn-echo after exactly 2 τ.* Reprint from Lien[30]

At 2τ the magnetization is at its maximum, but since the different isochromats precess with different Larmor frequencies the phase coherence that make up the reformed transverse magnetization will soon start to fan out again. If now a new 180˚ pulse is applied at t = 3τ after the initial 90˚ pulse the process of rephasing could start over again producing a new echo at t = 4τ. In a CPMG sequence there is usually a large number of echoes referred to as an echo-train.

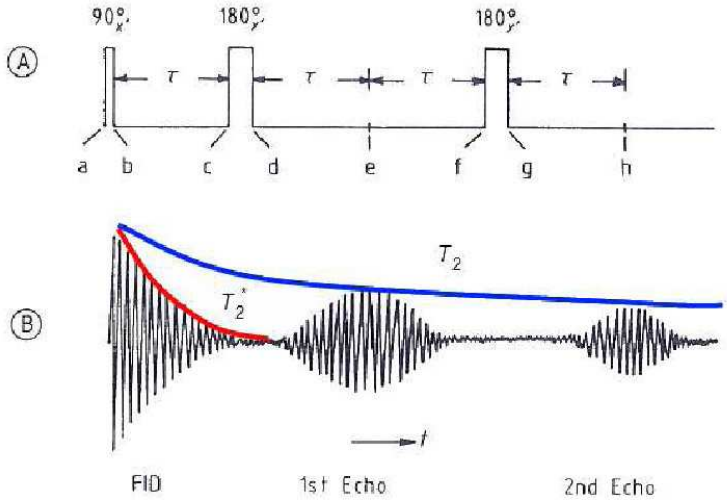

Figure 3-10: *An example of a pulse sequence* ***A****, and a schematic of an echo-train* ***B****.* Modified reprint from Lien[30].

The reproduced magnetization is an echo of the original magnetization, but the magnitude is not the same. As seen in figure 3-11 the magnitude of the polarization will decrease during the process and that the rate of dissipation follows the characteristic time constant T_2. In figure 3-10 there is indicated two curves associated with two different time constants. T_2^* represent the characteristic time constant for a FID (free induction decay) and the slope of the curve originate from the combination of the time dependent and the time independenet factors.

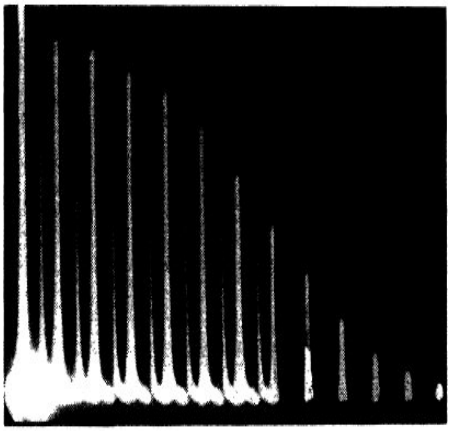

Figure 3-11: *An echo-train of a water sample. The separation between echoes is 1/60 sec.* Reprint from Hahn [33]

3.4 Relaxation mechanism

The use of nuclear magnetic resonance as a technique for measuring porous media parameters such as saturation, porosity and mobility has become increasingly important over the past 20 years. In the following section we will have a look at the special precautions that needs to be taken when dealing with nuclear magnetic resonance in porous media.

Bulk relaxation

Bulk relaxation is the process concerning protons that relaxate without any interactions from other external factors than the medium itself. For water the main process is the interaction with dissolved oxygen, but also ferromagnetic or paramagnetic ions dissolved in the brine such as iron and manganese could greatly increase the relaxation rate. Concentrations in the range of 0,01 mol/L of the ferromagnetic ions would drastically increase the relaxation rate[34]. In the absence of paramagnetic components, the nuclei interact with nuclei within their own molecule or with nuclei in neighbouring molecules through dipolar coupling[38].

Since water commonly is the wetting phase it will resides along the pore wall in the porous media. Oil on the other hand is often the non-wetting phase, consequently it resides in the centre of the pore space, and is prevented from making contact with the pore wall. In this situation the oil signal is dominated by the bulk relaxation, and the water signal is dominated by the surface relaxation. The shift of the relaxation times for oil and water can be studied to analyse the wettability of the rock.

Surface relaxation

Surface relaxation occurs as a consequence of interactions between the excited nuclei and the grain surface of the rocks. In a liquid the molecules will experience so called Brownian movement first explained by Einstein in 1905[39]. According to Einstein the average diffusion length x during a time t can be expressed as

$$\langle x^2 \rangle^{1/2} = \sqrt{6Dt} \qquad 3\text{-}20$$

where D is the molecular self diffusion coefficient. The pore size of common sandstone is in the range of 0.0015-0.015cm, and with D = 2.5 x 10^{-5} cm^2/sec for pure water at ambient temperature and pressure. This gives plenty of time for the molecule to interact with the surface wall during a NMR experiment[34]. The pore surface usually contains paramagnetic or ferromagnetic impurities, which got a magnetic moment several order of magnitude larger than that of hydrogen. When the excited nuclei interact with these minerals, it will affect both the energy transfer related to T_1 relaxation and the dephasing related to T_2 relaxation. Consequently, the relaxation occurs considerably faster for a

nuclei in contact with the pore wall than for the relatively slow relaxation for a nuclei in the interior of the pore.

Surface relaxation and bulk relaxation is the two of the main mechanism controlling relaxation in a porouse media. In a 100% brine saturated pore the measured relaxation is a combination of the bulk and the surface relaxation

$$\frac{1}{T_i} = \left(1 - \frac{\delta S}{V}\right)\frac{1}{T_{ib}} + \frac{\delta S}{V}\frac{1}{T_{is}} \qquad , i = 1,2 \tag{3-21}$$

where T_{ib} and T_{is} is the contribution from bulk relaxation and surface relaxation respectively and S/V is the ratio of the pore surface to fluid volume[30]. Since $\frac{1}{T_s} \gg \frac{1}{T_b}$ we rewrite the equation and we get

$$\frac{1}{T_i} = \rho_i \frac{S}{V} \qquad , i = 1,2 \tag{3-22}$$

where $\rho_i = \delta/T_{is}$ is called surface relaxivity and is a measure of the relaxing strength of the grain surface[6].

Diffusion relaxation

Water, gas and light to medium viscosity oil exhibit significant diffusive movement at normal pressure and temperature conditions. This is not an issue in a NMR experiment where the external magnetic field is constant. Because all the nuclei inside the sample precess at the same frequency the NMR signal will be independent of any movement of the nuclei during the experiment. However, this is not necessary the case. Instead of a uniform field the field may vary throughout the sample. This may be a result of internal susceptibility differences or as a result of an extra applied field. Since the field now does not have a uniform strength, but vary dependent on position in the sample, it is called a gradient field. If the gradient is applied parallel to B_0, the magnitude of the gradient field becomes a function of the z-coordinate of the **r** vector. In this case the precession frequency is dependent on both the static field and the field gradient

$$\omega(r) = \gamma \boldsymbol{B_0} + \gamma g \cdot r \tag{3-23}$$

where the first term is due to the static field as shown in equation 5-8, and the second term is due to the gradient **g**. If this gradient field is applied to a nucleus it will precess in the magnetic field with a higher frequency because of the added phase. Then after some time the nuclei is decoded by reversing the polarity of the gradient field, erasing the added phase. If the nuclei have not moved between the encoding and the decoding, the spin will refocus as normal after 2τ. If the nuclei on the other hand has moved from a position of low gradient field, to a position with slightly higher gradient field the echo is

not perfect. This causes a dissipation of the measured signal which is proportional to the distance the spins have moved.

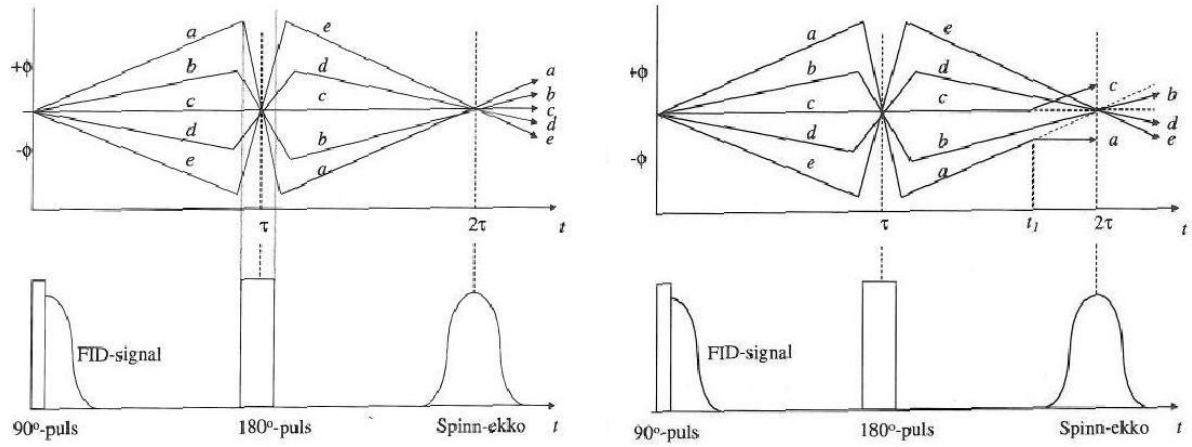

Figure 3-12: *The evolution of five isochromats: Left; the isochromats are stationary and refocused perfectly at 2τ. Right; two of the isochromats change place just before the resurrected echo. Because they precess with different velocities in the pre and post phase of the 180° pulse they can`t go back into phase. Hence, the echo is incomplete and the measured magnetization is weaker than normal.* Reprint from Lien [29].

For a fluid in a porous media, this adds a third relaxation mechanism to the system. In total, three different mechanisms, all acting simultaneously, contribute to the total relaxation of the spin system. Hence, the measured relaxation is given as the sum of the different contribution as

$$\frac{1}{T_2} = \frac{1}{T_{2\,surface}} + \frac{1}{T_{2\,bulk}} + \frac{1}{T_{2\,diffusion}} \qquad 3\text{-}24$$

$$\frac{1}{T_1} = \frac{1}{T_{1\,surface}} + \frac{1}{T_{1\,bulk}} \qquad 3\text{-}25$$

for transverse and longitudinal relaxation respectively. $1/T_{i\ surface}$ is the contribution from surface relaxation, $1/T_{i\ bulk}$ is the contribution from bulk relaxation and $1/T_{2\ diffusion}$ the contribution from diffusion in a field gradient (i =1,2). There is no diffusion term in the longitudinal relaxation, because the diffusion process is not related to energy transfer, and consequently it is only capable of dissipating the transverse magnetization.

For a regular CPMG experiment the effect from diffusion can be included in 3-21 to write 3-24 as

$$\frac{1}{T_2} = \left(1 - \frac{\delta \cdot S}{V}\right)\frac{1}{T_{2b}} + \frac{\delta \cdot S}{V}\frac{1}{T_{2S}} + \frac{(\gamma g \tau)^2 D}{12} \qquad 3\text{-}26$$

where δ is the thickness of the surface area S and V is the volume of the pore. D is self-diffusion constant, g is the assumed constant gradient and T_E is the *inter-echo spacing*.

As expressed in equation 3-26 the contribution from diffusion on the relaxation rate increases if one or more of the following parameters are changed:

a) The echo spacing is wider.
b) The gradient is increased
c) The molecular self diffusion is increased.

In a given system the self diffusion is fixed, so in order to control the effect from diffusion g or τ, or a combination of these two parameters are changed.

3.5 Introducing Pulsed Field Gradients

In the early years of NMR, the use of a constant gradient field during a CPMG-experiment was performed to find the diffusion coefficient. However, there are some limitations related to this. As the gradient is increased to allow the observation of smaller values of diffusion coefficient, the isochromates feels a broadening of the magnetic field strength. This causes a variation in the Larmor frequencies, which eventually leads to a reduction of the FID duration and a dissipation of the echo. To avoid these problems Stejskal and Tanner[40] introduced a technique where they reduced the strength of the gradient field during the time when the RF-pulse are being applied and also at the time of the appearance of the echo. This method is called pulsed gradient field. The modified Bloch equation for the Stejskal Tanner sequence modified by Torrey is given by

$$M(z,t) = M_0 \exp(-i\gamma G_0 z t) \exp\left(1 - \frac{t}{T_2}\right) \exp(-\tfrac{1}{3} D\gamma^2 G_0^2 t^3) \qquad 3\text{-}27$$

where the first exponential is a dephasing term, the second is due to transverse relaxation and the third represent dissipation due to diffusion. In a CPMG sequence the first term cancels out after the first echo and the equation is reduced to

$$M(z,\tau) = M_0 \exp\left(\frac{2\tau}{T_2} - \frac{2}{3} D\gamma^2 G_0^2 t^3\right) \qquad 3\text{-}28$$

3.6 Internal gradients

One of the key advantages of the utilization of NMR technique in oil field industry is the ability to extract mineral independent parameters from fluid filled rocks.[6] However, even though the matrix doesn't contribute to the NMR signal (because it doesn't contain any hydrogen nuclei) it will affect the signal in other ways. We have already talked about the surface relaxivity of the pore wall which "helps" the nuclei to undergo relaxation, but the magnetic property of the rock itself is also making an

impact on the NMR signal. When a fluid filled porous media is placed in a homogeneous magnetic field, the *magnetic susceptibility* contrasts between the different materials in the sample generate a variation in the magnetic field strength inside the void space. This is known as *susceptibility gradients* or more commonly, *internal magnetic field gradients*[35]. As the internal gradients are induced by the external field the size of the gradients are also proportional to magnitude of the external magnetic field. Consequently the presence of internal gradients will increase with higher field strength. This must be carefully considered in the interpretation of the measured signal. During the evolution of the NMR technology the use of increasingly higher magnetic field strength for obtaining higher resolution leads to a subsequently higher contribution from the internal gradients. But the presence of internal gradients is not only an experimental challenge. It is also exploited in several fields. In functional MRI the magnitude of the internal gradients are used to determine the change of blood flow related to neural activity in the brain, and the use of paramagnetic contrast agents to deliberately induce internal field inhomogeneities are routinely used in medical MRI[41]. In a fluid saturated sedimentary rock system, numerous researchers have shown that the presence of internal gradients could reveal information about fluid composition, diffusion, wettability and pore size distribution [35, 42-45].

The magnetic susceptibility, χ, is a parameter reflecting how an external magnetic field will magnetize a specific substance and is defined by

$$\chi = M/B_0 \qquad 3\text{-}29$$

where B_0 is the static field and M the induced magnetization[30]. Based on the sign and magnitude of the magnetic susceptibility scientist have divided the various substances into three groups.

- Diamagnetic substances got a small but negative value of magnetic susceptibility. This induces a magnetic field in the opposite direction of B_0 when placed in a static magnetic field. Consequently, the effective magnetic field is reduced in the presence of such a substance.
- Paramagnetic substances got a small, positive value of magnetic susceptibility. When placed in a magnetic field, they will induce a small magnetic field parallel to the applied field, which will increase the effective magnetic field.
- Ferromagnetic substances got a large positive magnetic susceptibility. When placed in a magnetic field the induced magnetic field causes a significant impact on the effective magnetic field. While paramagnetic substances are demagnetized when the external field is turned off, the ferromagnetic materials got a permanent magnetization. Ferromagnetic materials include iron, manganese, cobolt and nickel and are all present in most reservoir rocks[46-47].

Bulk water is a diamagnetic substance, while grain and cement in a porous rock could contain paramagnetic or ferromagnetic impurities. Consequently a considerable contrast in magnetic

susceptibility between the fluids and the matrix could exist. When a fluid saturated porous media is placed in an external, homogeneous magnetic field this contrast between the fluid and the solid grains magnetic susceptibility can induce large local field inhomogeneities inside the pore. The magnitude of this internal gradient is proportional to the susceptibility difference between the solid and the fluid, and inversely proportional to the size of the pore. In addition, the magnetic field strength of the internal gradients will vary inside a single pore being stronger at the pore surface, and weakest in the middle of the pore. However, finding a detailed function of internal gradient vs pore size is somewhat difficult. This is because the magnetic field inhomogeneities are also influenced by the grain shape, the aspect ratio of the pore, and the microgeometry of the pore network. But as a rule of thumbs, the smallest pores are associated with the largest internal gradient[42].

3.7 NMR and pore size distribution

NMR as a tool for measuring pore size distribution was first established by Brownstein and Tarr [48-49]. As noted in section 3.4 the relaxation can be described by a surface relaxing term and a bulk term. When the duration of the experiment is kept short it is only a small fraction of the volume in a pore that can contribute to the surface relaxation.

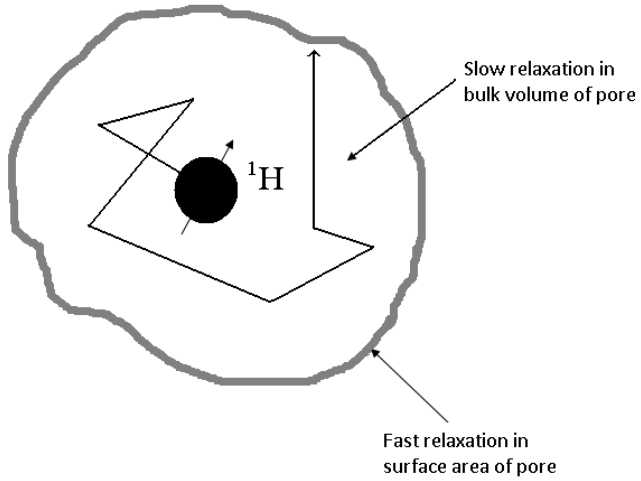

Figure 3-13: *Schematics of a pore split into a bulk volume (white), V, and "surface volume"(dark grey), δS. The diffusive movement of a single nucleus during a CPMG sequence is indicated with a black line.*

Brownstein and Tarr divided the relaxation into primarily two regimes: the fast and the slow diffusion regime. In the slow regime, the relaxation rate is primarily controlled by the ability to transport spin from the interior of the pore and into contact with the pore wall. In the fast diffusion regime, the rate of relaxation is controlled by the "relaxating strength" of the pore wall, i.e the probability of the pore wall to alter the energy level of a spin. These two regimes are also referred to as the diffusion limited- and the surface limited case respectively. In the surface limited case the rate of diffusion is very large compared to the relaxation induced by surface contact. As a result of this the polarization of the spins

in an isolated pore is quickly averaged trough diffusion and the magnetization decays uniformly across the pore.

From equation 3-21 we learned about the link between relaxation rate and pore geometry. Because T_{2b} >> T_{2s} the first term in equation 3-21 is ignored and it is reduced to

$$\frac{1}{T_2} = \frac{\delta \cdot S}{V}\frac{1}{T_{2s}} \equiv \rho \frac{S}{V} \qquad 3\text{-}30$$

where $\rho = \delta/T_{2s}$ is referred to as the surface relaxivity and is a measure of the relaxating processes that take place on the mineral surface. Extensive research on the field have shown that this constant is often independent of the size of the pore[43, 45]. This equation now states that the transverse relaxation time is directly proportional to pore size.

3.8 NMR relaxation in a porous media

In a naturally occurring porous media we find a spectrum of pore sizes, and most of the pores are interconnected. If we assume a fully brine saturated media satisfying the fast diffusion approximation, spins from pores with unequal size will relaxate at slightly different rates based on the contrast in surface to volume ratio, producing a spectrum of T_2-values.

$$\boldsymbol{M}(t) = \boldsymbol{M}_0 \sum_{j=1}^{n} f_j \exp\left(-\frac{t}{T_2}\right), \qquad \sum_{j=1}^{n} = 1 \qquad 3\text{-}31$$

where M(t) is the magnetization at time t, M_0 is the initial magnetization and f_j is the volume fraction of pores for the corresponding relaxation time T_{2j}. The relationship between pore size and T_2 values for water are illustrated in figure 3-14, and a schematic interpretation of equation 3-31 is shown at the bottom of the same figure. As found in equation 3-30 the T_2 values are proportional with the volume to surface ratio of the pore. Hence, the fluid in a large pore will have a longer relaxation time than a fluid in a smaller pore. Because of the high surface relaxivety in sandstone, we often find a good correlation between the pore size and T_2 relaxation. In carbonate on the other hand a weak surface relaxivety allows the spins to migrate, causing a diffusional coupling between neighbouring pores. T_2 measurement could then merge into an intermediate state giving a T_2 distribution that differs from the actual pore size distribution. [6]

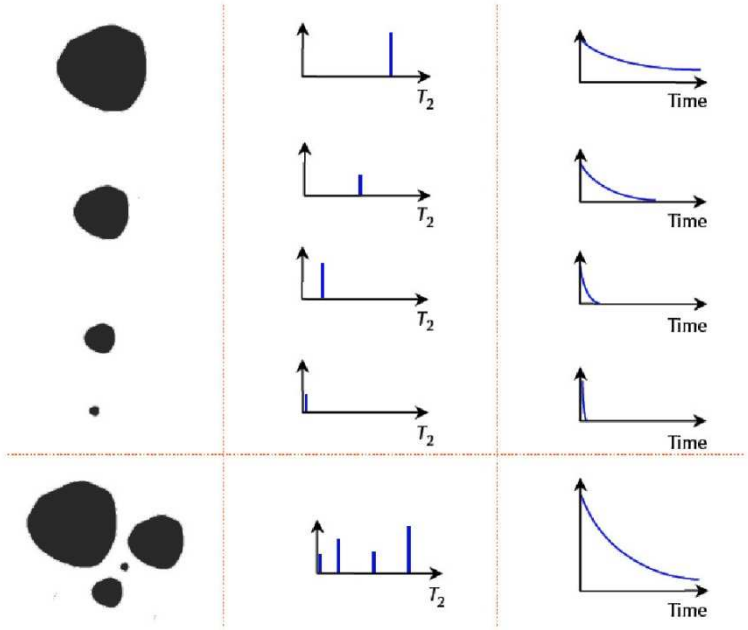

Figure 3-14: *The rate of relaxation is proportional to the surface to volume ratio, i.e the size of the pore. The figure is a schematically interpretation of how the different pore sizes contribute to the total T_2 spectrum.* Reprint from Coates et al.[6]

When a scientist measures the T_2 distribution whit the goal of finding the pore size distribution, the raw date is a magnetization vector that decreases with time. The rate at which the magnetization falls back to its equilibrium state is controlled by a sum of the spectrum of the T_2 values as formulated in equation 3-31. In order to decode the raw data and find the T_2values we must solve equation 3-31 for f_j. This prosess, referred to as echo-fit have proven to be an inverse problem and non-unique solutions may be found.

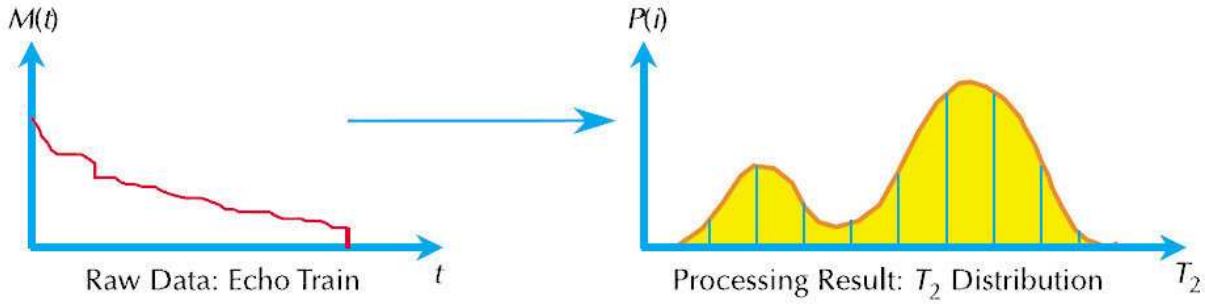

Figure 3-15: *Schematically interpretation of the echo mapping needed to translate the raw data into a T_2 distribution. Reprint from Coates et al. [6]*

The T_2 distribution from a porous sample is a continuous function, in the same way the pore size distribution is a continuous function. To simplify the fitting process the decoding program assumes that the T_2 distribution consist of a finite sum of decaying exponentials referred to as bins. Since all of the signal in a NMR experiment originate from the pore fluids, some important conclusions could be drawn from the magnitude of the signal. With proper calibration the shaded are under the T_2 distribution curve for a 100% water saturated core is equal to the porosity of the sample. For a water saturation $< 100\%$ we can, based on the assumption that fluid in smaller pores gives a faster T_2

relaxation, classify the T_2 spectrum into a range of sectors as shown in figure 3-16.

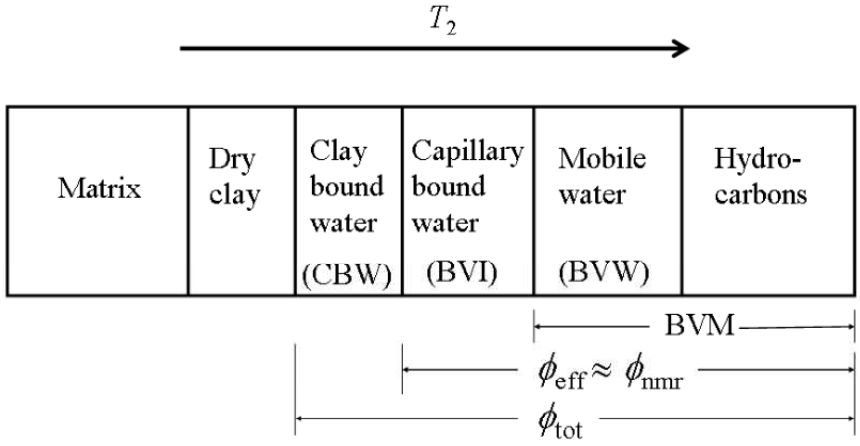

3-16: *Based on the assumption that smaller pores gives a shorter T_2 relaxation, the relaxation spectrum can be classified into a range of sectors. This is an example from a water wet reservoir.* Reprint from Lien[30]

In commercial logging of an oil field reservoir the common situation[6] is water wet reservoir where the hydrocarbons will reside in the interior of the large pores and the water is situated in the smaller pores, and possible as films in larger pores. Because the oil has no contact with the pore wall, the hydrocarbon fraction has no contribution from the surface relaxation and consequently the bulk relaxation is the dominating factor. Hydrocarbons will in this scenario have the longest T_2 relaxation rate. *Bulk volume water (BVW)* is water from the pores where the capillary forces are weak enough to allow mobility of the water. The volume of the hydrocarbons and the movable water is the *Bulk Volume Movable (BVM)* in logging terminology. *Capillary bound water(CBW)* and *Clay Bound Water (CLW)* is the fraction of water that cannot move around in the reservoir. Because of its close proximity to the surface wall this water has a very short transverse relaxation. These relaxation rates are the shortest that commercial logging instruments can detect. Any signal emitted from the matrix is undetectable for the logging instrument because of the short time between the excitation and relaxation.

The discrimination between BVI and BVW is usually determined by a fixed value referred to as the cut-off-value, T_{2co} dividing the T_2 distribution into two components. One where the pores are filled with bonded water, and the other where the water is free to move. For a number of years this has been 32 ms and 92 ms for sandstone and carbonate respectively. However a second method called spectral BVI exist which is based on the fact that a single pore could contain more than one fluid.

The ability to distinguish between movable and immobile fluids as shown in figure 3-16 is one of NMR loggings biggest success. From this information it is possible to estimate the absolute permeability by using Coates equation[30]:

$$k = \left(\frac{\phi_{NMR}}{C}\right)^4 \left(\frac{BVM}{BVI}\right)^2 = \left(\frac{\phi_{NMR}}{C}\right)^4 \left(\frac{\phi_{NMR}-BVM}{BVI}\right)^2 \quad [md] \qquad 3\text{-}32$$

3.9 Wettability determination from NMR

From chapter 3.4 we learned that because the surface interactions is the dominating factor in relaxation in a porous rock, the relaxation rate of a fluid is greatly dependent on its position relative to the surface. Because of the close relationship between surface phenomena and T_2 relaxation, nuclear magnetic resonance got a high potential for use in a wettability measurement setup. If we are able to determine which fluid that interact with the pore surface this will tell us a great deal about the fluid distribution inside the rock and consequently about its wetting state.

Brown and Fatt[32] considered in 1956 the feasibility of using NMR as a wetting test. They measured the relaxation rate of 5 different ratios of water wet and oil wet sand, and found a linear relationship between the relaxation rate and the amount of oil wet sand. Based on the assumption that there is a linear relationship between the NMR response and the amount of oil wet material in place, they proposed a method of determine the wetting state of a reservoir core. The NMR response should be measured at strongly water wet, and strongly oil wet conditions in addition to its native condition, and from the linear relationship between the measurements the native wettability could be established.

Hsu et al[50] conducted in 1992 a similar experiment on carbonate core samples where the wetting state was altered in order to create preferentially water wet and preferentially oil wet systems. T_1 relaxation rate was measured both at water wet and oil wet conditions, before the wettability was measured by the combined USBM/Amott test. Hsu et al found that for oil wet samples the longitudinal relaxation rate was reduced with about 50 percent compared to the water wet samples. They suggested that the difference was due to weaker interactions between the water and the pore surface in the oil wet cores because of the presence of hydrocarbon residue on the pore surface. They finally concluded that in order to measure wettability on a reservoir rock, NMR response from both oil wet, water wet and native wet state is needed. Because of the intricate pore structure and pore size distributions of a reservoir rock, and the relaxation rates dependencies on these parameters a true objective wetting test was not yet possible.

In 1998 Howard conducted a series of T_1 relaxation experiments on chalk samples at wettability ranging from strongly water wet to weakly oil wet in order to find a quantitative description of the wettability. He introduced the relationship

$$T_n = CS_w^b \qquad 3\text{-}33$$

where T_n is the normalized relaxation time for a sample, C is an empirical correction factor and S_w the water saturation. In his equation, b is correlated to wettability, and he found a strong linear relationship between the factor b and the Amott wettability index.

A more complex relationship between the NMR and wettability was introduced by Fleury and Deflander[51]. The model is based on the ratio of pore surface contacted by water and oil respectively and states that

$$I_{NMR} = \frac{S_w\left(\frac{1}{T_w}-\frac{1}{T_{bw}}\right)-C_p S_o\left(\frac{1}{T_o}-\frac{1}{T_{bo}}\right)}{S_w\left(\frac{1}{T_w}-\frac{1}{T_{bw}}\right)+C_p S_o\left(\frac{1}{T_o}-\frac{1}{T_{bo}}\right)} \quad 3\text{-}34$$

In this equation S_w, S_o are the water and oil saturations, T_w,T_o the dominant relaxation times for water and oil respectively and T_{bw}, T_{bo} the relaxation times at bulk state. C_p is the water-oil surface relaxivity ratio, given as

$$C_p = \frac{\rho_w}{\rho_o} = \frac{\frac{1}{T_{w,100\%}}-\frac{1}{T_w}}{\frac{1}{T_{o,100\%}}-\frac{1}{T_{bo}}} \quad 3\text{-}35$$

where $T_{w,100\%}$ and $T_{o,100\%}$ are the dominant relaxation times for water and oil respectively at 100% saturation. When Fleury and Deflander compared the result to the USBM wettability index they found a god correlation in the range $-0{,}3 < I_{USBM} < 1$.

Pursuing the same basic idea of correlating the ratio of the pore fluids in contact with the pore wall to a wettability index Al-Marooqi et al[7] used a pore scale model to investigate the effect of wetting and its relationship with NMR relaxation times. The model was based on an idealising bundle of capillary tubes, with an equilateral triangle shape and size from a given pore size distribution. The model was then used for calculating the volume of, and the surface area contacted by each phase. Both the model and the experimental data showed that, at S_{wi} the T_2 distribution is a function of the ratio of water contacting the surface (wetting the surface), and Mahrooqi argued that since his model is based on the same factors controlling the Amott-Harvey index the result was comparable. He proposed a NMR-wettability index using the relationship between the logarithmic mean T_2 value, T_{2m}, from two different saturations.

$$I_{ic}^{NMR} = \left(\frac{T_{2m}^{S_{wi}}-T_{2m}^{Sor}}{T_{2m}^{S_{or}}}\right) \quad 3\text{-}36$$

The index showed good correlation to the AH-index for cores at strong wetting conditions, but for intermediate wet cores the correlation was not as god. This was argued that might be the effect of other factors such as sample mineralogy and pore size distribution.

While Mahrooqi neglected the effect from internal field gradients, and the effect from diffusivity Freedman et al[52] demonstrated a way of obtaining a coupled diffusivity and transverse relaxation signal by applying a complex NMR sequence to the sample. This new technique made it possible to separate the NMR response from two fluids if there is a contrast in diffusivity, such as between water and oil. By comparing the brine distribution at 100% brine saturation with S_{or} conditions and the oil

distribution at S_{wi} and S_{or} with bulk oil distribution, Freedman et al. were able to differentiate mixed wet samples from water wet samples.

The same procedure has later been used by Chen et al[9] in order to examine the wettability changes caused by the presence of oil based mud. By using the contrast in diffusivity to separate the relaxation distribution at partial saturation from water and oil, Chen et al. was able to calculate the effective surface relaxivity for water and oil separately. This effective surface relaxivity was then used to calculate the NMR wettability index as follows:

$$I_c^{NMR} = I_w^{NMR} - I_o^{NMR} = \frac{\rho_{2,w,eff}}{\rho_{2,w,max}} - \frac{\rho_{2,o,eff}}{\rho_{2,o,max}}$$

$$= S_w \frac{\left(\frac{1}{T_{2,w}} - \frac{1}{T_{2,w,B}}\right)}{\frac{1}{\left(T_{2,w,S_W=100\%}\right)_{water\ wet}} - \frac{1}{T_{2,w,B}}} - S_o \frac{\left(\frac{1}{T_{2,o}} - \frac{1}{T_{2,o,B}}\right)}{\frac{1}{\left(T_{2,o,S_O=100\%}\right)_{oil\ wet}} - \frac{1}{T_{2,o,B}}} \qquad 3\text{-}37$$

where $T_{2,w,B}$,$T_{2,w,B}$ and $T_{2,w,Sw=100\%}$, is the relaxation times of water at bulk, after forced imbibition and at 100% saturation respectively. $T_{2,o,B}$,$T_{2,o,B}$ and $T_{2,o,So=100\%}$, is the relaxation times of oil at bulk condition, after forced displacement, and at 100% saturation respectively. When comparing result from measurements on Berea cores to the Amott-Harvey index they found a good linear correlation.

Flaum et al. [53] conducted a series of experiments correlating diffusivity and transverse relaxation in naturally oil wet West Texas dolomite and Berea sandstone polluted by oil mud additative. He argued that the divergence of diffusivity from bulk fluid values could give information about the wettability of the system. A diffusion coefficient above the bulk diffusion would indicate the presence of internal gradients, while values below bulk suggest the presence of restricted diffusion. He presented the data in the form of 2D diagrams enabling good visualization of the result. In addition to the interpretation detailed above, the separation of the fluids based on diffusivity also gave the potential of more detailed monitoring of the changes in the each fluids relaxation.

Taking this one step further Seland et al.[35] investigated the correlation between internal gradients, diffusivity and transverse relaxation rate for fluid saturated packings of glass spheres of various wettability. The experiments were performed on a 2 MHz Bruker Avance DMX200 instrument with an applied gradient strength in the range 0-900 G/cm. The samples contained originally water wet glass spheres with size ranging from 4-60 μm in diameter which was prepared in 10mm NMR tubes. In order to have both water-wet and oil-wet samples some of the tubes were treated with excess trimethylchlorsilane in a mixed solvent pair of toluene-pyridine kept under an atmosphere of argon gas. Because the strong internal gradients are associated with close proximity to the pore surface, the knowledge of which component that experience the strongest internal gradient gives valuable information about the fluid distribution and the wettability of the system. Seland et al. performed a series of experiments with various saturations and wetting state and was able to differentiate between

various wettabilities based on the location of the water signal. In order to present his results he expressed it in the form of D-T_2 and G_0-T_2 2D-diagrams using the inverse Laplace software developed by Callaghan.

Recently Pavlin et al.[54] presented a paper investigating the same relationship between internal gradients, diffusivity and transverse relaxation for a Berea outcrop, and concluded that the use of $G_0 - T_2$ correlation was potentially more sensitive for wettability measurements than the D-T_2 correlation.

4. Experimental methods

Review of the experimental methods used in the thesis.

4.1 Drying procedure

The Berea sandstone cores were cut from a larger stone with a metal saw and water as cooling, cleaning and lubricant agent. In order to clean the cores from any water absorbed during the cutting, the cores was placed in a heating cabinet for three days until the weight of the cores stabilized, confirming that no more water remained in the core.

4.2 Measuring porosity

Porosity is one of the most fundamental parameters of a sedimentary rock, and knowledge of its magnitude is required in most core analysis. The core sample is first placed in a heat cabinet at 80°C in order to completely vaporise any fluids still trapped in the pore volume. Then weight, length, height and diameter are measured. Each parameter is measured three times, and the arithmetical mean is calculated in order to minimize any human error or inaccurate values due to uneven shape of the core. The core is then placed in a core holder, and a confining pressure of 20 bar is applied before it is put under a vacuum pump to extract the air. When the air pressure in the core is below 1 mBar, the core is flooded with synthetic sea water (Appendix table 1) with 5 bar over pressure in order to fully dissolve the air still trapped inside the core. A precise pump is utilised, and the amount of water needed to fill the core is recorded. This amount is the pore volume of the core. The porosity is then calculated from the following equation

$$\phi = \frac{V_p}{V_b} \cdot 100\% \qquad 4\text{-}1$$

where V_b is the total bulk volume of the core sample.

To quality check the porosity the now fully water saturated core sample is weighted again. Because the density difference between air and synthetic seawater is known, the porosity is calculated with the following equation

$$\phi = \frac{\frac{m_{wett} - m_{dry}}{\rho_{water}}}{V_b} \cdot 100\% \qquad 4\text{-}2$$

where m_{wett} and m_{dry} is the weight of the dry core and the fully saturated core respectively and ρ_{water} is the density of synthetic seawater.

The error from this calculation is the function of uncorrelated variables. We use the error propagation formula 4-3 to find the total error. For a general function F dependent on the uncorrelated variables x,y,z... with the corresponding errors $\delta_x, \delta_y, \delta_z$... this is given by the formula:

$$\delta_F = \sqrt{\left(\frac{\partial F}{\partial x}\delta_x\right) + \left(\frac{\partial F}{\partial y}\delta_y\right) + \left(\frac{\partial F}{\partial y}\delta_y\right) + ..} \quad 4\text{-}3$$

4.3 Measuring permeability

As described in section 2.2, permeability is defined through Darcy's law. It is based on the following assumptions [1]:

1. The flow within the pore space must be laminar.
2. The core must be 100 % saturated with a single fluid.
3. No chemical or physical reactions can occur between the saturating fluid and the rock.
4. The flow angle must be constant. In this case, the permeability was measured horizontally in order to avoid the effects of gravity.
5. The saturating fluid is incompressible.

The generalized Darcy law (Equation (2.3)) can be rewritten as

$$K = \frac{\mu L}{A}\frac{Q}{P_2 - P_1} \quad 4\text{-}4$$

Since the cross-sectional area *A*, and the viscosity μ, are known, we can find the permeability by flooding the core sample at constant flood rate and measure the production, Q and the pressure drop, $\Delta P = P_2 - P_1$. The fully saturated sample was placed in a core holder with an applied sleeve pressure of 20 bars to prevent any fluid from bypassing the core. To prevent any air bubbles in the sample, which can cause fluid discontinuity and thus influence the measured pressure drop, the whole system was ensured to be filled with brine prior to the measurement by using a valve to bypass the core holder. In addition a back pressure of 10 bars was applied to dissolve any air still trapped in the core. Schematic of the setup is shown in figure 4-1

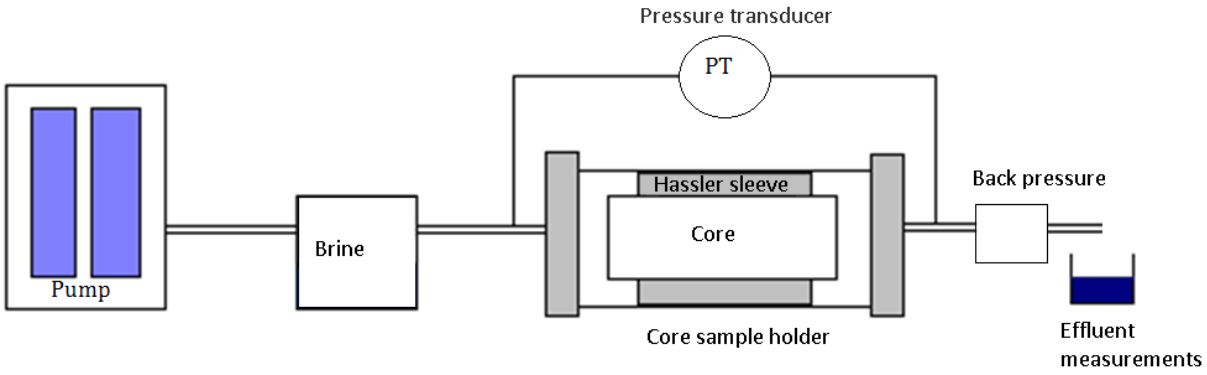

Figure 4-1: *Experimental setup for measuring absolute permeability.*

According to equation 4-4, a linear relationship exist between the absolute permeability K and $\Delta Q / \Delta(P_B - P_A)$. Experimental uncertainty was thus reduced by running the experiment with several different flow rates and using linear regression to fit the data.

4.4 Changing fluid saturation

When finished measuring the permeability of the cores, we want to change the fluid saturation of the cores. In order to change from a water saturated core to a crude oil saturated core, this is a two step process. For the mineral oil saturated cores only step number one is necessary.

Step 1. Marcol 152 displacing water. A drainage prosess.

Because of the favourable density difference between water and oil, the coreholder is placed in an upright position as shown on figure 4-2, where oil is injected from the top, and water is produced from the bottom. The produced water is collected in a graduated cylinder, and the volume of the displaced water is measured. This is a non-miscible process and is performed in two steps:

1. First one pore volume of oil is injected at low rate (< 0,1 mL/min). The low rate is chosen in order to delay the time of first oil production, and maximising the effect from gravity.
2. Then 10 pore volumes of oil are injected at high rate (> 2 mL/min). This high injection rate is chosen in order to increase the viscous force acting inside the pores and mobilise as much as possible of the water.

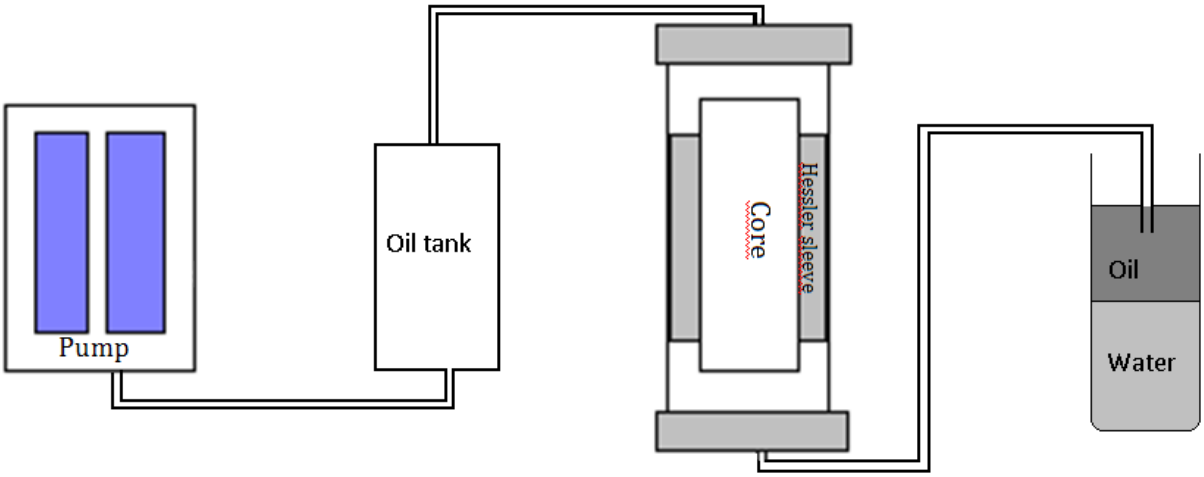

Figure 4-2: *Displacement process setup. The volume of produced water is measured, and saturation is calculated.*

When the production of water stops, the displacement process is terminated and the saturation is calculated from the following formula:

$$S_w = 1 - \frac{V_{wp}}{P_v} \qquad 4.4 \qquad\qquad S_o = 1 - S_w \qquad 4.5$$

where V_{wp} is the produced water volume.

Step 2. Displacing Marcol 152 with crude oil

The crude oil we are using in this thesis is a North Sea stock tank oil. The viscosity of this crude oil is in the range of 50-55 cP. Compared to water which have a viscosity of only 1 cP this makes a highly unfavourable mobility ratio. In order to achieve a more effective displacement situation we want to dilute the crude oil by adding 40% Xylene to the crude prior to flooding the cores which gives a viscosity of only 4,0 cP.

The displacement of Marcol with crude oil is a miscible process. We start the displacement by flooding the core with low rate (0.1 mL/min) for the first porevolume, and continue by flooding 4-5 porevolumes at medium rate (0.5 mL/min)

4.5 Changing fluid saturation to S_{or}

To increase the amount of information from the system we want to conduct the NMR experiments at both irreducible water saturation, S_{wi}, and at residual oil saturation, S_{or}. In order to achieve this we flooded the cores with synthetic sea water while recording the produced oil volume. The flooding was conducted upflanks and at three different injection rates. First water was injected at 0.1 mL/min. After 2 pore volumes this did not give any more production and the injection rate was first increased to 0.3

mL/min and then after another 2 pore volumes again increased to 0.6 mL/min. The total volume of water injected was approximately 10 pore volumes for each core. The relatively low injection rate was chosen in order to maintain the stability of any aging effect.

4.6 Results

		Error (abs)	1A	1B	2A	2B	S1	S2
Diameter	(cm)	± 0.01	3.74	3.87	3.77	3.76	3.7	3.76
Length	(cm)	± 0.02	5.91	5.94	5.82	5.86	6.00	6.23
Unsaturated Weigth	(g)	± 0.01	143.38	144.70	140.84	142.38	-	-
Saturated Weigth	(g)	± 0.01	154.14	153.89	151.61	153.22	-	-
Bulk Volume	(cm^3)	± 0.01	65.08	66.54	64.89	65.07	64.51	69.18
Pore volume	(cm^3)	± 0.01	12.68	12.62	12.68	12.29	12.35	13.27
Porosity	(%)	± 0.01	19.77	18.97	19.55	18.89	19	20
Absolute Permeability	(mD)	± 0.5	84.4	79.0	99.0	100.2	103.8	90.2
Oil endpoint Permeability	(mD)	± 0.5	103.62	100.38	66.05	104.91	-	-
Water saturation,	S_{wi}	± 0.01	0.31	0.31	0.29	-	0.30	0.26
Water saturation,	S_{or}	± 0.01	0.61	0.75	0.72	-	0.82	0.75
		Pore fluid and ageing state						
Marcol			x	x				
Heimdal Crude Oil					x	x	x	x
Aged							x	x

Table 4-3: *Core specifications*

		Error (abs)	R1	R2
Diameter	(cm)	± 0.01	3.73	3.73
Length	(cm)	± 0.02	5.73	5.79
Bulk Volume	(cm^3)	± 0.01	62.61	63.27
Pore volume	(cm^3)	± 0.01	12.24	12.45
Porosity	(%)	± 0.01	19.55	19.68
Absolute Permeability	(mD)	± 0.5	89.7	85.1

Table 4-4: *Core specifications reference cores at S_w=1*

5. Wetting test

In order to measure the wettability of the cores, the combined USBM/Amott test was performed.

Figur 5-5: *Image showing the production of oil after 5 minutes from a non-aged Berea sandstone. Since the oil clings strongly to both the core and to the glass, the imbibitions cell must be carefully "whirled" to force oil up to the graduated cylinder where it is recorded. PHOTO: Joar Vevle*

The test starts with cores at irreducible water saturation placed in an imbibition cell filled with synthetic sea water (appendix table 1). The spontaneous oil production is then recorded as a function of time for two weeks. The initial oil production is very fast so the production is recorded every hour the first 6 hours, every 12 hours the first two days and on a daily basis until the end of the imbibitions process.

After two weeks the cores are dismounted from the imbibtion cells and mounted in an Exxon-holder. This core holder is specially designed to operate with the Beckman J6B Centrifuge, and has been modified with a translucent plastic cup to measure the amount of produced fluid and a centrifuge line which transports the displacement fluid around the core. The centrifuge rotor is able to hold up to 4 cores at the same time with a maximum of 0,3 gram difference in weight. In order to balance the centrifuge, lead wire is winded around the production cup and secured with tape before the core holders are placed in the specially designed centrifuge arm.

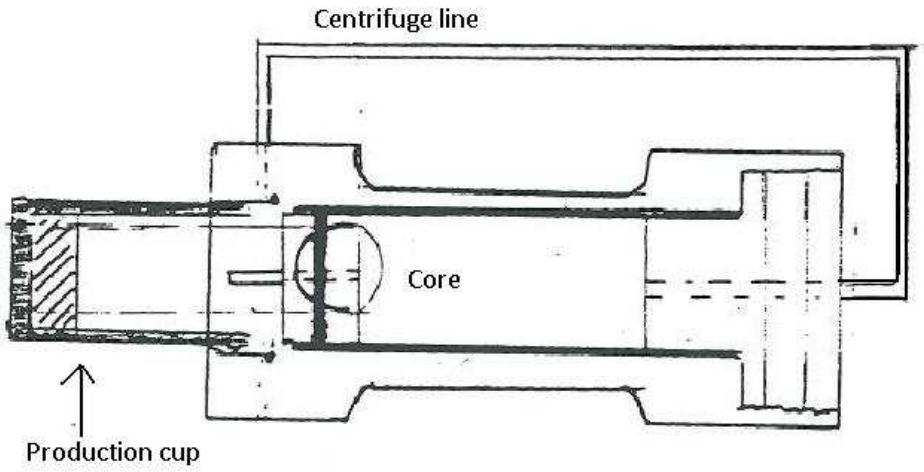

Figur 5-2: *Schematic of the Exxon core holder equipped with a plastic cup for produced oil and a centrifuge line for the displaced water. Modified reprint from Norsk Hydro[55]*

The experiment starts at 400 RPM and continues in steps of 200 RPM up to 3000 RPM, or until vibrations stops the centrifuge. At every speed step we allow 24 hours of spinning in order to achieve an hydrostatic equilibrium between the two fluids[56-57].

At the end of the centrifuge run the produced fluids are recorded, and the cores are placed in imbibition cells filled with oil. The spontaneous imbibion of oil is now measured for a period of two weeks or until no production is recorded for 7 days.

5.1 Results

Spontaneous imbibition

To correlate differences in fluid and core properties the modified scaling group of Mason et al[58] is used where t_D is the dimensionless time.

$$t_{D,Ma} = t\sqrt{\frac{k}{\phi}}\frac{\sigma}{\mu_w(1+\sqrt{\mu_{nw}/\mu_w})}\frac{2}{L_c^2}$$

k is the permeability, φ is the porosity, σ the interfacial tension, and μ_w and μ_o the viscosity for water and oil respectively. L is the length of the core.

Free imbibition of water

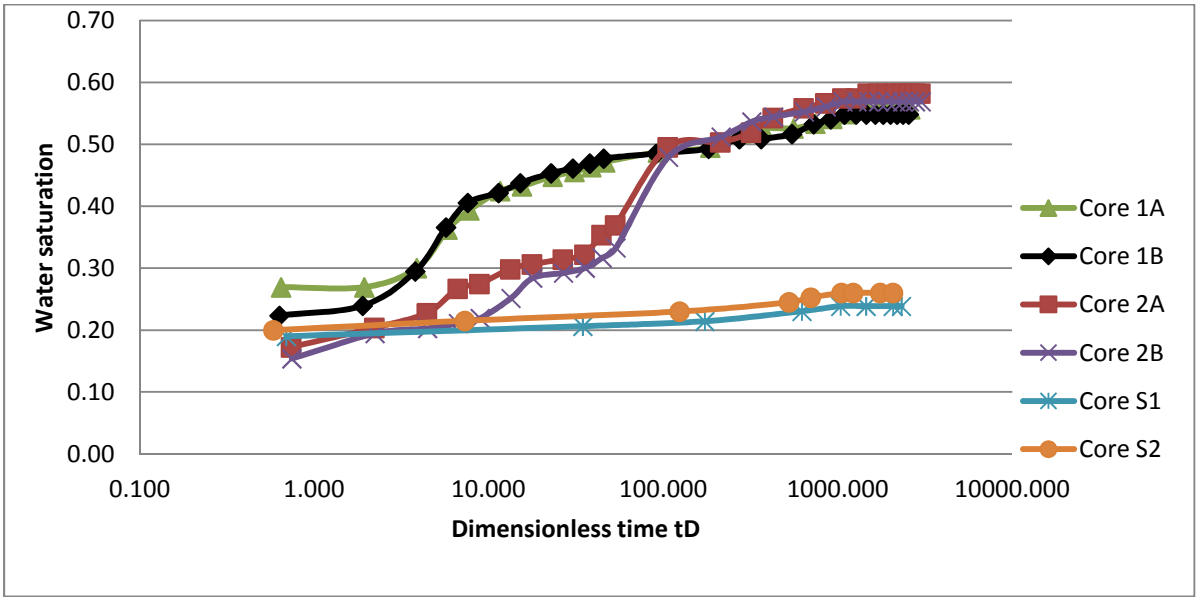

Figur 5-3: *Graph showing the free imbibition of water as a function of the dimensionless time t_D*

As seen in figure 5-1 the four non-aged cores have a large spontaneous imbibition of water compared to the aged cores. Another striking observation is that the cores filled with Marcol (1A and 1B) show a significant faster oil production in the early part of the spontaneous imbibition compared to the crude filled (2A-2B). This is however merely a delay in the production and we observe that after dimensionless time 100 000, (24 hours), the crude oil production from the non-aged cores have regained the lead and at the end of the experiment (after 2 weeks) the cumulative production is slightly higher for these cores.

The production from the aged cores is significantly slower than the rest, and we observe only a 4-6 percentage points increase in the water saturation.

Forced water imbibition

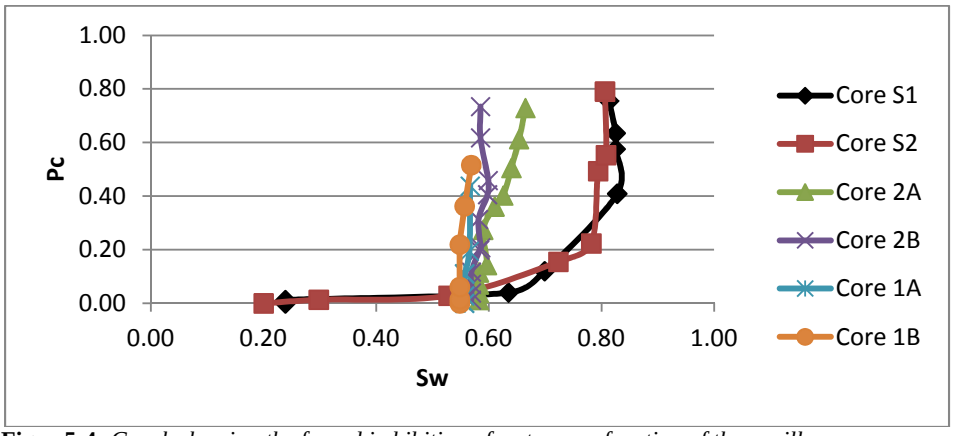

Figur 5-4: *Graph showing the forced imbibition of water as a function of the capillary pressure*

In the forced imbibition of water by centrifuge method we clearly see a difference between the aged cores and the non-aged cores. The non-aged cores had a large oil production in the spontaneous imbibition test and consequently have a limited volume of oil available for production in this test. We observe that core 2A have a 4 percentage points change in fluid saturation, and that the other non-aged cores are having smaller saturation change. The aged cores have a quite significantly change in saturation from 24% to 80%.

Free imbibition of oil

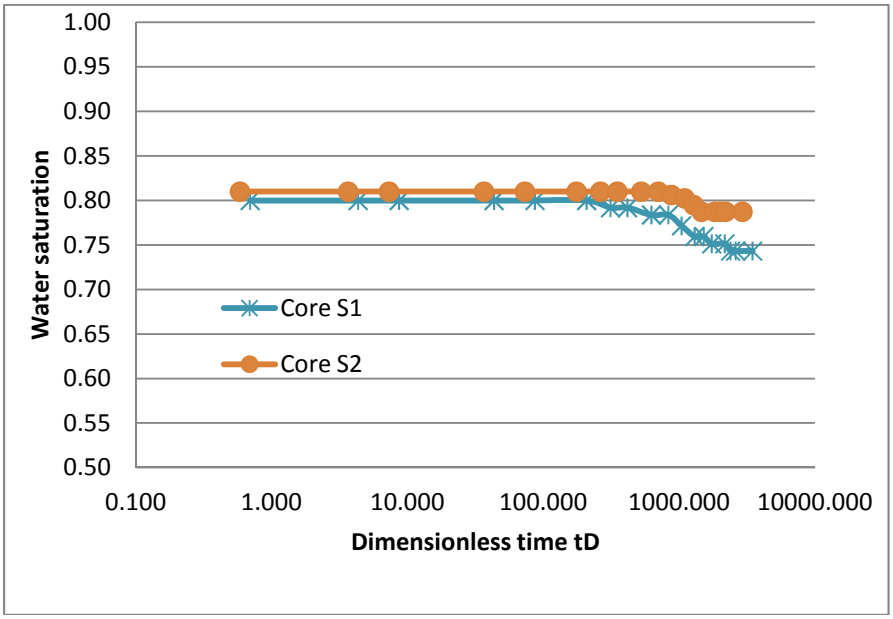

Figur 5-5: *Graph showing the free imbibition of oil as a function of dimensionless time* t_D.

After the forced water imbibition part of the experiment all the cores was at irreducible oil saturation. The remaining oil is now trapped inside the pore space by capillary pressure as explained in chapter 2.3. As there were no imbibtion of oil from the non-aged cores we have not plotted them in the graph. The aged cores showed some production of water in the mid part of the experiment.

Forced imbibition of oil

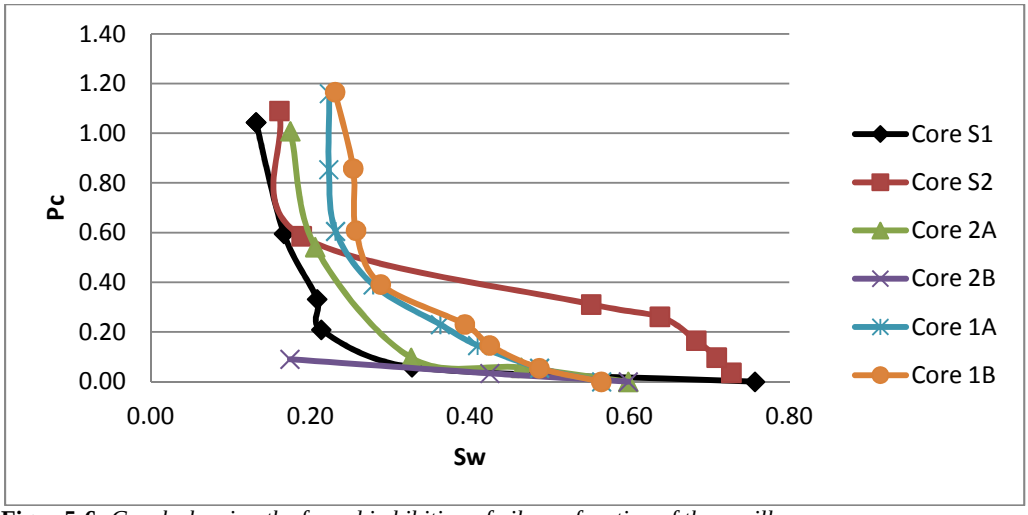

Figur 5-6: *Graph showing the forced imbibition of oil as a function of the capillary pressure*

As the spontaneous imbibition of oil proved to be quite inefficient, the majority of the movable water resides in the core at the start of this experiment. We observe that the different cores produce its water in highly different ways, from core S1 which produces close to all of its movable fluids during the few first steps of centrifuge spinning to core S2 which produces the majority of its water in the mid part of the experiment. Core 1A, 1B and to some extent core 2A have a highly coincidently graphs with a steady water production through the first half of the experiment. Core holder 2B broke at stage two of the centrifuge experiment and consequently lost all of its pore fluids.

Summary of the wetting test

	Amott Index	USBM Index
1A	0.98	1.63
1B	0.96	1.06
2A	0.91	1.05
2B	* 0.96 *	* 1.51 *
S1	-0.01	0.20
S2	0.07	0.71

Table 5-7: *Summary of the wetting test. * Core 2B: Broken core holder.*

From table 5-4 we learn that the non-aged cores are strongly water wet, and that the aged cores are neutrally wet according to the Amott index and weakly water wet according to the USBM index. From chapter 2.5.4 we remember that Dixit et al. showed an analytical relationship between the Amott and the USBM test. In figure 5.5 we have plotted the two indices, and in accordance with the method from chapter 2.5.4 we conclude because $I_{USBM} > I_{AH}$ and $-0.5<I_{AH}<0,5$, core S1 and S2 have a tendency towards a Mixed Wet Large state (MWL). Core holder 2B broke at a late state of the experiment, and the result from this core should be interpreted accordingly.

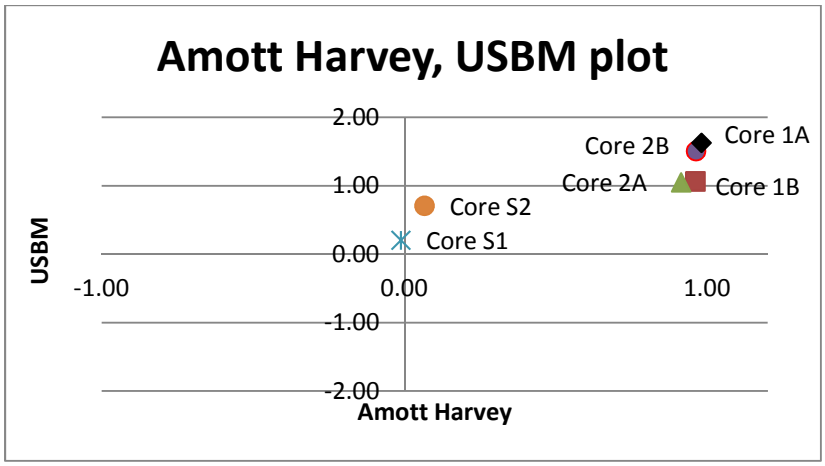

Figure 5-8: *Amott and USBM index plotted for each graph.*

5.2 Conclusion

We observe that our non-aged cores have a small deviation from 100% water wet state due to an inefficient spontaneous imbibition of water, and a small forced oil production. This could be the effect of us not allowing enough time for the cores to reach equilibrium state in the spontaneous imbibition test. In fig 5-3 we observe that after two weeks of spontaneous imbibition of water the production is flat, but it could be argued that if we allowed another two weeks off imbibition, the remaining mobile oil could have been produced spontaneously. According to Cuiec[59] the length of time before reaching the equilibrium could range from a few hours to up to two months, depending on the rock and fluid parameters. In addition our small core plugs, with a corresponding low pore volume produces a very small quantity of fluid making the room for error larger. Both in the spontaneous imbibition, and particularly in the forced imbibition, it is possible to misread the volume of produced fluid leading to a fail in calculations.

We conclude that the wetting test we applied was able to detect a change in wettability due to ageing in the two aged cores. The Amott and USBM test show some deviation in wettability, ranging from neutral wet according to Amott, and weakly water wet according to USBM. From the work of Dixi et al[26] and Skauge et al[14] we conclude that core S2 have a clear tendency towards Mixed Wet Large (MWL). Core S1 has a much lower USBM index, which could indicate a more Fractional Wet (FW) situation, where the oil-wet pores are more evenly distributed in the pore size distribution, but we are still regarding it as MWL. This is in good accordance with the belief that crude oil will displace the water in the largest pores during flooding at the initial strongly water-wet state, and the alternation of wettability will happen in the pores containing the oil, leaving the smaller water filled pores more prone to water.

6. NMR

All of the experiments in this thesis was performed on a 12 MHz Maran Ultra DRX spectrometer from Resonance Instruments (now Oxford Instruments). The instrument is capable of delivering a gradient strength of 225 gauss/cm, and operates at 35˚C. In order to ensure stable temperatures during the experiment, the sample was left in a heating cabinet over night prior to the NMR experiments. To eliminate the effect from evaporation, and avoid contamination of the NMR probe, each sample was wrapped in plastic foil.

6.1 Calibration of instrument

When I started on the measurements, the instrument had just returned from a service due to critical failure in the control unit, and upon arrival it showed a significant shift in signal to noise ratio and P90 pulse length compared to previous values. In order to set up the instrument to this new regime, a total of 80 experiments was performed at various parameter settings.

Number of scans

In order to improve the signal to noise ratio (S/N), it is a common practice to perform a high number of scans and stack the signals. The real signal from the fluids in the core will multiply, and the noise will, based on statistical theory, distribute equally in the signal improving S/N with the square root of number of scans. Hence adding 100 scans will improve S/N with a factor of 10.

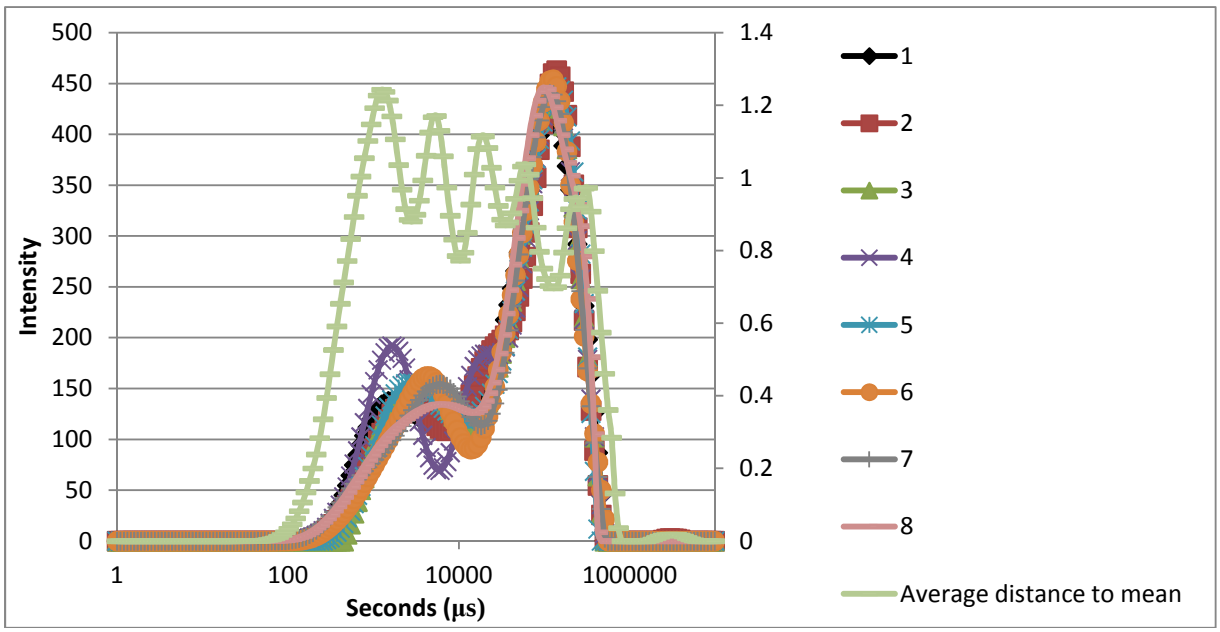

Fig 6-1: *NMR response from 7 successive experiments with 16 scans.*

When performing 16 scans, we clearly see that the variance in the experiment is significant. For each point the average distance to the mean is calculated, and we observe that it is close to 1 and largest for small T_2. In addition to a point to point variance there also exists a contrast in the total signal detected.

This is equal to the integral of the function, and we observe a 6 percent difference between the smallest and strongest signal detected.

When performing 32 scans, the signal to noise ratio is improved by almost 50% giving a much smoother graph and a better correlation between each data set. The average distance to mean is reduced to 0.6, and the largest difference in signal strength is 3%.

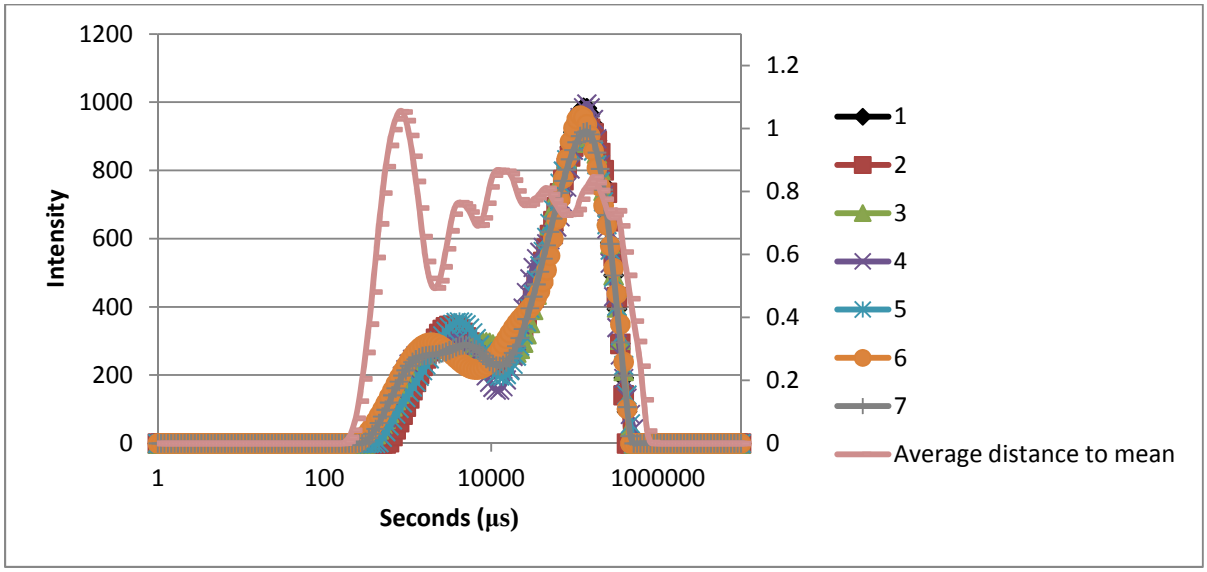

Figure 6-2: *NMR response from 7 successive experiments with 32 scans.*

Based on fig 6-1 and 6-2 we concluded to perform 32 scans from each experiment.

Setting of relaxation delay (RD)

After performing one scan the nuclei in the sample must have sufficient time to reach equilibrium before the next scan is performed. If this is not achieved it will result in a decrease in signal amplitude in the successive scan, and spurious data could be collected. In addition each echo is produced by sending a small portion of energy into the sample. This energy is later converted to heat which needs to be transported away from the sample. Because the NMR response of a nucleus is highly dependent on the sample temperature, a failure to allow sufficient time for the heat to dissipate will lead to spurious data towards the end of the experiment.

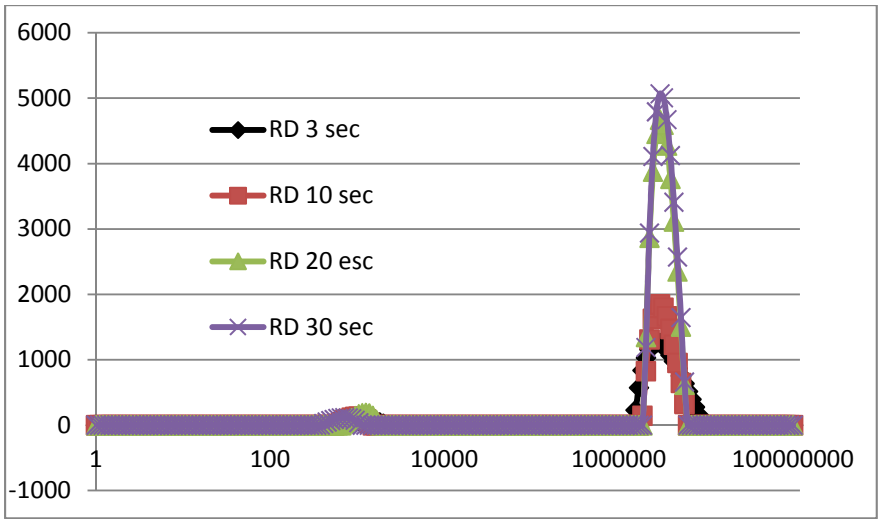

Fig 6.3: *NMR response from four experiments with 32 scans. RD varied between 3 and 30 seconds.*

In fig 6-3 we can see that the signal intensity increases significantly when increasing the receiver delay from 3 to 20 seconds. We also observe a slight increase in signal intensity when changing it it to 30 seconds. Based on fig 6-3 and the fact that S/N makes it imperative to perform a high number of scans which could lead to a change of temperature in the sample RD was set to 30 seconds.

Setting of τ

τ is the interval between the initial 90˚ pulse and the 180˚ repahsing pulse, and it controls the smallest available value of T_2. If τ is set to 500 μs, no faster value than 500 μs can be recorded. In chapter 3.5 we learned that a given nuclei will have a relaxation rate, and consequently a characteristic time constant, T_2, based on the state of the surroundings. The relaxation rate of a hydrogen nuclei imbedded in a shale, will be faster than for a identical nuclei in the water phase. This implies that if we fail to allow sufficient time for the signal from clay bound water to die, out some of the signal in our echo train will consist of clay bounded water signal which is not of our interest. τ was set to 200 μs.

6.2 Procedure

T2

A fundamental part of any NMR experiment is the transverse relaxation time, T_2. This characteristic time constant is the measure of how fast the transverse magnetization is attenuated for a given sample, and it is measured through the technique of Carr, Purcell, Meiboom and Gill (CPMG). This sequence consists of one 90˚ pulse and a loop of n 180˚ pulses as shown in fig 6.4.

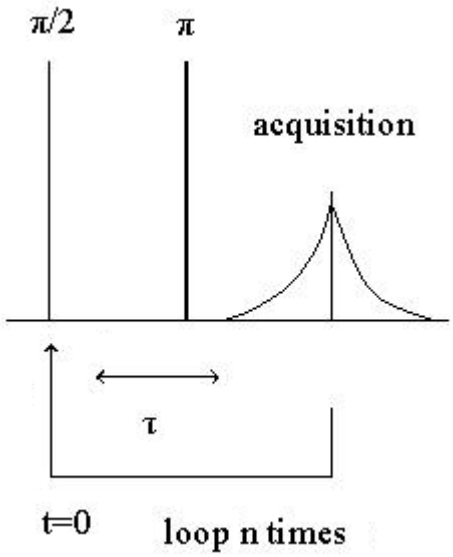

Figure: 6.4: *Schematical presentation of the CPMG spin echo experiment.*

In a typical experiment 4000 echoes is acquired, and the attenuation of the transverse magnetization is calculated by curve fitting to the following equation.

$$I = I_0 e^{-n\left(\frac{2\tau}{T_2}\right)} \qquad 6\text{-}1$$

The relaxation rate of a fluid in a porous rock is highly dependent on the amount of fluid in contact with the pore surface because of the highly effective surface relativity. In a strongly water wet rock the oil is limited to the interior of the pore while the water resides along the pore wall. In this situation the short NMR signal will be associated with water, and the long T_2 values would originate from the oil phase. When the wettability of the rock is shifted towards a more neutral or oil-wet situation, the distribution of the fluid inside the pore will also change. Some of the oil could then be in direct contact with the surface of the pore causing the T_2 value of oil to decrease. The purpose of this sequence is to detect this shift in relaxation rate.

Combined T1 and T2 measurement

The combined T_1 and T_2 experiment is an ordinary CPMG train preceded by a stimulated echo pulse.

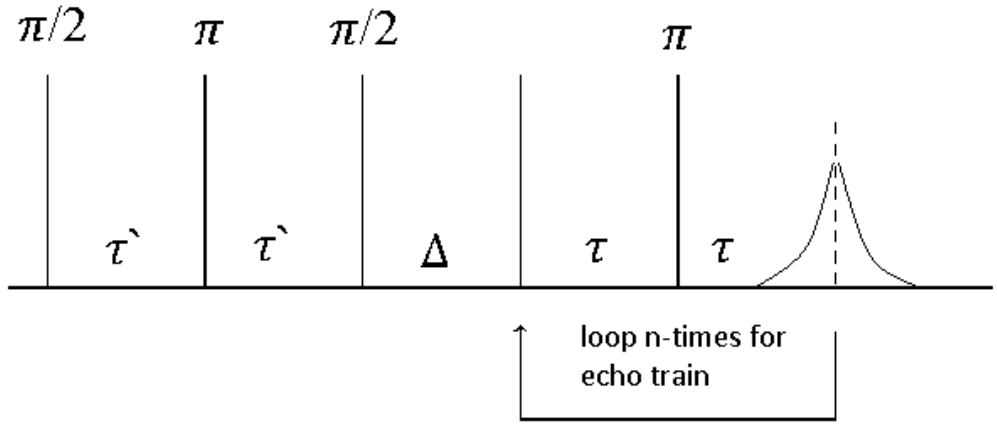

Fig 6.5: *Schematic of combined T1-T2 measurement.*

The echo attenuation for this sequence is given by equation

$$\ln\left(\frac{I}{I_0}\right) = -\frac{\Delta}{T_1} - \left[\frac{2\tau`}{T_2} + \gamma^2 G_0^2 D \frac{2\tau`^3}{3}\right] - n\left[\frac{2\tau}{T_2} + \gamma^2 G_0^2 D \frac{2\tau`^3}{3}\right] \qquad 6\text{-}2$$

This sequence is applied in order to gain information about the correlation between the longitudinal and the transverse relaxation process. By comparing the two characteristic time constants we are able to tell which mechanism that is the controlling factor in the relaxation process. As we remember from chapter 3 T_1 relaxation is related to the increase of magnetization in z-direction. This process is controlled by the energy transfer rate from the nuclei to the surroundings or lattice. The characteristic time constant T_2 is related to the reduction of magnetization in the transverse plane because of depahsing of precession. This process is both sensitive to the energy transfere associated with T_1 relaxation and by the existents of internal field gradients. From this simple explanation we see that if $T_1 = T_2$ the controlling factor in the relaxation process must be the energy transfer from the excited nuclei to the surroundings. This situation where the two characteristic time constants are equal is common for a bulk fluid. Because the different nuclei have roughly the same surroundings they will also experience roughly the same magnetic field leading to a relatively long dephasing time. On the other hand if the nuclei in the sample experience a large variety in local magnetic field there will be a considerable variation in the subsequent Larmor frequency. This situation could happen for a fluid close to the pore wall in a porous media. Because of the magnetic susceptibility differences between the fluid and the material composing the matrix there will be induced a large variation in the Larmor frequencies, which leads to a quick dephasing of the transverse magnetization. Because $T_1=T_2$ indicates fluid at bulk condition, and $T_1 \neq T_2$ indicates a fluid close to the pore wall the knowledge about the T_1T_2 ratio could reveal a great deal about the wetting state of the porous media.

Internal gradient – T_2 measurement

As a consequence of susceptibility differences between the solid grains and pore fluids, there will be a considerately impact on the NMR response due to internal gradients. In a fairly homogeneous rock, such as Berea sandstone, the strength of these internal gradients is a function of the pore size and the proximity to the pore wall. The strongest internal gradients are associated with small pore sizes and close proximity to the pore wall, and small internal gradients are located in the interior of the largest pores.

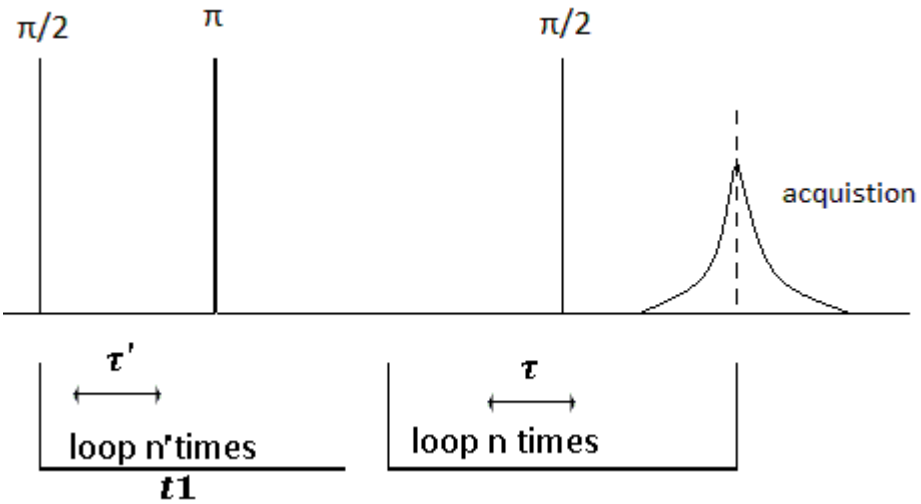

Fig 6.6: *Schematical interpretation of the combined G_0 – CPMG sequence.*

The echo attenuation for this sequence is given by the following equation:

$$M(\tau`, 2n\tau) = \int\int f(DG_0^2, T_2) e^{-\frac{t1+2n\tau}{T_2}} e^{-\frac{\gamma DG_0^2 \tau`^2 2n`\tau`}{3}} dT_2 d(DG_0^2) \qquad 6\text{-}3$$

By applying this sequence we are able to gain information about the correlation between the transverse magnetization and the internal gradient strength. Because strong internal gradient are associated with the wetting fluid, this correlation could generate valuable information about the wetting state of the rock.

Diffusion - T2 measurement

When T_2 relaxation curves are analyzed from an ordinary CPMG measurement of a multicomponent porous media system, the broadening of the line width caused by the presence of internal gradients makes it difficult to find direct information regarding the type of environment experienced by each component. A combination of the pulsed field gradient (PFG) method and a CPMG experiment will increase the amount of information obtained from the NMR experiment and adding insight to the study of the system[60].

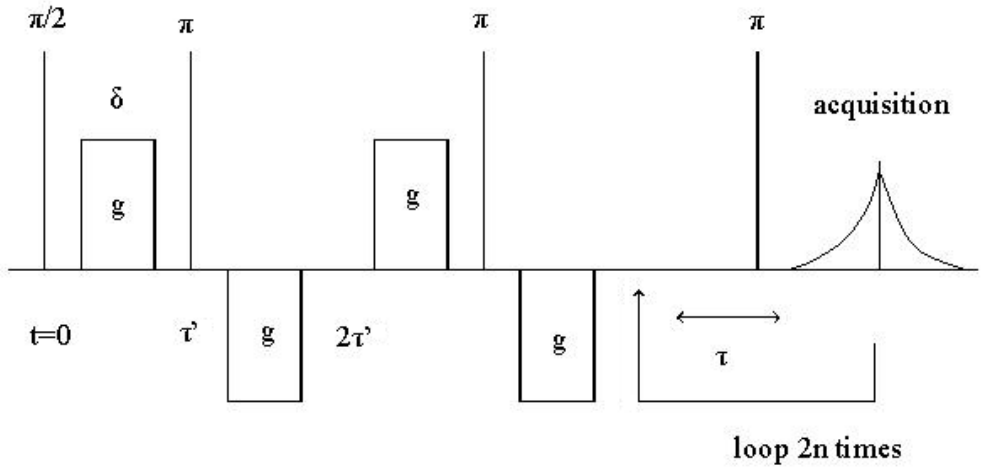

Figure: 6.7: *Schematical presentation of the PFG and CPMG spin echo experiment.*

Bipolar gradients are applied in order to suppress cross terms between applied and internal gradients. The echo attenuation for such a sequence corrected for sinusoidal shaped gradients, can be written:

$$\ln\left(\frac{I}{I_0}\right) = -\left(-\frac{2n\tau}{T_2} + \gamma^2\left(\frac{4g}{\pi}\right)^2 \delta^2 D(2\tau')\left(\frac{3}{2}\tau' - \frac{\delta}{8}\right)\right) \qquad 6.4$$

The purpose of applying this sequence is to distinguish between the fast and the slow diffusing components. This is done by performing several experiments with continuously increasing gradient, strength to a point where the signal from the fast diffusing component is sufficiently suppressed. With the use of the 2D Laplace Inversion program, we are then able to correlate a specific diffusion coefficient to a specific relaxation value.

When measuring diffusion weighted T_2 values from the systems Seland et al, were able to distinguish quite easily between the signal from oil and water based on diffusivity. They also found that when mowing from water wet system to oil wet system, the measured diffusivity of oil was decreased indicating that the diffusion of oil is more restricted in this system. The properties of water on the other hand was indicating less restriction on the water phase, with diffusivity and transverse relaxation times closer to bulk properties.

7. Results

The result section is divided into four parts for the four experiments performed

7.1 CPMG experiment

CPMG – Bulk fluids

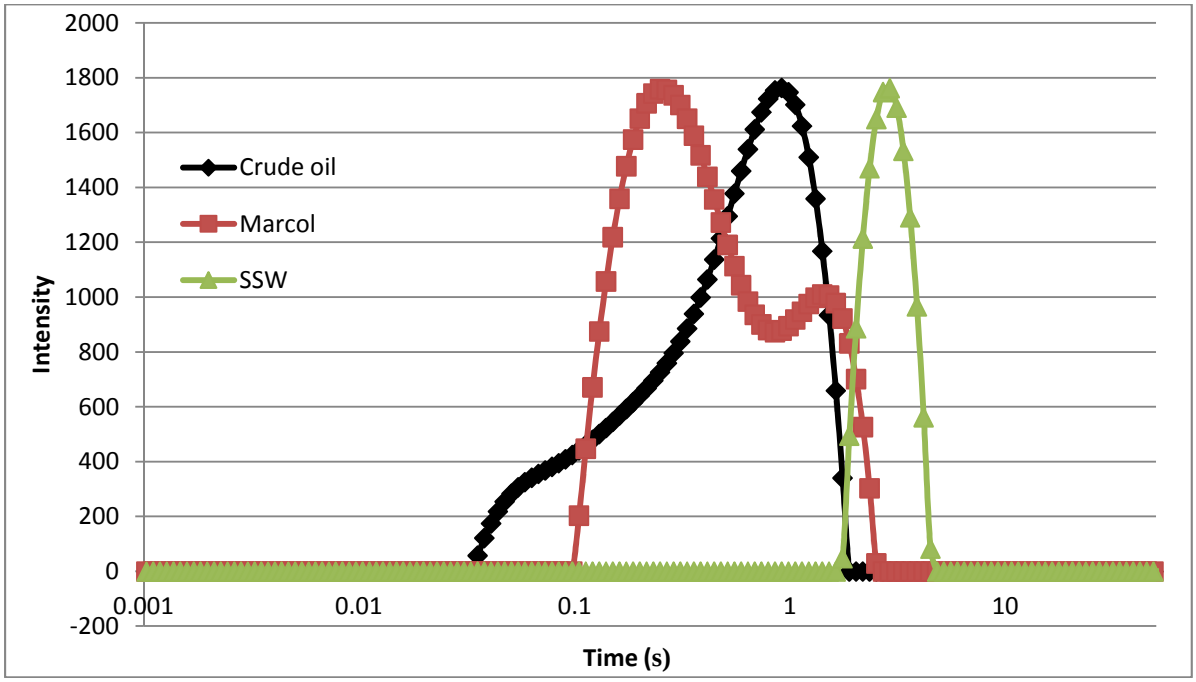

Figure 7-1-1: *Transverse relaxation values for the three fluids at bulk condition.*

Based on figure 7-1-1 we can easily state that the three fluids got different composition. The water got a sharp peak at 3 seconds. Because of the homogeneous nature of the water the peak of the T_2 value is very distinct.

Marcol got two peaks at 0.2 seconds and 1.4 seconds respectively. Marcol is a pure mineral oil produced by Exxon Mobile, and should produce a sharp peak in the same way water did. However, because of the very high viscosity of the clean Marcol it was decided to dilute it with 40% xylene. When calculating the integral of the T_2 distribution we recognize that 70 per cent of the signal is located in the 0,2 second peak, and 30 per cent is located in the peak at 1.4 second. Since we know the volumetric ratio of the mixture we conclude that the peak at the lowest T_2 value originates from the pure Marcol and the longest T_2 relaxation is from the diluting agent Xylene.

Crude oil got an entirely different T_2 distribution with a large peak at 1 second, and a tail for smaller T_2 values down to 0.04 seconds. Crude oil is diluted with the same ratio of Xylene, and when investigating the distribution a little closer we see that the large peak at 1 second is due to the Xylene, and the broad tail is from the pure crude oil. The broad tail we observe in the crude oil is typical for this fluid. This is due to the high number of components in the crude.

From fig 7-1-1 we have observed that the pore fluids got some variations in transverse relaxation. The largest contrast is between the oil and the water, but also some variation is seen between the oils. Because of this we expect to see some variation in the NMR respons when measuring the transverse relaxation times in the cores. Largest contrast is expected between the water filled cores and the oil filled cores, but we also expect that cores saturated with crude oil should produce a broader T_2 distribution than the cores filled with mineral oil.

CPMG measurements at S_{iw}

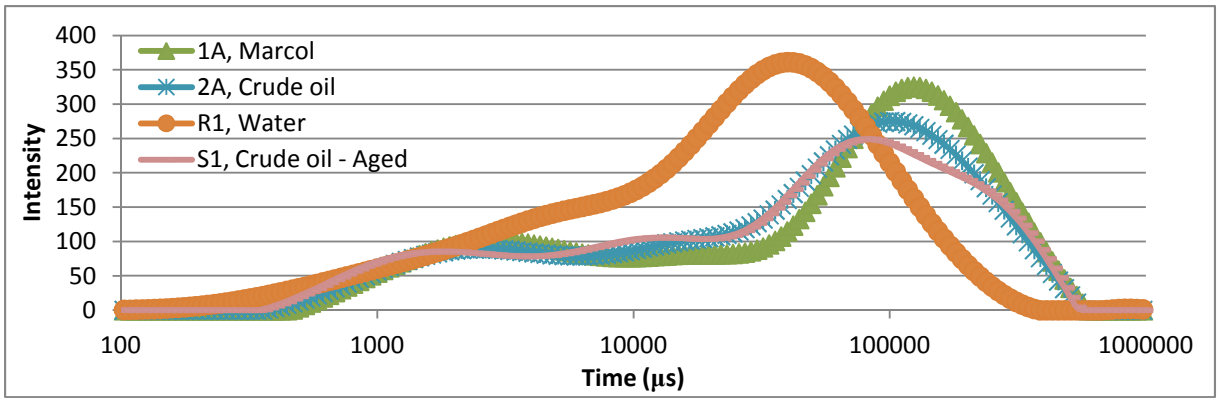

Fig 7-1-2: *Plot of the transverse relaxation at Siw for four cores.*

We observe that the water filled reference core got a significantly divergent T_2 distribution. This is a typical NMR respons from a core at 100% saturation. The large peak at 0.04 second comes from water in large pores, where the majority of the water is located. The tail for decreasing T_2 values originates from water in smaller pores where the increased surface to volume ratio gives an increased chance for the fluid to undergo surface relaxation.

When comparing the T_2 values from saturated cores with the corresponding T_2 values for the corresponding bulk fluid, we identify two important aspects. While transverse relaxation times for bulk fluids is longest for water, the core at $S_w = 1$ got the fastest relaxation times of the four systems we are investigating. This is due to the fact that all of the fluid in the completely water saturated system got access to the pore wall, and it indicates that the requirement for the fast diffusion approximation is fulfilled. In core 1A, 2A and S1 the oil is more restricted from reaching the pore surface because of the presence of water as films and/or water fills the smallest pore entirely.

We observe that core 2A and S1 got the broadest peak of the three cores with two pore fluids. We can also see that these cores got a higher intensity of nucleus relaxating at the interval 0.1 second to 0.5 second. This is in good correlation to the result from the measurements on the fluids at bulk condition where crude oil had a long tail for shorter T_2 values.

Since core 1A, 2A and S1 got two fluids present in the system this complicates the analysis of the T_2 signal. From fig 4-3 we know that the saturation at irreducible water saturation is approximately 30

per cent water, and fairly consistent for all of our cores. From fig 5-8 we found that our oil wet cores are mixed wet large (MWL) indicating that most of our oil will reside in the largest pores. This will also hold for the strongly water wet non-aged cores. Consequently this implies that most of the oil signal will come from oil residing in the largest pores, giving long relaxation values and the water signal comes from the smallest pore producing short T_2 values. In fig 7.1-3 we have performed a qualitative analysis of the T_2 distribution from the non-aged core 2A.

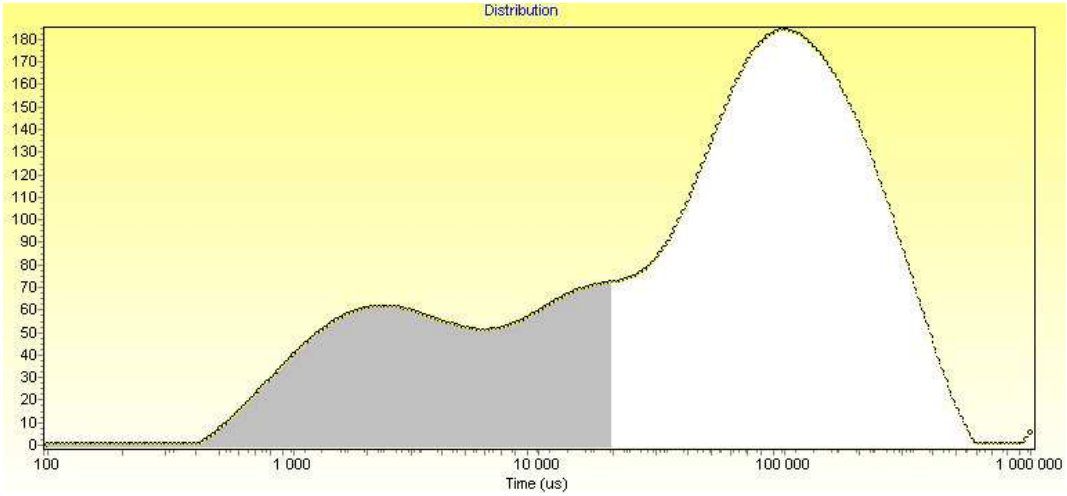

Fig 7-1-3: *Qualitative analysis of the T2 distribution for core 2A where 30 per cent of the area is coloured grey.*

When colouring the lower 30 per cent of the distribution, corresponding to 30 per cent water, we can see that this divides the distribution into a large white peak at 0.1 second and a long grey tail down to 200 μs. This coincides with our understanding of the fluid distribution presented above, but it is sadly very inaccurate. Because of the broadening of the peaks there is hard to tell the exact position of the fluids. In addition, this approach neglects that T_2 relaxation is dependent on other factors than pore size. As we saw in figure 7-1-1 above the crude oil got broad T_2 distribution which makes it a bit harder to do a clean correlation between T_2 values and pore size. From chapter 4 we could see that the aging procedure have resulted in a wettability of the core S1 and S2 close to neutral. This implies that some of the oil will be located close to the pore wall resulting in faster T_2 relaxation. Since the intention of the relaxation measurements is to measure the effect from aging the approach from fig 7-1-3 will not work.

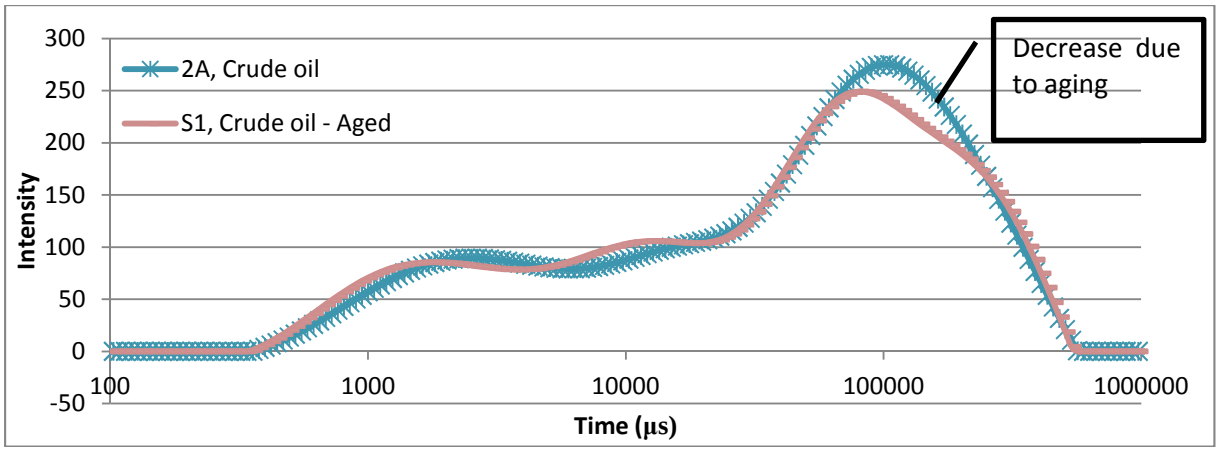

Figure 7-1-4: *Comparing the T_2 distribution from aged core, S1, and non-aged core, 2A.*

When comparing the non-aged and aged cores we observe a shift towards faster relaxation values in the T_2 peak at 0.1 second originating from the oil phase. When comparing the peak from aged and non-aged core we observe a 6% decrease in the measured T_2 signal. We can also see a slight increase in intensity of T_2 values at 0.01 seconds. With reference to table 4-3 we state that the only thing differencing the two samples is the wetting state, and we conclude that the changes we see in T_2 relaxation is because of this change towards more neutral wet. The physical explanation on what`s happen is that because of the altered wetting state of the pore surface there have been a transportation of fluid from the interior of the pore, towards the pore surface compared to in the non-aged core. This oil that now have the opportunity to diffuse into contact with the pore surface will have a smaller T_2 causing a decrease in the peak at 0.1 second and an increase in the peak at 0.01 second.

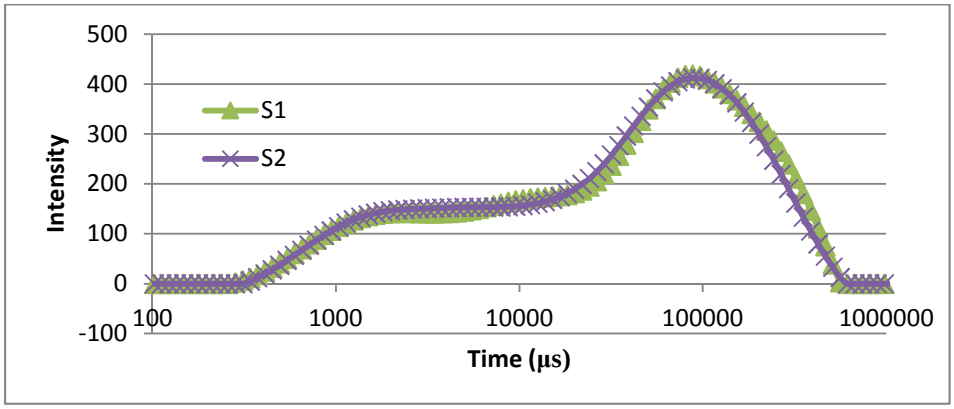

Figure 7-1-5: *Comparing the T_2 distribution from two aged cores S1 and S2*

When comparing the CPMG signal from the two aged cores S1 and S2 we observe that the T_2 distribution is virtually identical. This coincides well with table 4.3 where all the core characteristics are close to identical. Even though they don`t share the same saturation and wetting state, this is not enough to give them a difference notable in the T_2 distribution.

CPMG measurements at S_{or}

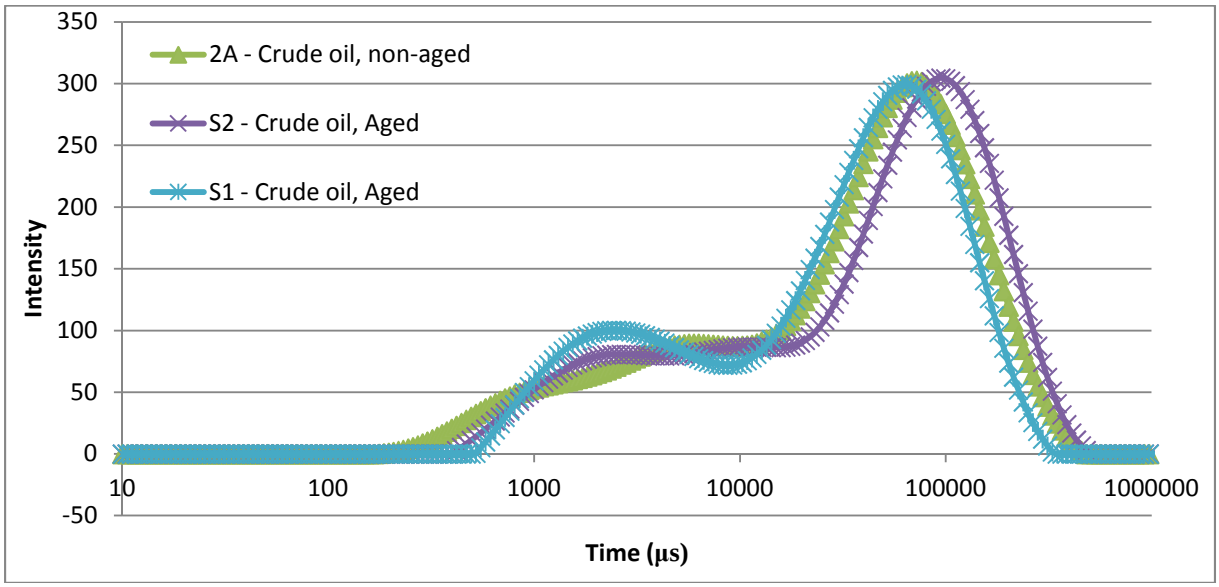

Figure 7-1-6 *Comparing T_2 distribution from crude oil saturated cores at aged and non-aged state.*

When we compare the T_2 distribution from the crude oil saturated cores we observe a distinct contrast between the aged and the non-aged cores. Where the non aged core got a continuously decreasing tail towards faster T_2 relaxation, the two aged cores, and in particularly S1, shows a distinct peak at 2 ms. We also notice that when comparing the main peak in the two aged cores S1 have a shorter T_2 values than what is seen in S2. This could come as a consequence of the wetting state. As noted in section 5.2 both our aged cores are considered mixed-wet-large. This is a situation where the largest pores are oil-wet, and the smaller pores are water-wet. But as seen in figure 5.8 the core S1 is close to being fractionally wet. In this wetting state the oil-wet pores are more randomly distributed between small pores and large pores. Because the oil resides in slightly smaller pores in core S1 compared to S2 this may explain why the main peak of S1 have smaller T_2 values than what is seen in S2.

7.2 Difusion-T_2 correlation

Difusion-T_2 correlation – S_{wi}

First of all we take a look at the diffusion-T_2 correlation for the bulk fluids.

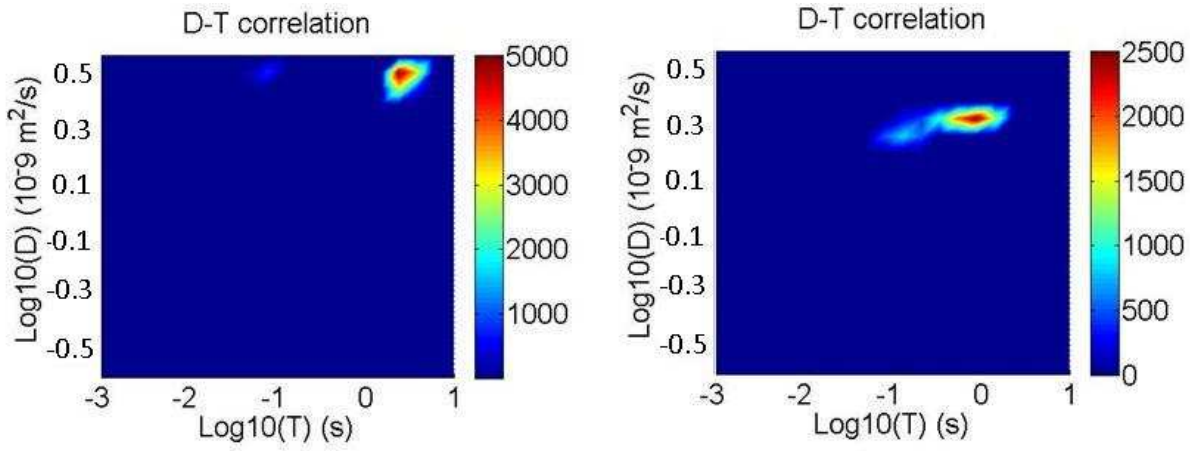

Figure 7-2-1: *Image showing diffusion-T2 correlation for brine and crude oil at bulk condition. Brine to the left.*

Because the measured diffusivity is strongly dependent on the strength of the gradients applied, the calibration of these gradients is important. In our experiment we have chosen to set bulk diffusion of water to $2.9*10^{-9}$ m^2/sec which is well known in the literature [61]. For the rest of the diffusion experiment water at bulk conditions have been used as calibration.

As seen in figure 7-2-1 brine produces a distinct peak at 3 second at a diffusion coefficient of $2.9*10^{-9}$ m^2/sec. We also observe that the T_2 distribution found in this experiment coincides quite good with the distribution found in the standard CPMG experiment.

The crude oil got a main peak for diffusion coefficient of $1.75*10^{-9}$ m^2/sec and a transverse relaxation rate ranging from 1 second to 0.1 second. In addition we notice that the fastest relaxating components in the oil, associated with heavier components, have a lower diffusivity. This is in accordance with the expected result.[62] Water consists of only one component and at ambient pressure and temperature conditions it is expected to have a high diffusivity. Our oil is a multi component system and because of the higher viscosity we expect a lower diffusivity.

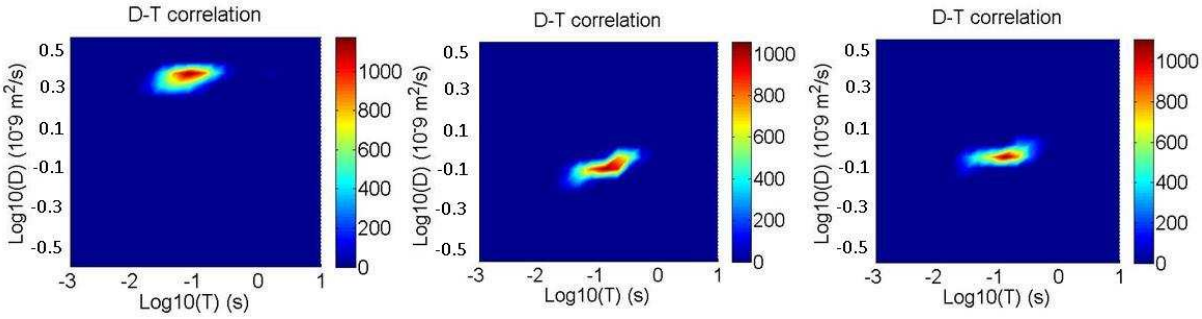

Figure 7-2-2: *Image showing diffusion-T_2 correlation for brine saturated core to the left. A non-aged core at S_{wi} in the middle and aged core at S_{wi} to the right*

The fully brine saturated core got a diffusion coefficient of 1.75 $*10^{-9}$ m^2/sec, which is lower than the water in bulk phase and as expected according to previous experiments[63]. Because of the restricting nature of the pore wall the measured diffusion coefficient appears to be lower. The much faster transverse relaxation rate found in the water phase is due to the interaction between the fluid and the pore wall. We observe that when the echo train is preceded by a diffusion encoding sequence some of the water signal is lost. We can see that a lot of the signal associated with water, having T_2 values around 0.001 second is lost because of dephasing of molecules diffusing in internal gradients.

When looking at the systems with two fluids present we can see that the entire signal at low T_2 values, which is likely to originate from the water phase, is lost because of the effect explained above, and only oil signal is preserved. We can see that the non-aged core got a T_2 distribution ranging 1 second to 0.01 second with a diffusion coefficient of 0.6-1.5 $*10^{-9}$ m^2/sec, where the faster diffusing components got the longest transverse relaxation values. This behaviour is in good accordance with what was observed for the oil at bulk conditions. However, in the bulk signal in figure 7-2-1 the majority of the oil signal had the fastest diffusion. In figure 7-2-2 the opposite situation appears. This is explained by another mechanism. Because of the wetting state of the non-aged core the oil will reside in the interior of the pores. In the largest pores the oil phase has more space to move, and we measure a diffusion coefficient closer to the bulk values. In the smaller pores the oil feel more restriction due to the presence of the water film and the confined space, hence a lower apparent diffusivity is measured. The combination of these two mechanisms form the signal observed in figure 7-2-2.

In the aged core the transverse relaxation values is close to what we measured in the non-aged core, but the diffusion coefficient is more uniform throughout the T_2 distribution. This may be a consequence of the differnet wetting state. Because the oil is the wetting phase in some of the pores, it will cover a larger surface area, presumably both the interior of the pore and close to the pore wall. In this situation the oil may experience less restriction and the apparent diffusion is higher than for the non-aged case. Seland et al[64] found the opposite situation when investigating water and oil in

packings of water-wet and oil-wet glass beads. In the strongly oil wet case he found that the oil was experiencing more restriction, giving a lower apparent diffusion coefficient. The system he investigated was however quite different from what we are looking at. He used glass spheres with oil-wet surface packed in a small tube. After he introduced the pore fluid he used ultrasonic stirring in order to distribute the fluids inside the sample, giving a more uniform fluid distribution throughout the sample allowing oil to enter a wider range of pore sizes. In this situation a high ratio of the oil will be located close to the pore wall as surface films, contributing to the reduced diffusion coefficient. Because of the aging technique applied to our cores, fluid distribution is highly dualistic, where the majority of the oil is located in the largest pores. A change towards oil wet will then only enlarge the oil globes and increase the apparent diffusivity.

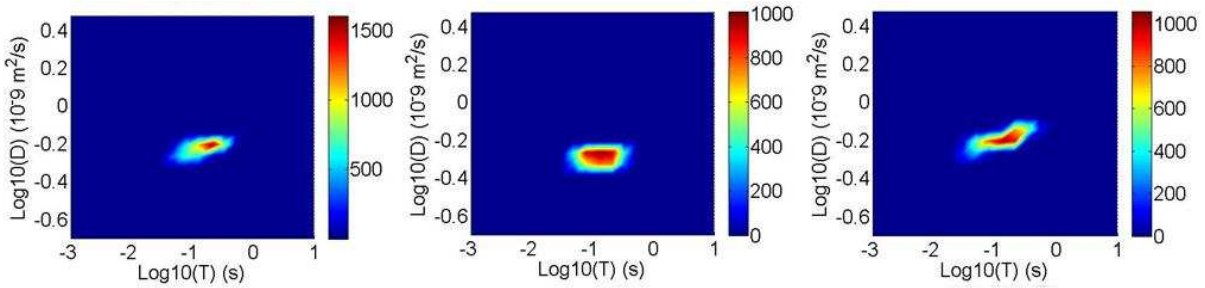

Figure 7-2-3: *Image showing diffusion-T_2 correlation for the marcol saturated core to the left, it`s sister core 1B in the middle and crude oil saturated core 2A to the right.*

Finally I want to present the data from the cores saturated with marcol and water. As we observed in the standard CPMG experiment the NMR respons from Marcol is not behaving like the crude oil. This makes it hard to draw any definite conclusions regarding the wetting state from these samples, because we don`t know whether the measured signal is influenced by wetting or by the pore fluid. In figure 7-2-3 we observe that 1A show some of the same characteristics as 2A. Observe that the intensity scale is not identical, which means that the tail for smaller T_2 values is more distinct than it seems. The lower diffusivity for small T_2 values could come from the restriction small oil droplets feel from the presence of the water phase. In core 2B we see that the intensity of the signal is more evenly distributed in the signal peak. This could indicate a better continuity of the oil phase as explained for core S1, or it means that the oil phase is more evenly distributed between large and medium sized pores. Given the very strong water wet state of this core we believe that the latter is more plausible.

Difusion-T_2 correlation – S_{or}

When changing the saturation to S_{or} most of the oil was produced from the cores. Through flooding with water a saturation of S_{or} = 0.2-0.3 was achieved. This drastically changes the measured diffusivity of the pore fluid.

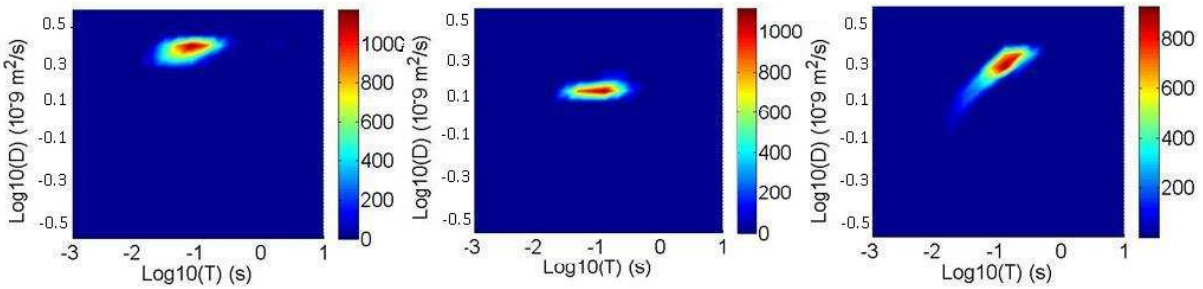

Figure 7-2-3: *Image showing diffusion-T_2 correlation for brine saturated core to the left. A non-aged core at S_{or} in the middle and aged core at S_{or} to the right*

When changing to water being the most dominant pore fluid we would expect the water phase to give a clear voice in the 2D image from the core. Because of the nature of the NMR sequence applied the small percentage of water found in the smallest pores in cores at Swi was thought to have died out before we were able to measure it. In the S_{or} case the percentage of water is so big that it is obliged to fill more than just the smallest pores, and because of the longer T_2 values associated with the larger pores we should be able to detect some signal from the water phase in this experiment. Furthermore, because of the even longer T_2 values of the oil phase we should also be able to detect some signal coming from the oil phase. What we expect from this experiment is two distinct peaks, one originating from the oil phase, the other originating from the water phase.

However when we are looking at fig 7-2-3 we are only seeing one peak for each core. We are observing that the diffusion coefficient have been increased for both of our crude oil filled cores (in the middle and to the right in fig 7-2-3). For the non-aged core we now observe a uniform diffusivity closer to bulk properties for oil. We believe that the majority of the signal we now observe is originating from the water phase. Because the two peaks have blended together we do not see two peaks as expected, but rather one peak that got some of its characteristics from both fluids.

In the aged case we observe a diffusivity ranging from 0.7-1.75*10^{-9} m^2/sec where the lowest diffusivity is observed for the fastest relaxating components. Inside the pore the high volumetric ratio of the water phase now has displaced the oil from most of the pore, and the oil phase can now roughly be divided into two locations. Some of it resides in the interior of the pore as droplets. The other part of the oil phase is now, because of the altered wetting state of the rock located as oil films on the pore surface. Because the water phase now lays strict limitations on the oils ability to diffuse, we are measuring a smaller diffusion coefficient for this oil. In fact this is the opposite situation to what we

observed in the S_{wi} case. When oil was the most abundant pore fluid in the rock, the altered wetting state allowed oil to contact the surface of the rock which increased the continuity of the oil phase. In that case we observe an increase in the measured diffusivity. In the S_{or} case on the other hand, the oil films are being so restricted by the water phase that we are measuring a decrease of the diffusion coefficient for decreasing T_2 values. However, we notice that the diffusivity in the aged core has increased significantly more than what we see in the non-aged cores. This could come as a consequence of the much higher water saturation in S1. According to table 4-3 the saturation is S_w=82 and S_w=0.72 in S1 and 2A respectively. Because of this higher saturation of water in S1 the signal will have more of the water characteristics than in the non-aged core 2A. Since water at bulk conditions have higher diffusivity than oil it results in the signal in fig 7-2-3.

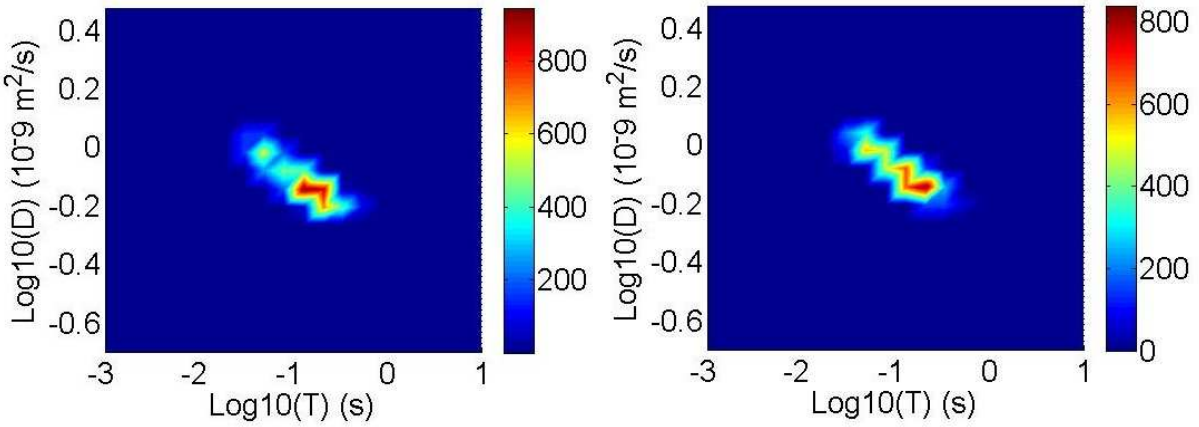

Figure 7-2-3: *Image showing diffusion-T_2 correlation for the two marcol saturated cores. 1A and 1B from left to right.*

The core saturated with marcol got a very peculiar signal in the S_{or} case. With increasing diffusion coefficient for decreasing T_2 values these cores don`t behave quit dissimilar to what we have found in the previous cases, and what we expect from the theory. However when we look at table 4-3 we observe that the saturation in core 1A and 1B is S_w=0.61 and S_w=0.75 respectively. This means that in core 1A the water affect the signal to a very high degree, increasing the apparent diffusion coefficient. This could explain the high diffusivity for low T_2 values in core 1A. In core 1B the saturation is almost identical to what we find in core 2A, and we would expect that it showed some of the same features. When it does not this is likely because of the nature of the marcol in core 1B. In the CPMG experiment we saw that marcol at bulk conditions got a high peak at low T_2 values compared to crude oil (fig 7-1-1). This high peak that corresponds to pure marcol, most likely have a higher diffusivity than the heavy components of the crude oil with similar T_2 values. Hence this could explain the high diffusion coefficient we observer at low T_2 values in core 1A and 1B compared to 2A

7.3 Internal gradient-T_2 correlation

Internal gradient-T_2 correlation – S_{wi}

The standard user interface of the Maran Ultra DRX spectroscope does only allow single scans, so in this thesis where each core sample have been scanned more than 70 times a automated script was developed in order to have the experiments done in a timely manner. Because of some misunderstandings and poor quality control of our script we vary τ in equation 6.3. This means that instead of varying the echo distance in the first loop, we varied it in the second loop, meaning that we got a decoding from internal gradients in both the first and the second half of equation 6.3. Because this equation no longer is valid we can no longer decode the effect from internal gradients

Unfortunately this error was not detected before after flooding to S_{or}. Because of limited time and because we did not want to subject the cores for another flooding of oil it was decided that it was sufficient to only present data from S_{or}.

Internal gradient-T_2 correlation – S_{or}

When the water saturation increases in the water wet core, the water displaces most of the bulk oil leaving only droplets of oil in the interior of the largest pores. In the more oil wet core some of the remaining oil will reside as surface films experiencing high internal gradients and fast T_2 relaxation. In water wet cores the oil will according to the theory primarily remain as oil droplets in the largest pore, while water occupies the volume close to the surface and the small pores.

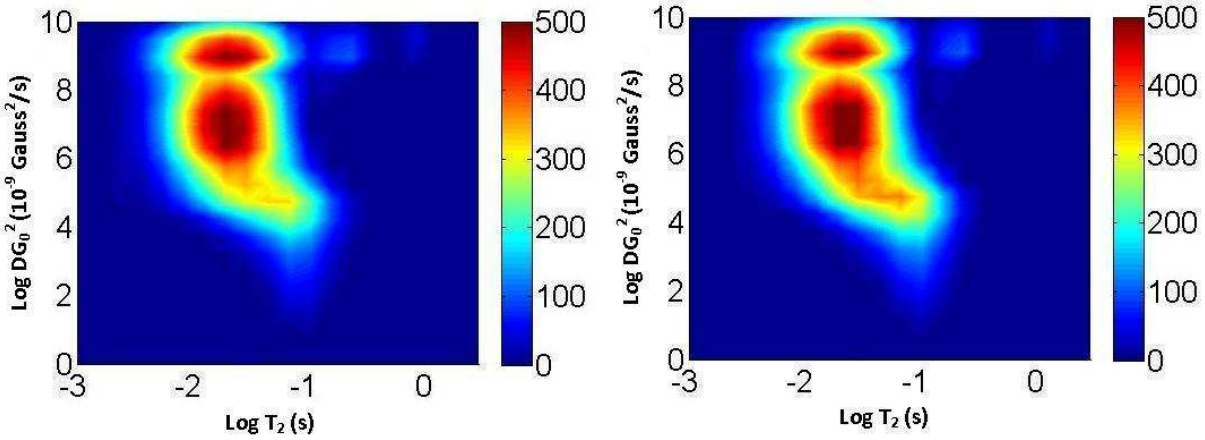

Figure 7-3-1: *Image showing G_0-T_2 correlation for two brine saturated cores. R1 to the left and R2 to the right.*

In figure 7-3-1 we see the 100 per cent brine saturated reference cores. We observe that the 2D image correspond poorly with the corresponding CPMG plot in section 7.1 having a distribution entirely located between 0.1 and 0.01. The reason this happens is because of the nature of the NMR sequence applied. Because of the encoding for internal gradients part that precedes the echo train all T_2 values shorter than 0.005 have died out before the acquisition of the transverse magnetization starts. However, since the fluid represented by these short T_2 values are thought to be water in small pores and micro pores in all of our samples we believe that this should not affect our experiment in any negative way

.

In figure 7-3-1 we observe that fluid with small T_2 values are experiencing high internal gradients and fluid with long T_2 values are experiencing much smaller internal gradients. This is in good accordance with our theory in section 3.6 and with other experimental results[64]

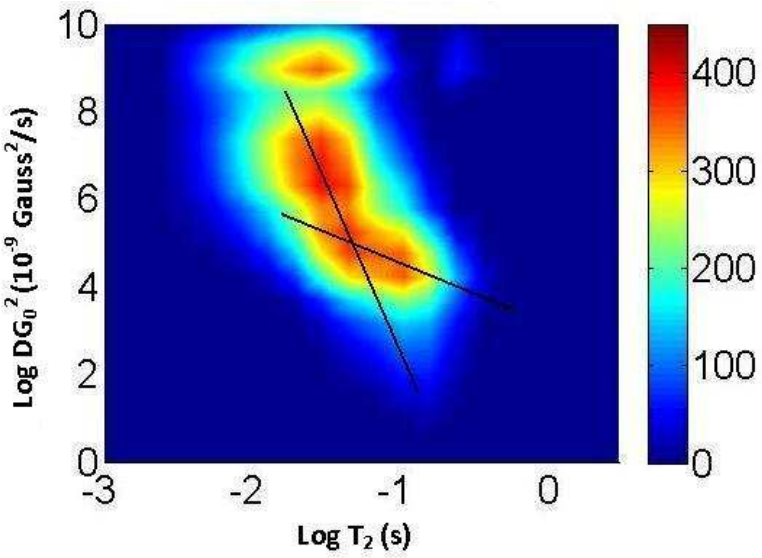

Figure 7-3-3: *Image showing G_0-T_2 correlation for the non aged core 2A with two lines representing DG_0/T_2 ratio.*

When comparing the 2D image from the water filled reference cores and the core saturated with crude oil and water at S_{or} we notice that the signal in core 2A extends further towards long T_2 values. This coincides well with what we saw in the standard CPMG experiment in figure 7-1-2. Because this is a two component system where one of the fluids have strict limitations on the ability to contact the pore surface this inevitably leads to longer T_2 values in the T_2 distribution. We also recognise a distinct shape. While the DG_0/T_2 ratio is constant and strongly decreasing for short T_2 values it flattens out significantly at T_2=0.08 second. This is indicated by the two trend lines. We believe that the reason for this behaviour is the presence of the oil phase. Because the oil has very little contact with the pore surface it will experience a much weaker range of internal gradients. With reference to our theory in chapter 3.6, internal gradients are dependent on the distance between the internal gradient centres and the nuclei. Even if the oil is separated from the surface by only a thin layer of water, this could impact the effect from internal gradients. Since we in this core have reached S_{or} there is likely to be a large volume of water separating the small droplets of oil from the surface.

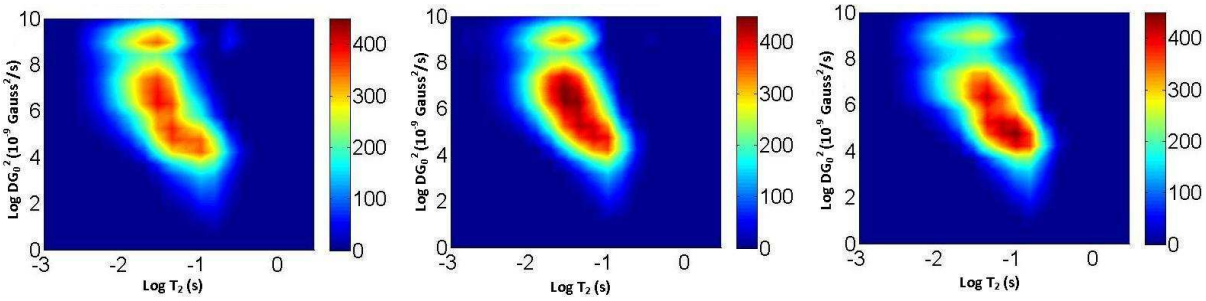

Figure 7-3-4: *Image showing G_0-T_2 correlation for the non-aged core 2A, and the aged cores S1 and S2 from left to right respectively.*

When comparing the non-aged cores to the aged cores we instantly recognise a difference between the two wetting states. While the non-aged core got a significantly shift at T_2=0.08, we do not see any of

this in the two aged cores. We believe that this is because the altered wetting state has allowed the oil phase to contact the surface. Because the oil likely to have more contact with the surface in these cores we do not see the same shift in the trend for core S1 and only a slight shift in core S2.

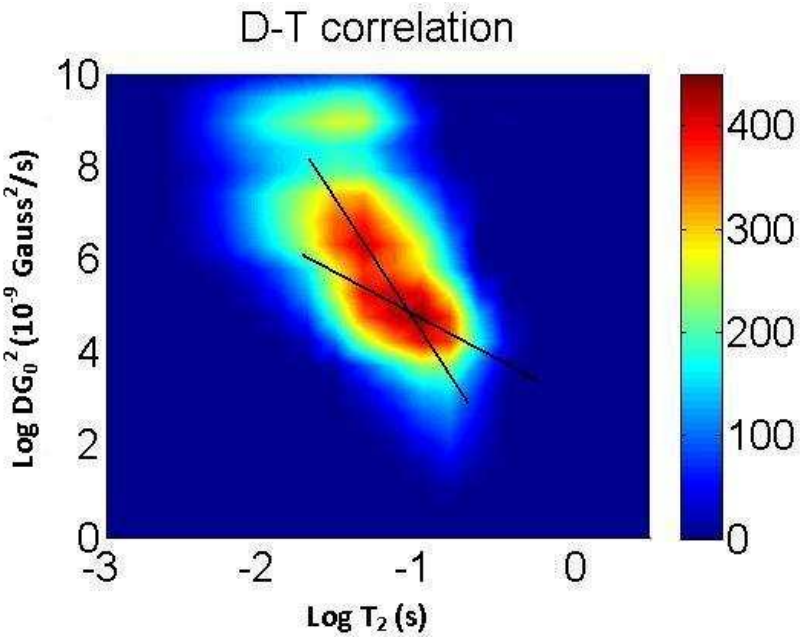

Figure 7-3-5: *Image showing G_0-T_2 correlation for the aged core S2 including trendlines*

When looking at core S2 we observe that there is a weak shift in the trend lines at 0.1 seconds. Although being weak this indicates that the oil phase in this core does not have as strong connection to the surface as we observe in core S1. This is also confirmed by the wetting test in section 4.6 and the data from standard CPMG experiment explained in section 7.1

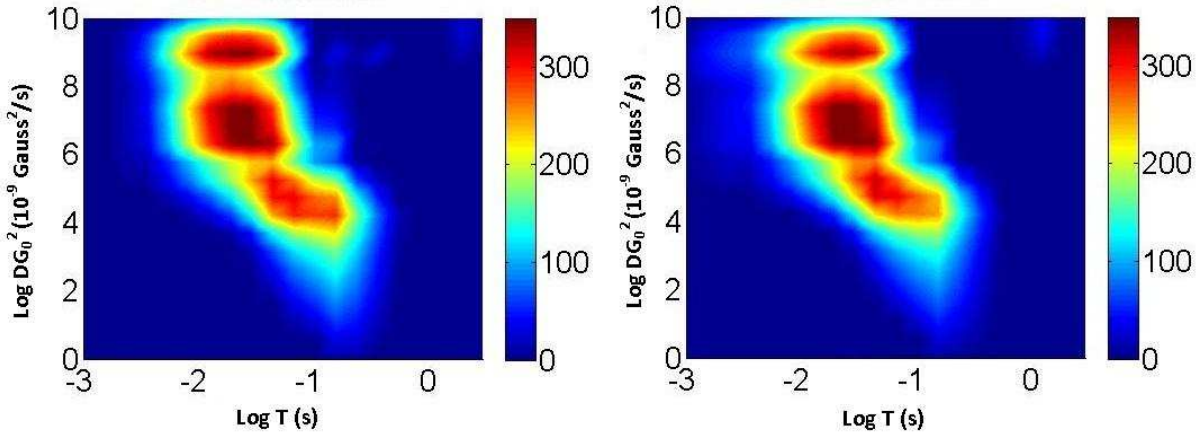

Figure 7-3-6: *Image showing G_0-T_2 correlation for the non-aged marcol saturated cores 1A and 1B from left to right respectively.*

We observe that the marcol saturated cores got many of the same characteristics as the non-aged core 2A. The 2D image from these two core also have a hinge point at 0.05 second indicating that the oil are restricted from contacting the surface of the pore. We observe that because of the smaller T_2 values

of marcol, we see that more of the signal is located at low T_2 values and that the hinge point is located at a slightly lower T_2 value.

7.4 T1-T2 correlation

T_1-T_2 correlation – S_{wi}

For a nucleus in a porous media there are two major contributors to relaxation of its excited state. Interactions between the nuclei and the surroundings that cause energy transfer to the surroundings, and dephasing of phase coherence which causes a reduction of the transverse magnetization. For T_1 only the former is contributing to the relaxation, but in T_2 relaxation the dephasing of phase coherence is both affected by the energy transfer to the surroundings and by the influence of internal gradients. Consequently if we find that our T_1T_2 plot is close to the T_1=T_2 line it means that all the water molecules in the rock have an identical T_1/T_2 ratio and that relaxation in this rock is caused by a single mechanism throughout the sample. Any distribution of T_1 and T_2 is only due to the variation in the local surface to volume ratio, or pore size distribution. If the opposite situation occurs, and the T_1 T_2 plot deviates significantly from the T_1=T_2 line, we know that the impact from internal gradients are an important factor in the dephasing of precession in T_2 relaxation. Because these mechanisms are highly dependent on the position of the nuclei inside the porous body, knowledge of the T_1/T_2 ration could reveal information about the wetting state of the rock.

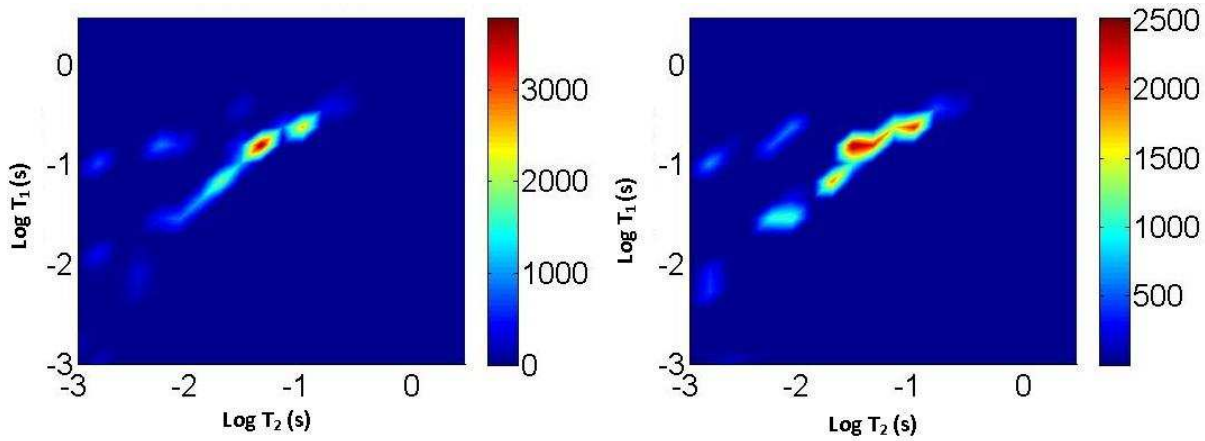

Figure 7-4-1: *Image showing T_1-T_2 correlation for the two brine saturated cores.*

In fig 7-4-1 we see the reference cores at 100% water saturation. We immediately notice the trend in both cores that the T_1 /T_2 ratio is close to the T_1=T_2 line. If we introduce a line, T_1=T_2 (fig 7-4-2) we also acknowledge that the signal stays at the positive side of the T_1/T_2 line. In other words, T_1 is always bigger than T_2. This coincides well with the theory from chapter 3.2. Because the characteristic time constant T_1 is related to the increase of magnetization in z-direction and T_2 is related to the dissipation of magnetization in the x-y-plane it would be impossible for the sample to reach equilibrium before the transverse magnetization is fully dissipated.

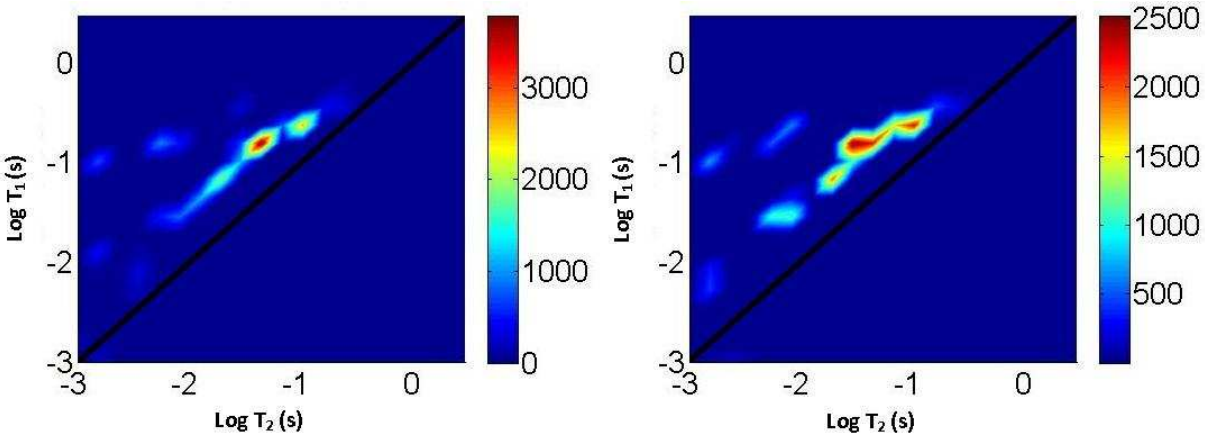

Figure 7-4-2: *Image showing T_1-T_2 correlation for the two brine saturated cores whit a black line at T_1=T_2.*

Finally, by calculating the T_1/T_2 ratio for every increment we are able to find the mean T_1/T_2 ratio, or more precisely the slope of the T_1/T_2 curve. In the reference cores R_1 and R_2 our calculated T_1/T_2 ratio was 1.22 and 1.32 respectively. This is roughly what other researchers have found before. Kleinberg et al conducted a large survey measuring the T_1/T_2 ratio of 105 rock core samples. This survey consisted of a large variety of lithologies and he calculated a mean T_1/T_2 ratio of 1.62[47].

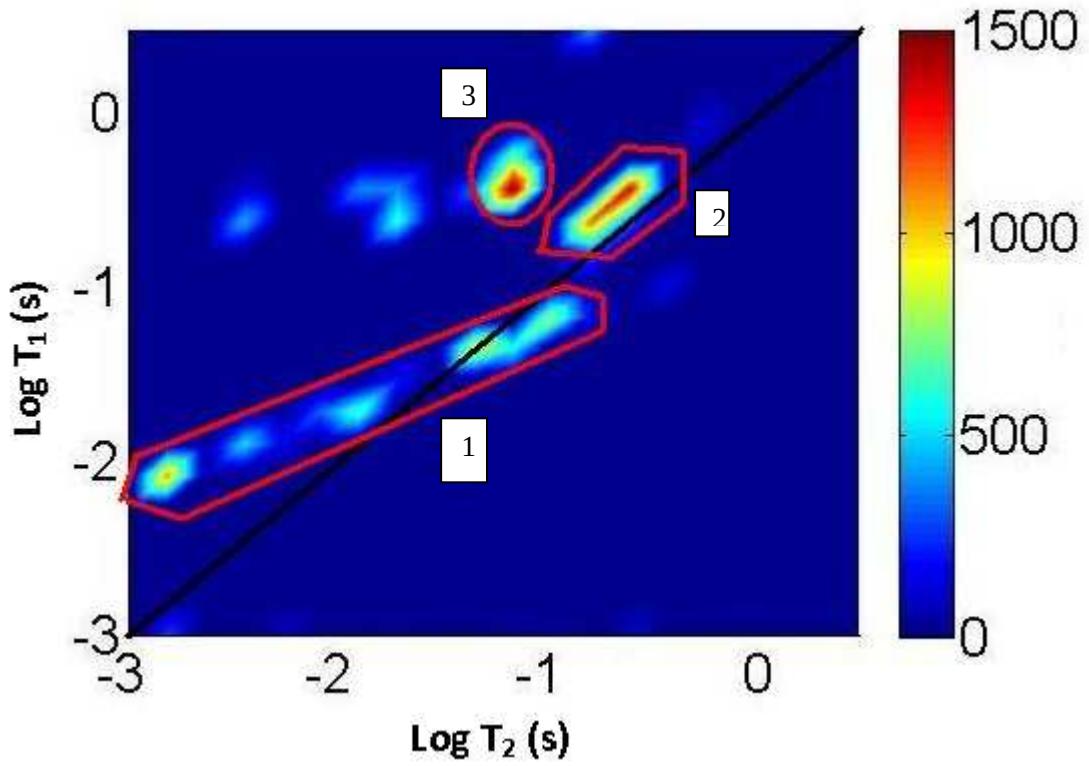

Figure 7-4-3: *Image showing T_1-T_2 correlation for the non-aged crude oil saturated core 2A at S_{wi}.*

While the 100% brine saturated cores got one very distinct trend line the cores at S_{wi} is not as unambiguous. When looking at core 2A (fig 7-4-3) we clearly see three different segments. Some of

the signal forms a distinct trend line from 0.001 second to 0.1 second having a T_1/T_2 ratio of 2.18. As we can see this is considerately higher than what we found in the cores at S_w=1. We also notice that the signal has a larger range on the T_2 scale, ranging all the way from 0.001-0.5 second, compared to the cores at S_w =1 which only got a clear signal from 0.01-0.2 second. Further we notice two other points of interest. Very close to the T_1=T_2 line we find a cluster of intense signal (2), and close to this another cluster marked with the number 3 which differs slightly in T_1 value and strongly in T_2.

In figure 7-4-3 we notice that the signal cluster marked with the number 1 extend beyond the T_1=T_2 line. This is by definition impossible, and must therefore be regarded as a system error. One explanation for this behaviour is the technique that was used in order to construct the 2D image. This technique limits us to a maximum of 20 data points when calculating the 2D image which results in some degree of inaccuracy. With this in mind we state that some of the signal that extend across the T_1=T_2 line must have been produced by an error in the 2D Laplace inversion software giving an artificially long T_2 or short T_1 value. With this in mind it is tempting to merge segment 1 and 2 in figure 7-4-3 into one larger segment. This would in addition explain the slightly high T_1/T_2 ratio we calculated, but since this behaviour is seen in all the cores at S_{wi} we have decided not to do this.

When comparing the signal in core 2A with the signal from the 100% brine saturated cores we clearly see that the crude filled core extends more distinctively towards short T_2 values. From figure 4-3 and 4-4 we acknowledgement that even though these is two separate cores, the only feature that differs them significantly is the fluid saturation. Therefore we explain the long tail towards short T_2 values with the saturation state. Because most of the pore volume and in particularly the interior of the large pores is occupied by the oil phase the water will be restricted from diffusing inside the pore space. The water films will therefore experience the pore as smaller than it really is, because the volume occupied by the oil phase is inaccessible for the water. This results in a higher ratio of spins with small T_2 values than would have been the case for a single fluid system. Another explanation is that the intensity ratio between the signal at small T_2 values and the signal at long T_2 values is different in the two cores. In figure 7-1-2 we see that the brine filled reference core got a high intensity peak representing the bulk water and a relatively low intensity tail representing the water in small pores. Core 2A on the other hand got slightly higher intensity in the signal at small T_2 values, and slightly lower intensity in the signal at long T_2 values. The combination of these two mechanisms deceives us when comparing the 2D image from the two cores. The tail for smaller T_2 values appears less distinct in the brine saturated cores because the intensity of the bulk water is so strong. In the crude oil filled core the presence of the oil phase forces the water phase to experience a higher T_2 rate at S_{wi}. Because the intensity of the bulk phase is weaker and the intensity of the signal at small T_2 values is stronger, the tail for smaller T_2 values appears more distinct in this core.

The third segment in figure 7-4-3 is located quite far from the T_1=T_2 line. Having a much higher T_1 value than T_2 value, we know that the fluid represented by this signal is not being relaxated by a single surface mechanism. Since the T_2 rate is close to 10 times faster than the T_1 rate we conclude that depahasing of precession because of internal gradients must be a key factor. What we observe for this segment of the signal is quite typical for the bulk fluid. Because internal gradients are only capable of affecting the transverse magnetization the longitudinal magnetization is left almost unchecked giving a high T_1/T_2 ratio. It is likely to believe that the fluid represented by the signal in segment 3 is oil trapped as droplets in the interior of the pore. Because it has virtually no contact with the pore surface the longitudinal magnetization is only slightly decreased, but because of the presence of internal gradients the transverse magnetization is dissipated.

After stating that the fluid represented by segment 1 in figure 7-4-3 is water in small pores, and that the fluid in segment 3 is oil at bulk conditions segment 2 remains a puzzle. From the discussion in section 7.1 and from literature[6, 34] it is likely to believe that in a water wet sandstone the signal with the longest T_2 relaxation rate is oil. Because our core is at S_{wi} the oil should according to our theory from chapter 2.4 occupy all the largest pores, hence give a signal at long T_2 values. Consequently we have to recognise the signal as originating from the oil phase, but this doesn`t explain the T_1/T_2 ratio close to 1. To answer this we look at the oil phase distribution in the porous media. Because there is an abundance of oil in this core, the oil phase occupies the interior of the largest pores *and* the medium sized pores. In the medium sized pores the presence of internal gradients causes dissipation of T_2 but is not affecting T_1. This is what we see in segment three. In the middle of the largest pores the strength of the internal gradients are so weak that they are not capable of dephasing the phase coherence and hence T_1=T_2. Hence the fluid represented by segment 2 in figure 7-4-3 should be regarded as oil. Furthermore we know from table 4.3 that core 2A contain 71 per cent oil. When comparing this to the 2D image we notice that the two peaks in segment 2 and 3 combined contains 61 per cent of the total signal intensity in the 2D image. This is 10 per cent less than what we expected and indicate that some of the oil signal has been blended into the water signal.

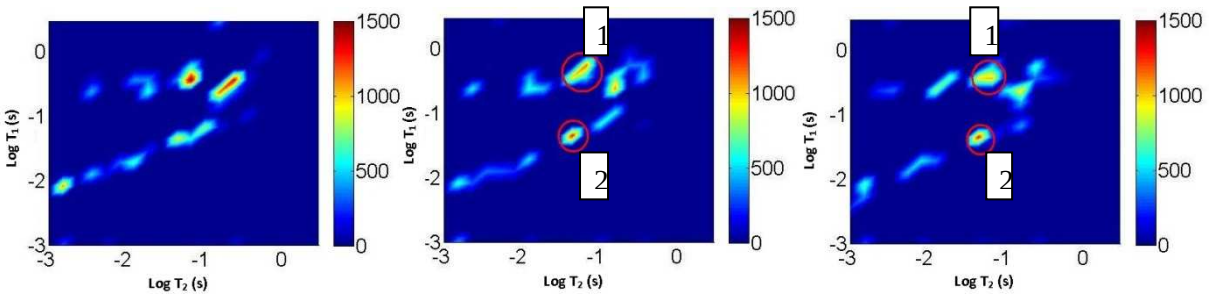

Figure 7-4-4: *Image showing T1-T2 correlation for a non-aged crude oil filled core to the left and two aged cores filled with crude oil, S2 in the middle and S2 to the right at S_{or}.*

When comparing the non-aged core 2A with the aged core S1 and S2 we observe much of the same characteristics. However we observe a slight decrease in the signal associated with bulk fluid in the aged cores compared to the non aged core. Since this is observed in both the aged cores we conclude that the effect must come as a consequence of the altered wetting state. Because the oil phase got some contact with the surface of the pore the longitudinal relaxation rate is decreased. In the 2D image we see this as a decrease in peak (1) and an increase in peak (2).

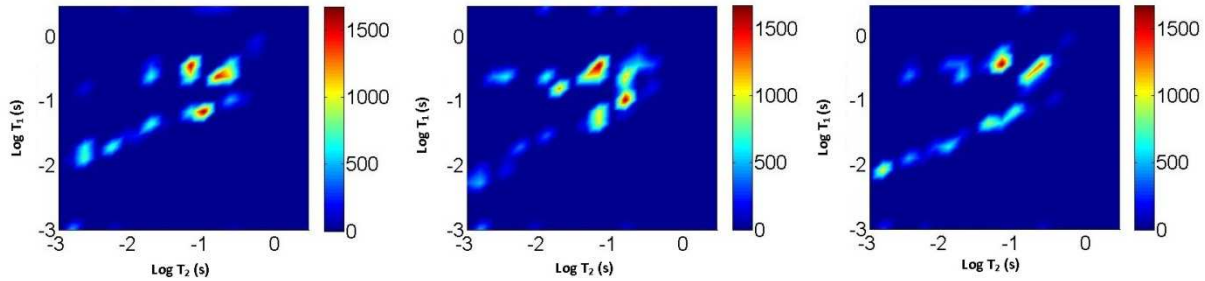

Figure 7-4-5: *Image showing T1-T2 correlation for a non-aged marcol filled core 1A to the left, it`s sister core 1B in the middle and non-aged crude oil filled core 2A to the right.*

In the cores saturated with marcol we find much of the same characteristics as we did in core 2A. However we see observer that much of the signal is located at the T_1=T_2 line at T_2 values we previously have associated with the wetting phase (marked in figure 7-4-6).

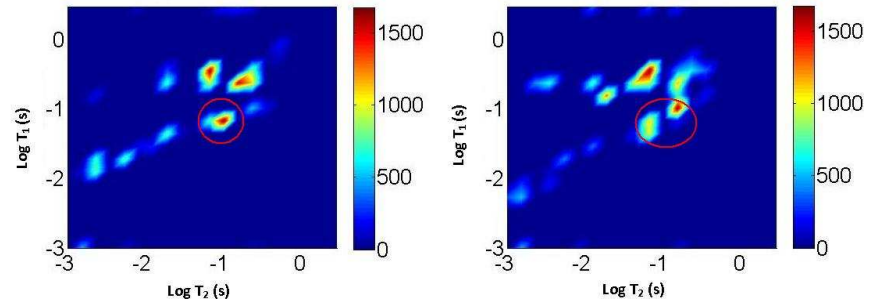

Figure 7-4-6: *Image showing T1-T2 correlation for a non-aged marcol filled core 1A and 1B from left to right. Red circle indicates marcol at bulk conditions.*

This behaviour is could be caused by the short T_2 values of the marcol. Because marcol got shorter T_2 values than crude oil the oil located in the largest pores got slightly shorter T_2 values. This oil is equivalent to the oil labelled “segment 2” in core 2A.

T_1-T_2 correlation – S_{or}

When the oil saturation in the cores reaches S_{or}, water will occupy the largest volume of the pore. In a water-wet media the water will cling to the surface, forcing the oil to form small droplets in the middle of the largest pores. In a partly oil-wet media like we have reasons to believe we are dealing with in core S1 and S2 some of the oil will stay close to the pore surface forming oil film.

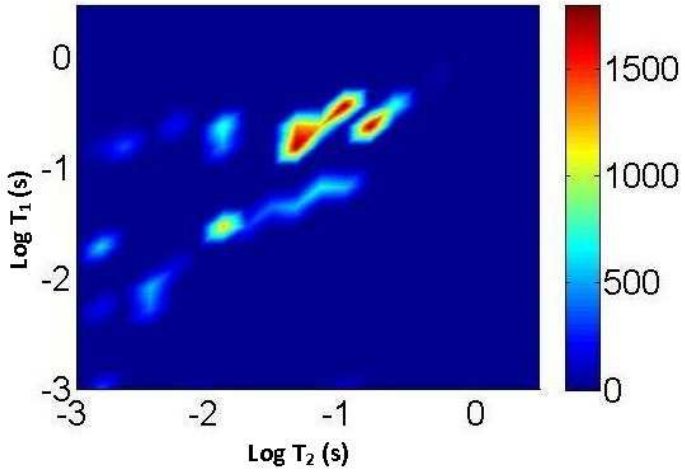

Figure 7-4-7: *Image showing T1-T2 correlation for the non-aged core 2A at S_{or}.*

When we look at the non-aged core at residual oil saturation we observer that there has been a considerately change in T_1/T_2 behaviour compared to the S_{wi} case. The majority of the signal at short T_2 values has dissipated leaving only some weak peaks. In some way the 2D image starts to look like the image produced from the core at 100% water saturation in fig 7-4-1. This behaviour is as anticipated. Even though the restriction caused solely by the matrix is constant, since the water phase now occupies the majority of the pore space the restriction on the water phase residing close to the pore wall has decreased. Consequently a smaller volume of water is having a short T_2 value because it no longer being trapped between the pore surface and the non-wetting phase. On the other hand a larger volume of the water now has longer T_2 values, so the combination of these two effects gives an apparent loss of signal decreasing towards small T_2 values and an increase in the signal at long T_2 values. These results are also coinciding with what we found in the standard CPMG experiment in section 7.1.

.

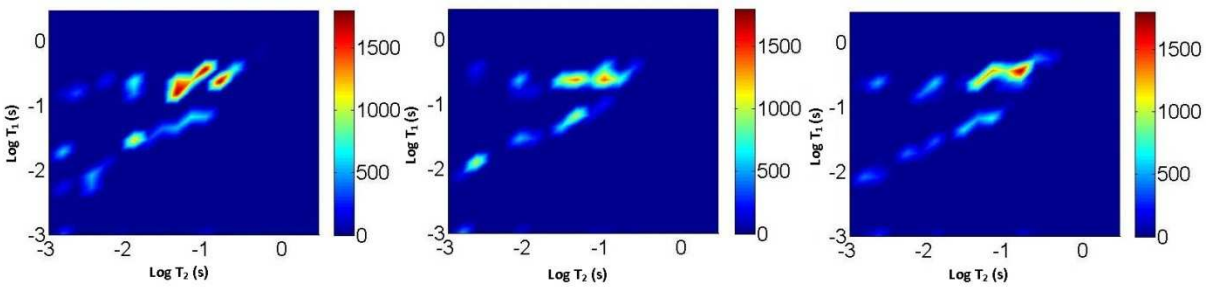

Figure 7-4-8: *Image showing T1-T2 correlation for a non-aged crude oil filled core to the left and two aged cores filled with crude oil, S1 in the middle and S2 to the right. Saturation: S_{or}*

When comparing the non-aged core with the two aged cores we see that in all three cores the majority of the signal is located around 0.1 second. We also see that all of the cores got a tail, even though it is weak, for decreasing T_2 values with a T_1/T_2 ratio of 1.80, 1.67 and 1.80 for 2A, S1 and S2 respectively. We also notice that even though all of the cores got the same main characteristics it is 2A and S2 that have the most in common. We see that both these cores got high signal intensity at T_2=0.1 second, and that S1 got slightly lower signal intensity at the same place. Some of the signal intensity seems to have shifted towards smaller T_1 values as explained in fig 7-4-7.

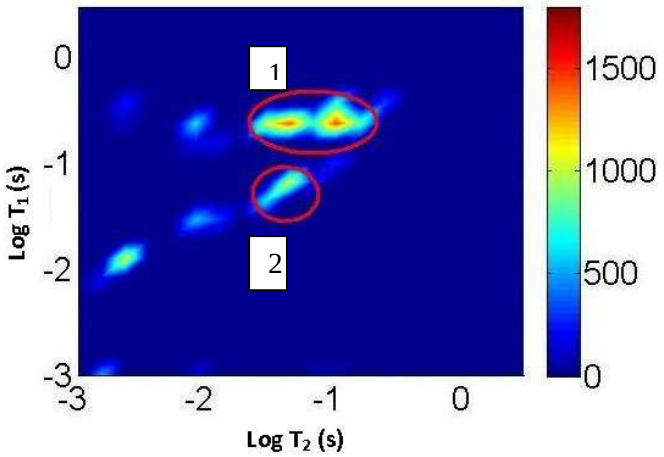

Figure 7-4-9: *Image showing T1-T2 correlation for the aged core S1 at S_{or}*

Even though it is a weak trend we are able to see a lower intensity in segment 1 (fig 7-4-9) and a higher intensity in segment 2. We believe that this is due to the wetting state of the rock. Because some of the oil is able to contact the pore surface it has a smaller T_1 value than what is seen in the other cores and has a T_1/T_2 ratio close to 1. Because the water phase occupies the majority of the pore space the oil feels more restriction, resulting in a smaller T_1 and T_2 value than what is seen in the water phase.

We don`t see the same trend in S2. This could mean that what we see in S1 is just faulty data, but it could also mean that the alternation of the wetting state in core S2 is not sufficient enough to produce any measurable result in this test. With reference to figure 5-8 we see that S2 is slightly more water-wet than S1, according to both USBM and Amott test. This indicates that our results from this section are genuine, and that we are able to detect small changes in wettability by the use of T_1/T_2 correlation.

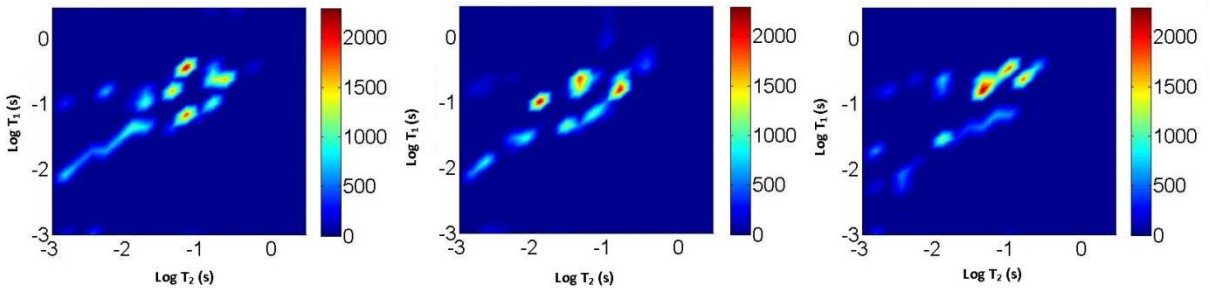

Figure 7-4-6: *Image showing T1-T2 correlation for a non-aged marcol filled core 1A and 1B to the left and in the middle respectively, and 2A to the right.*

When looking at the marcol filled cores we observe some of the same effects that were seen in the crude filled core in figure 7-4-7. However, in the core 1B we observe one peak at T_2=0.001 second where T_1>T_2. Following the same thought as we did in the previous section this behaviour indicates an oil in medium sized pores where the T_2 is dissipated by the presence of internal gradients, and T_1 is not affected in the same degree. We believe that this behaviour is explained by the slightly lower T_2 values in the marcol.

8. Conclusion

In this work a new technique for obtaining wettability data has been investigated. The technique utilizes the principles of nuclear magnetic resonance to measure internal properties of fluid and rock in order to gain information about system of different wettabilities. This information is then compared to a reference system in order to find qualitative information about the wetting state. To correlate our results to traditional wettability data we have also used a standard wetting test in the form of the combined USBM/Amott test to analyse our cores.

In the standard wetting test we found that the aged core showed significant altered wetting state compared to the non aged. All our non-aged cores proved to be strongly water-wet regardless of pore fluid. Our aged core at the other hand had become neutrally wet and was characterised as MWL.

In the NMR part of the experiments all of our experiments showed some sensitivity to the change in wettability. Even though the NMR response from oil and water were highly overlapping, we were able to distinguish between the aged and the non-aged core based on the wetting state from our CPMG experiment. When comparing the T_2 distribution from the aged and the non-aged core we found that there had been a reduction in the main peak and increase in intensity at shorter T_2 values of the aged core`s T_2 distribution. This is described as an effect of changed wettability state, where the altered wetting conditions cause oil to come into contact with the pore surface. In our other experiments concerning diffusion we expected to separate the fluids based on the diffusion coefficient. This did not happen, but because the measured signal still had diffusion information we were able to distinguish between the water-wet and the neutral-wet cores. When measuring the cores at S_{wi} we saw an increase in diffusivity in the aged cores compared to the non-aged core. We have explained that this happen because the continuity of the oil phase have be4en increased in the aged cores, hence the oil in aged cores feel less restriction than the oil in the non-aged cores. In the case of S_{or} we see a decrease in diffusion that may be caused by oil trapped in films at the pore surface, where the diffusion is limited.

In the part of the experiment concerning internal gradient no information was collected at S_{wi}, but at S_{or} good indicators of wettability alternation was detected. Because the oil is behaving more like the wetting phase we saw an indicator of changed NMR signal in the aged cores. This was revealed as a hinge point in the DG_0/T_2 curve. By the use of internal gradient – T_2 correlation, some indicators of the slightly different wettabilities in the two aged cores was also found.

When applying the T_1-T_2 correlation sequence we found that the altered wettability of the aged cores caused the oil phase to behave more like the wetting phase. In more detail we saw an increase of oil signal associated with the oil phase being relaxated by a single surface mechanism. This indicates that the oil is contacting the pore surface which is a good indicator of the surface being oil wet.

In this thesis we used two sets of non-aged cores. One saturated with Marcol/Xylene and the other saturated with the same fluid that was used in the aged cores. The idea was to investigate the impact from the pore fluid on the measured wetting state. This however proved to be a challenge in the NMR part of the experiment. Because the Marcol/Xylene blend had a NMR response which was quite dissimilar to the one found in the crude oil blend it became impossible to draw any conclusions from the samples containing Marcol. There was no way of telling which effect was originating from the wetting state and what came as a consequence of the pore fluids. However, in the USBM/Amott test, they showed no sign of altering the wettability of the rock, indicating that having an inert oil saturating a core at room temperature should not alter the wetting state of the rock.

All in all we have showed the strength of using specialized NMR sequences to detect the alternation of wettability due to aging in Berea sandstone. When only relying on the standard CPMG experiment we only found small indications on the change in wettability, but when combining this with the three other mechanisms some good indicators were made. In particular the internal gradient encoding sequence proved powerful as a tool to detect change in wettability. However, even though we were able to find indicators of altered wettability, this technique are not whiteout flaws. The use of NMR as a probing tool for measuring effects from changed wettability relies heavily on the interpretation of the measured data. Intricate knowledge about the mechanisms taking part in both NMR and in wettability is necessary in order to get any results. We also did some small attempts to find a quantitative measure of the wettability in our cores based on the theory from chapter 3.9, but this attempt have not been presented because the results did not coincide with our other results. Because this was found to be outside the scope of this thesis we did not investigate this any further.

From the work done in this thesis we have showed some of the strength of NMR spectroscopy as a detector of fluid and rock properties. We have shown that the wettability state of the rock may affect the NMR signal to a degree where it is detectable and that the use of NMR in core analysis could give valuable information, complementing other investigation methods.

9. Further work

During the work on this thesis some issues have emerged that would benefit from further attention. For a new method to be widely accepted, it needs to be tested on a large number of samples. A weakness of the data presented here is the limited number of sample cores tested. Testing a larger number of heterogeneous samples would increase the reliability of the method.

If another attempt to do similar experiments on multiple pore fluids, effort should be made in order to keep the pore fluids NMR response as similar as possible. If this is not done, the difference in pore fluid characteristics would lead to a situation where you can not tell if a change is due to wettability changes or the difference in pore fluid.

It would also be interesting to investigate the evolution of the aging process. In this thesis the original plan was to investigate the NMR response of various cores while they were undergoing aging procedure. This could not be achieved because of malfunction of essential hardware, but pursuing that original idea to investigate how the wetting state develops during aging could give valuable information about wetting as well as aging procedures.

10. Appendix

TABLE 1 – Compostion of synthetic seawater

	Recipe (g / 2L)	**Actual** (g / 2L)
NaCl	49,78	49,72
$CaCl_2 \cdot 2H_2O$	3,452	3,46
$MgCl'_2 \cdot 6H_2O$	22,248	22,18
$NaHCO_3$	0,384	0,43
Na_2SO_4	8,096	8,11
KCl	1,336	1,33
Tot salt		85,23 g
Water		1914,77 g

TABLE 2 - Properties of Marcol 182.

Property	**Test methode**	**Min**	**Max**
Appearance	Visual	Clear and bright	Clear and bright
Odour		Absent	Absent
Viscosity at 20 ˚C [cP]	Calculated	47	53.5
Viscosity at 22 ˚C [cP]	RHEOPLUS	67	67
Density at 20 ˚C [Kg/m3]		847	862

TABLE 3 – Crude characteristics

API:	**Test methode**	
S.G.:		0.9043
Sulphur (mass%):		0.52
Pour Point (°C):		<-42
TAN (mg KOH/g):		2.9
Nickel (wppm):		2.5
Vanadium (wppm):		12.0
Viscosity at 22 ˚C [cP]	RHEPLUS	71

11. Referanser

1. Zolotukhin, A.B. and Ursin, J.-R., (2000), *Introduction to Petroleum Reservoar Engineering*, Kristiansand: Høyskoleforlaget.
2. Anderson, W.G., (1986), *Wettability Literature Survey- Part 2: Wettability Measurement, SPE 13933.* Journal of Petroleum Technology. **38**(11): p. 1246-1262.
3. Anderson, W.G., (1986), *Wettability Literature Survey- Part 1: Rock/Oil/Brine Interactions and the Effects of Core Handling on Wettability.* Journal of Petroleum Technology. **38**(10): p. 1125-1144.
4. Amott, E., (1959), *Observations Relating to the Wettability of Porous Rock, SPE:1167.* Petroleum Transactions, AIME. **216**: p. 156-162.
5. Donaldson, E.C., Thomas, R.D., and Lorenz, P.B., (1969), *Wettability Determination and Its Effect on Recovery Efficiency, SPE 2338-PA.* SPE Journal. **9**(1): p. 13 - 20.
6. Coates, G.R., Xiao, L., and Prammer, M.G., (1999), *NMR Logging: Principles and Applications*: Haliburton Energy Services.
7. Al-Mahrooqi, S.H., et al. (2005). *Wettability Alteration During Aging: The Application of NMR to Monitor Fluid Redistribution*. in *Society of Core Analyst*:Toronto
8. Al-Mahrooqi, S.H., et al., (2006), *Pore-scale modelling of NMR relaxation for the characterization of wettability.* Journal of Petroleum Science and Engineering. **52**(1-4): p. 172-186.
9. Chen, J., Hirasaki, G.J., and Flaum, M., (2006), *NMR wettability indices: Effect of OBM on wettability and NMR responses.* Journal of Petroleum Science and Engineering. **52**(1-4): p. 161-171.
10. Freedman, R., et al. (2002). *Wettability, Saturation, and Viscosity Using the Magnetic Resonance Fluid Characterization Method and New Diffusion-Editing Pulse Sequences, SPE 77397*. in *SPE Annual Technical Conference and Exhibition*:San Antonio, Texas
11. Selley, R.C., (1998), *Elements of petroleum geology*, San Diego: Academic Press.
12. Honarpour, M. and Mahmood, S.M., (1988), *Relative-Permeability Measurements: An Overview, SPE 18565-PA* Journal of Petroleum Technology. **40**(8): p. 963-966.
13. Graig, F.F., (1971), *The Reservoir Engineering Aspects of Waterflooding*. 2nd ed. SPE Monograph Series. Vol. 3, Dallas, : American Institute of Mining, Metalurgical, and Petroleum Engineers.
14. Skauge, A. and Ottesen, B. (2002). *A Summary Of Experimentally Derived Relative Permeability And Residual Saturation On North Sea Reservoir Cores*. in *International Symposium of the Society of Core Analysts*. SCA 2002-12
15. Anderson, W.G., (1986), *Wettability Literature Survey- Part 1: Rock/Oil/Brine Interactions and the Effects of Core Handling on Wettability, SPE 13932.* Journal of Petroleum Technology. **38**(10): p. 1125-1144.
16. Salathiel, R.A., (1973), *Oil Recovery by Surface Film Drainage In Mixed-Wettability Rocks, SPE 4104-PA.* Journal of Petroleum Technology. **25**(10): p. 1216-1224.
17. Chilingar, G.V. and Yen, T.F., (1983), *Some notes on wettability and relative permeabilities of carbonate reservoir rocks, II.* Journal Name: Energy Sources (N.Y.); (United States); Journal Volume: 7:1: p. Medium: X; Size: Pages: 67-76.
18. Treiber, L.E., Owens, W.W., (1972), *A Laboratory Evaluation of the Wettability of Fifty Oil-Producing Reservoirs, SPE 3526-PA.* SPE Journal. **12**(6): p. 531-540.
19. Lyutin, L.V.a.B., T. A, (1970), *Adsorption of asphaltenes in a stratum and its effect on permeability and oil production.* Tr., Vses. Neffegazov..Nauch.-IssIed. Inst. **53**(117-30): p. Sited in Anderson, W.G., (1986), Wettability Literature Survey- Part 1:

Rock/Oil/Brine Interactions and the Effects of Core Handling on Wettability, SPE 13932. Journal of Petroleum Technology. 38(10): p. 1125-1144.
20. Graue, A., Viksund, B.G., and Baldwin, B.A., (1999), *Reproducible Wettability Alteration of Low-Permeable Outcrop Chalk, SPE 55904-PA.* SPE Reservoir Evaluation & Engineering. **2**(2): p. 134-140.
21. Graue, A., et al., (2002), *Alteration of wettability and wettability heterogeneity.* Journal of Petroleum Science and Engineering. **33**(1-3): p. 3-17.
22. Lien, J.R., (2007), *Reservoarteknikk I*: University of Bergen.
23. Holmes, S., (2002), *Capillary Pressure & Relative Permeability Petrophysical Reservoir Models*, Denver, Colorado, USA: Digital Formation, Inc.
24. Aamot, E., (1959), *Observations Relating to the Wettability of Porous Rock, SPE 1167-G.* Trans. AIME. **216**: p. 156 - 162.
25. Sharma, M.M. and Wunderlich, R.W. (1985). *The Alteration of Rock Properties Due to Interactions With Drilling Fluid Components, SPE 14302*. in *SPE Annual Technical Conference and Exhibition*:Las Vegas, Nevada
26. Dixit, A.B., et al., (2000), *Empirical Measures of Wettability in Porous Media and the Relationship between Them Derived From Pore-Scale Modelling.* Transport in Porous Media. **40**(1): p. 27-54.
27. Bloch, F., (1946), *Nuclear Induction.* Physical Review. **70**(7-8): p. 460-474.
28. Purcell, E.M., Torrey, H.C., and Pound, R.V., (1946), *Resonance Absorption by Nuclear Magnetic Moments in a Solid.* Physical Review. **69**(1-2): p. 37.
29. Levitt, M.H., (2008), *Spin dynamics: basics of nuclear magnetic resonance*, Chichester: Wiley. XXV, 714 s., [2] pl.
30. Lien, J.R., (2004), *En kort innføring i NMR logging.*
31. Hornak, J.P. *The Basics of NMR*. 1997; Available from: http://www.cis.rit.edu/htbooks/nmr/.
32. Brown, R.J.S. and Fatt, I., (1956), *Measurements of Fractional Wettability of Oilfield Rocks by the Nuclear Magnetic Relaxation Method.* Transactions of the American Institute of Mining and Metallurgical Engineers. **207**(11): p. 262-264.
33. Hahn, E.L., (1950), *Spin Echoes.* Physical Review. **80**(4): p. 580.
34. Dunn, K.-J., Bergman, D.J., and Latorraca, G.A., (2002), *Nuclear Magnetic Resonance - Petrophysical and Logging Applications*. Seismic Exploration. Vol. 32: Pergmanon.
35. Seland, J.G., et al., (2004), *Correlations between diffusion, internal magnetic field gradients, and transverse relaxation in porous systems containing oil and water.* Physical Review E. **70**(5).
36. Carr, H.Y. and Purcell, E.M., (1954), *Effects Of Diffusion On Free Precession In Nuclear Magnetic Resonance Experiments.* Physical Review. **94**(3): p. 630-638.
37. Meiboom, S. and Gill, D., (1958), *Modified Spin-Echo Method for Measuring Nuclear Relaxation Times.* Review of Scientific Instruments. **29**(8): p. 688-691.
38. Watson, A.T. and Chang, C.T.P., (1997), *Characterizing porous media with NMR methods.* Progress in Nuclear Magnetic Resonance Spectroscopy. **31**(4): p. 343-386.
39. Einstein, A., (1956), *Investigation on the Theory of Brownina Movement*: Dover Publication, inc.
40. Stejskal, E.O. and Tanner, J.E., (1965), *Spin Diffusion Measurements: Spin Echoes in the Presence of a Time-Dependent Field Gradient.* The Journal of Chemical Physics. **42**(1): p. 288-292.
41. Hürlimann, M.D., (1998), *Effective Gradients in Porous Media Due to Susceptibility Differences.* Journal of Magnetic Resonance. **131**(2): p. 232-240.

42. Sun, B. and Dunn, K.-J., (2002), *Probing the internal field gradients of porous media.* Physical Review E. **65**(5): p. 051309.
43. G.H. Sørland, K.D., H. C. Widerøe, J.R. Lien, and A. Skauge, (2007), *Absolute Pore Size Distributions from NMR.* Diffusion Fundamentals. **5**: p. 4.1-4.15.
44. Sørland, G.H., Aksnes, D., and Gjerdåker, L., (1999), *A Pulsed Field Gradient Spin-Echo Method for Diffusion Measurements in the Presence of Internal Gradients.* Journal of Magnetic Resonance. **137**(2): p. 397-401.
45. Mitra, P.P. and Sen, P.N., (1992), *Effects of microgeometry and surface relaxation on NMR pulsed-field-gradient experiments: Simple pore geometries.* Physical Review B. **45**(1): p. 143.
46. Hashemi, R.H. and Bradley, W.G., (1997), *MRI: the basics*, Baltimore: Williams & Wilkins. XI, 307 s.
47. Kleinberg, R.L., et al. (1993). *Nuclear Magnetic Resonance of Rocks: T1 vs. T2, SPE 26470*. in *SPE Annual Technical Conference and Exhibition*:Houston, Texas
48. Brownstein, K.R. and Tarr, C.E., (1979), *Importance of classical diffusion in NMR studies of water in biological cells.* Physical Review A. **19**(6): p. 2446.
49. Brownstein, K.R. and Tarr, C.E., (1977), *Spin-lattice relaxation in a system governed by diffusion.* Journal of Magnetic Resonance (1969). **26**(1): p. 17-24.
50. Hsu, W.-F., Li, X., and Flumerfelt, R.W. (1992). *Wettability of Porous Media by NMR Relaxation Methods, SPE 24761-MS*. in *SPE Annual Technical Conference and Exhibition*:Washington, D.C.
51. Fleury, M. and Deflandre, F., *Quantitative evaluation of porous media wettability using NMR relaxometry.* Magnetic Resonance Imaging. **21**(3-4): p. 385-387.
52. Hürlimann, M.D. and Venkataramanan, L., (2002), *Quantitative Measurement of Two-Dimensional Distribution Functions of Diffusion and Relaxation in Grossly Inhomogeneous Fields.* Journal of Magnetic Resonance. **157**(1): p. 31-42.
53. M. Flaum, J.C., G. J. Hirasaki. (2004). *NMR Diffusion Editin For D-T2 Maps: Application To Recognition Of Wettability Change*. in *SPWLA 45th Annual Logging Symposium, 2004*. Society of Petrophysicists & Well Log Analysts
54. Pavlin, T. and Seland, J.G., (2010), *Dynamic correlations between susceptibility gradients and T2- relaxation as a probe for wettability properties of liquid saturated.* Diffusion Fundamentals. **14**(8): p. 1-4.
55. Norsk Hydro (1990). *Sentrifugering med Vann/Olje ved romtemperatur med J6-B-Sentrifuge - Imbibisjon og Drenering*. in *Prosedyre for Kjerneanalyse*:Bergen
56. O'Meara Jr., D.J., Hirasaki, G.J., and Rohan, J.A., (1992), *Centrifuge Measurements of Capillary Pressure: Part 1 - Outflow Boundary Condition, SPE 14419.* SPE Reservoir Engineering. **7**(1): p. 133-142.
57. Omeregle, Z.S., (1988), *Factors Affecting the Equivalency of Different Capillary Pressure Measurement Techniques, SPE 15384-PA.* SPE Formation Evaluation. **3**(1): p. 146-155.
58. Mason, G., et al., (2010), *Correlation for the effect of fluid viscosities on counter-current spontaneous imbibition.* Journal of Petroleum Science and Engineering. **72**(1-2): p. 195-205.
59. Cuiec, L.E. (1975). *Restoration of the Natural State of Core Samples*. in *Fall Meeting of the Society of Petroleum Engineers of AIME*:Dallas, Texas
60. Seland, J.G., Soerland, G.H., Anthonsen, H.W., Krane, J., (2003), *Combining PFG and CPMG NMR measurements for separate characterization of oil and water simultaneously present in a heterogeneous system.* Applied Magnetic Resonance. **24**: p. 41-53.
61. Djurhuus, K., (2011), Personal communication

62. Hirasaki, G.J., Zhang, G.Q., and Huang, C.-C., (2000), *Interpretation Of Wettability In Sandstones With Nmr Analysis.* PetroPhysics.
63. Mitra, P.P., Sen, P.N., and Schwartz, L.M., (1993), *Short-time behavior of the diffusion coefficient as a geometrical probe of porous media.* Physical Review B. **47**(14): p. 8565-8574.
64. Seland, J.G., et al., (2004), *Correlations between diffusion, internal magnetic field gradients, and transverse relaxation in porous systems containing oil and water.* Physical Review E. **70**(5): p. 051305.